

THESIS

PERFORMANCE EVALUATION OF AN ADVANCED AIR-FUEL RATIO CONTROLLER
ON A STATIONARY, RICH-BURN NATURAL GAS ENGINE

Submitted by

Roshan Joseph Kochuparampil

Department of Mechanical Engineering

In partial fulfillment of the requirements

For the Degree of Master of Science

Colorado State University

Fort Collins, Colorado

Summer 2013

Master's Committee:

Advisor: Daniel Olsen

Christopher Hagen
Sybil Sharvelle

Copyright by Roshan Joseph Kochuparampil 2013

All Rights Reserved

ABSTRACT

PERFORMANCE EVALUATION OF AN ADVANCED AIR-FUEL RATIO CONTROLLER ON A STATIONARY, RICH-BURN NATURAL GAS ENGINE

The advent of an era of abundant natural gas is making it an increasingly economical fuel source against incumbents such as crude oil and coal, in end-use sectors such as power generation, transportation and industrial chemical production, while also offering significant environmental benefits over these incumbents. Equipment manufacturers, in turn, are responding to widespread demand for power plants optimized for operation with natural gas. In several applications such as distributed power generation, gas transmission, and water pumping, stationary, spark-ignited, natural gas fueled internal combustion engines (ICEs) are the power plant of choice (over turbines) owing to their lower equipment and operational costs, higher thermal efficiencies across a wide load range, and the flexibility afforded to end-users when building fine-resolution horsepower topologies: modular size increments ranging from 100 kW – 2 MW per ICE power plant compared to 2 – 5 MW per turbine power plant.

Under the U.S. Environment Protection Agency's (EPA) New Source Performance Standards (NSPS) and Reciprocating Internal Combustion Engine National Emission Standards for Hazardous Air Pollutants (RICE NESHAP) air quality regulations, these natural gas power plants are required to comply with stringent emission limits, with several states mandating even stricter emissions norms.

In the case of rich-burn or stoichiometric natural gas ICEs, very high levels of sustained emissions reduction can be achieved through exhaust after-treatment that utilizes Non Selective Catalyst Reduction (NSCR) systems. The primary operational constraint with these systems is

the tight air-fuel ratio (AFR) window of operation that needs to be maintained if the NSCR system is to achieve simultaneous reduction of carbon monoxide (CO), nitrogen oxides (NO_x), total hydrocarbons (THC), volatile organic compounds (VOCs), and formaldehyde (CH₂O). Most commercially available AFR controllers utilizing lambda (oxygen) sensor feedback are unable to maintain engine AFR within the required range owing to drift in sensor output over time.

In this thesis, the emissions compliance performance of an AFR controller is evaluated over a 6-month period on an engine driving a gas compressor in an active natural gas production field. This AFR controller differentiates itself from other commercially available products by employing a lambda sensor that has been engineered against sensor drift, making it better suited for natural gas engine applications. Also included in this study are the controller's responses to transient loads, diurnal performance, adaptability to seasonal variations in ambient temperature, fuel quality variations (in wellhead gas), engine health considerations for proper AFR control, and controller calibration sensitivity when replacing lambda sensors.

During the first three months of operation and subsequent diurnal tests, the controller's performance as a multi-point AFR control system was consistent, demonstrating appropriate AFR adjustments to variation in engine operation, over a wide range of ambient conditions, despite high consumption rate of engine lubrication oil. For the remainder of the test, high levels of lubrication oil consumption compromised the ability to verify controller performance.

ACKNOWLEDGEMENTS

This work was supported by Southern California Gas Company (SoCal Gas Co.) through Pipeline Research Council International. Research funding and project oversight was sponsored by Gregg Arney, Jeff Chini, and Firas Hamze of SoCal Gas Co.

First and foremost, I am immensely grateful to Dr. Daniel Olsen for his patient mentoring throughout my graduate program adventures. I want to extend my sincere appreciation to Lyle Delay and Justin Lisowski at Encana Corp. for the hospitality extended during site visits to Frenchie Draw and innumerable other professional courtesies; Dr. Chris Hagen at Oregon State University and Chris DeFoor at Woodward, Inc. for sharing their wealth of experience on best practices during field testing. I am also very grateful for the support and encouragement received from staff members and fellow student collaborators in the Department of Mechanical Engineering and at the EECL.

On a personal note, I am indebted to the Kochuparampil, Tshering–Copeland, Manriquez, and Ihde–Ksug families for their love, good counsel, and friendship.

TABLE OF CONTENTS

ABSTRACT	ii
ACKNOWLEDGEMENTS	iv
LIST OF TABLES	vii
LIST OF FIGURES	ix
1. Introduction	1
1.1 The Golden Age of Natural Gas	1
1.2 Classification of Internal Combustion Engines	5
1.3 Exhaust After-Treatment Systems	7
1.3.1 Catalytic Considerations	7
1.3.2 Oxidation Catalysts	10
1.3.3 Selective Catalytic Reduction (SCR)	11
1.3.4 Lean NO _x Trap (LNT)	12
1.3.5 Non-Selective Catalytic Reduction (NSCR)	12
2. Site Overview	18
2.1 Control Architecture	24
2.2 Emissions Sampling System	30
2.2.1 Portable Emissions Analyzer	33
2.2.2 Portable Gas Chromatograph	38
2.3 Project Timeline and Milestones	39
2.4 Test Matrix	42
2.4.1 Performance Evaluation Protocol	43
2.4.2 Evaluation of Engine Power Output	45
3. Results	47

3.1	Engine Tuning	47
3.2	Alarms/Faults	48
3.3	Engine Health	48
3.4	Steady-State Performance	54
3.4.1	Engine Condition: High Speed/High Load (HS/HL)	54
3.4.2	Engine Condition: Medium Speed/Medium Load (MS/ML).....	65
3.4.3	Engine Condition: Low Speed/Low Load (LS/LL)	68
3.5	Retuned Performance	72
3.6	Fuel Gas Composition	79
3.7	Diurnal Cycle	81
3.8	Remote Monitoring	82
3.9	Transient Performance	84
3.9.1	Load Steps.....	84
3.9.2	Shutdown	85
3.9.3	Startup	86
4.	Conclusions and Recommendations.....	89
5.	References	91
	Appendix A: Engine Specifications.....	94
	Appendix B: Emissions Analyzer Calibration Log	97
	Appendix C: Alarm/Fault Checks.....	100
	Appendix D: Transient Response	108
	Appendix E: Field Data	120
	Appendix F: Installation Details	133
	LIST OF ABBREVIATIONS.....	163

LIST OF TABLES

Table 1: Overview of currently available exhaust after-treatment systems [7, 16, 17, 18, 19]......	9
Table 2: Specifications of sensors fitted on ECOM J2KN portable emissions analyzer.....	34
Table 3: Calibration gases used for the portable emissions analyzer during field site visits.....	35
Table 4: Engine speed/load test matrix used for emissions monitoring and evaluation of E3RB performance	43
Table 5: Elemental composition of catalyst ash	51
Table 6: Summary of emissions trends @ HS/HL operation.....	60
Table 7: Calibration gas concentrations used during field test.....	98
Table 8: Calibration log for portable emissions analyzer	99
Table 9: Field data log from February 27 (Site visit # 1)	121
Table 10: Field data log from March 13 (Site visit # 2)	122
Table 11: Field data log from April 2 (Site visit # 3)	123
Table 12: Field data log from May 15 – Part 1/2 (Site visit # 4).....	124
Table 13: Field data log from May 15 and 16 – Part 2/2 (Site visit # 4)	125
Table 14: Field data log from June 25 (Site visit # 5)	126
Table 15: Field data log from 24-hour test on June 26 – Part 1/4 (Site visit # 5).....	127
Table 16: Field data log from 24-hour test on June 26 and 27 – Part 2/4 (Site visit # 5).....	128
Table 17: Field data log from 24-hour test on June 27 – Part 3/4 (Site visit # 5).....	129

Table 18: Field data log from 24-hour test on June 27 – Part 4/4 (Site visit # 5).....	130
Table 19: Field data log from August 20 (Site visit # 6)	131
Table 20: Field data log from August 24 – after retuning (Site visit # 6).....	132

LIST OF FIGURES

Figure 1: Map of U.S. shale gas and shale oil plays in the lower 48 states [25].	2
Figure 2: Cross-section of a horizontal well, showing hydraulically fractured fissures within the target formation [26].	4
Figure 3: Engine-out emissions of various constituents and engine power output (on y-axis) produced during a λ sweep (on x-axis) [Reprinted from 10].	7
Figure 4: NSCR (or TWC) conversion efficiencies (on y-axis) for various constituents over a range of operational ϕ (on x-axis) [Reprinted from 11].	13
Figure 5: Compressor station external view, with engine room (in foreground) and exhaust stack/tailpipe on elevated catwalk (in background).	18
Figure 6: Schematic of compressor station layout, comprising engine, compressor, piping from exhaust manifold to catalyst housing, and stack. The catwalk is mounted atop the cooling fan housing structure.	20
Figure 7: Profile view of the Waukesha L7044GSI engine inside the compressor station with left bank components labeled.	21
Figure 8: Gas compressor (in foreground) coupled to the engine (in background).	22
Figure 9: Lagging catalyst element (with ash on front face) being removed from the housing for cleaning.	23
Figure 10: Emit elements in the catalyst housing (leading element is on the right), with thermal-wrap around the frame for proper sealing. Direction of exhaust gas flow is from right to left.	23

Figure 11: The E3RB control module installed inside the compressor station at the test site.....	24
Figure 12: Layout of sensors and actuators for E3RB operation of a dual-bank engine (stereo control) [8].	25
Figure 13: Schematic of valves and sensors installed on the field engine to facilitate E3RB operation. NO _x sensors, coupled to onsite SCADA, provided remote emissions monitoring capability (not required by the E3RB system).	29
Figure 14: Pre-catalyst emissions sampling probe in exhaust manifold.	31
Figure 15: Post-catalyst emissions sampling probe in exhaust manifold.	32
Figure 16: Heated sample line (bottom left) connected to filter outlet, shrouded in thermal wrap. Handle of three-way valve is on the far right, with handle of purge air valve visible in the middle.	32
Figure 17: Heated sample line is routed from the sampling port on the elevated catwalk (left), through a ground level window in the engine room (middle), to the inlet of the heated head pump (right).	33
Figure 18: (Left) Portable emissions analyzer setup inside the engine room. (Right) Alternate arrangement for exhaust sampling: heated sample line (hanging in foreground) ready for direct connection to the sampling port on the analyzer.	33
Figure 19: Screenshot of SCADA page for Engine Data	36
Figure 20: Screenshot of SCADA page for Compressor Data	36
Figure 21: (Left) Pre-catalyst NO _x sensor. (Right) Post-catalyst NO _x sensor.	37
Figure 22: NO _x sensor control module installed inside sealed enclosure on elevated catwalk. ..	37

Figure 23: Portable fuel gas chromatograph station inside the engine room.....	39
Figure 24: Comparison of engine power output obtained using three different methods.	46
Figure 25: Tuned emissions level across the engine operating load range.....	47
Figure 26: Catalyst elements being blown out with compressed air to clear ash-masking.	50
Figure 27: Spectrogram of elemental composition of catalyst ash.....	51
Figure 28: Pre (right) and post (left) catalyst pressure taps affixed atop the catalyst housing.	52
Figure 29: Trend of pressure drop and temperature across catalyst elements at HS/HL operation.	53
Figure 30: Trends of pre-catalyst emissions and CO:NOx @ HS/HL operation.....	55
Figure 31: Trends of post-catalyst emissions and CO:NOx at HS/HL operation.....	56
Figure 32: Comparison of in-cylinder temperatures before/after spark plug change.	57
Figure 33: Catalyst efficiency @ HS/HL operation.....	59
Figure 34: Trends of E3RB parameters and pre-catalyst emissions @ HS/HL operation.....	62
Figure 35: Pre-catalyst NOx-CO crossplot @ HS/HL operation.....	63
Figure 36: Post-catalyst NOx-CO crossplot @ HS/HL operation.	64
Figure 37: Trends of other engine parameters and ambient temperature @ HS/HL operation. ...	64
Figure 38: Trend of pressure drop and temperature across catalyst elements at MS/ML operation.	65
Figure 39: Trends of post-catalyst emissions and CO:NOx at MS/ML operation.	66
Figure 40: Trends of E3RB parameters and post-catalyst emissions @ MS/ML operation.....	67

Figure 41: Post-catalyst NO _x -CO crossplot @ MS/ML operation.....	68
Figure 42: Trend of pressure drop and temperature across catalyst elements at LS/LL operation.	69
Figure 43: Trends of post-catalyst emissions and CO:NO _x at LS/LL operation.....	71
Figure 44: Trends of E3RB parameters and post-catalyst emissions @ LS/LL operation.	71
Figure 45: Post-catalyst NO _x -CO crossplot @ LS/LL operation.	72
Figure 46: (Coarse scale) Simulated ϕ sweep vs. post-catalyst emissions.	73
Figure 47: (Fine scale) Simulated ϕ sweep vs. post-catalyst emissions.	74
Figure 48: (Coarse scale) Simulated ϕ sweep versus catalyst efficiency.	74
Figure 49: (Fine scale) Simulated ϕ sweep vs. catalyst efficiency.	75
Figure 50: Simulated ϕ sweep vs. pre-catalyst emissions.....	76
Figure 51: (New tuning) Trends of post-catalyst emissions and CO:NO _x at HS/HL operation. .	77
Figure 52: (New tuning) Trends of post-catalyst emissions and CO:NO _x at MS/ML operation. 78	
Figure 53: (New tuning) Trends of post-catalyst emissions and CO:NO _x at LS/LL operation. ..	79
Figure 54: 12-hour trend of fuel gas composition and NO _x emissions.	80
Figure 55: 24-hour evaluation of E3RB performance.	82
Figure 56: Daily average NO _x trends obtained from SCADA.	83
Figure 57: Transient response of E3RB parameters during load step from HS/HL to MS/ML... 85	
Figure 58: Transient response of E3RB parameters during engine shutdown on March 12.	86
Figure 59: Transient response of E3RB parameters during engine startup on March 12.....	87

Figure 60: NO _x emissions during engine startup on March 12.....	88
Figure 61: CO emissions during engine startup on March 12.....	88
Figure 62: (Above) E3RB ToolKit Fault Log displaying the misfire alarm, designated by the control system as AL370. (Right) Realtime trend of E3RB parameters captured during the misfire event.....	101
Figure 63: E3RB ToolKit trends displaying alarms for System Lean (orange trend - above) and System Rich (magenta trend - below) conditions.....	102
Figure 64: E3RB ToolKit trend displaying an alarm during simulated failure of the post-catalyst HEGO sensor (identified as HEGO 3).....	103
Figure 65: E3RB ToolKit trend displaying an alarm during a simulated exceedance of the high temperature limit recorded by the post-catalyst temperature sensor (not installed).	104
Figure 66: E3RB ToolKit trend displaying an alarm during a simulated exceedance of the high temperature limit recorded by the pre-catalyst temperature sensor (not installed).....	105
Figure 67: E3RB ToolKit trend displaying an alarm during a simulated exceedance of the low temperature limit recorded by the pre-catalyst temperature sensor (not installed).....	106
Figure 68: E3RB ToolKit trend displaying alarm incidents during simulated failure of the pre-catalyst HEGO sensors; AL560/HEGO 1 – Right bank (above) and AL575/HEGO 2 – Left bank (below).	107
Figure 69: Transition from HS/HL to MS/ML on 27-Feb.....	109
Figure 70: Transition from MS/ML to LS/LL on 27-Feb.....	109
Figure 71: Transition from LS/LL to HS/HL on 27-Feb.....	110

Figure 72: Transition from HS/HL to MS/ML on 13-Mar	110
Figure 73: Transition from MS/ML to LS/LL on 13-Mar	111
Figure 74: Transition from LS/LL to HS/HL on 13-Mar	111
Figure 75: Transition from HS/HL to MS/ML on 02-Apr.....	112
Figure 76: Transition from MS/ML to LS/LL on 02-Apr.....	112
Figure 77: Transition from LS/LL to HS/HL on 02-Apr.....	113
Figure 78: Transition from HS/HL to MS/ML on 15-May.....	113
Figure 79: Transition from MS/ML to LS/LL on 15-May	114
Figure 80: Transition from LS/LL to HS/HL on 15-May.....	114
Figure 81: Transition from HS/HL to MS/ML on 25-Jun	115
Figure 82: Transition from MS/ML to LS/LL on 25-Jun	115
Figure 83: Transition from LS/LL to HS/HL on 25-Jun.....	116
Figure 84: Transition from HS/HL to MS/ML on 20-Aug.....	116
Figure 85: Transition from MS/ML to LS/LL on 20-Aug.....	117
Figure 86: Transition from LS/LL to HS/HL on 20-Aug	117
Figure 87: Transition from HS/HL to MS/ML on 24-Aug (after retuning).....	118
Figure 88: Transition from MS/ML to LS/LL on 24-Aug (after retuning).....	118
Figure 89: Transition from LS/LL to HS/HL on 24-Aug (after retuning).....	119

1. Introduction

Natural gas is used extensively in power generation and is becoming increasingly competitive with incumbent fuel sources, such as crude oil, in other end-use sectors such as transportation and industrial chemical production, while also offering notable environmental benefits over these incumbents.

1.1 The Golden Age of Natural Gas

The factors that drive natural gas demand and supply increasingly point to a future in which natural gas plays a greater role in the global energy mix. Global uncertainties afflicting the energy sector can be seen as opportunities for natural gas. When replacing other fossil fuels, natural gas can lead to lower emissions of greenhouse gases and other pollutants while diversifying the energy supply, thereby leading to improved energy security. It is capable of providing the flexible backup capacity required to augment higher grid penetration of renewable power sources such as wind and solar. Gas is a particularly attractive fuel for regions like China, India, and the Middle East, that are experiencing rapid urban development, causing a surge in energy demand [24].

The global resource base for natural gas is vast and widely dispersed (geographically). Conventional recoverable resources are equivalent to more than 120 years of current global consumption, while total recoverable resources could sustain current production levels for over 250 years. All major regions have recoverable resources equivalent to a minimum of 75 years of current consumption. Timely and successful development depends on a complex set of factors, including policy choices, technological capability, and market conditions. Once discovered, major gas resources can take several decades to reach production [24].

away from the straight vertical trajectories observed in traditional wells, instead deviating to reach a point that could be up to two miles away from the entry site [26].

One of the key enablers of this technique is measurement-while-drilling technology, or borehole telemetry, which permits engineers and geologists to monitor, in real-time, the progress of a drilling operation deep beneath the surface. Using this technology, the trajectory of a well can be accurately plotted and managed, as it curves from a vertical to a horizontal path. Another important enabler is the steerable downhole motor assembly. Conventional drilling of vertical wells occasionally require downhole motors, placed above the drill bit, to help penetrate particularly hard rock formations. Supplementing this with the capability to steer these motors implies that a given well-path can be redirected during real-time drilling operation, allowing for introduction of controlled deviation of the well-path, eventually steering the drill bit into a horizontal path [26].

Hydraulic fracturing is a process of creating fractures in tight rock formations, using high-pressure water containing a mixture of sand and other chemicals, to release the oil and natural gas trapped inside the rock formation. Pumping this pressurized fluid into a drilled well opens up tiny fissures in the rock formation, up to several tenths of an inch wide, allowing oil and natural gas trapped within to flow back to the surface (Figure 2). This technique has been used to extract oil and natural gas for decades, having been first deployed in Kansas in 1947 [26].

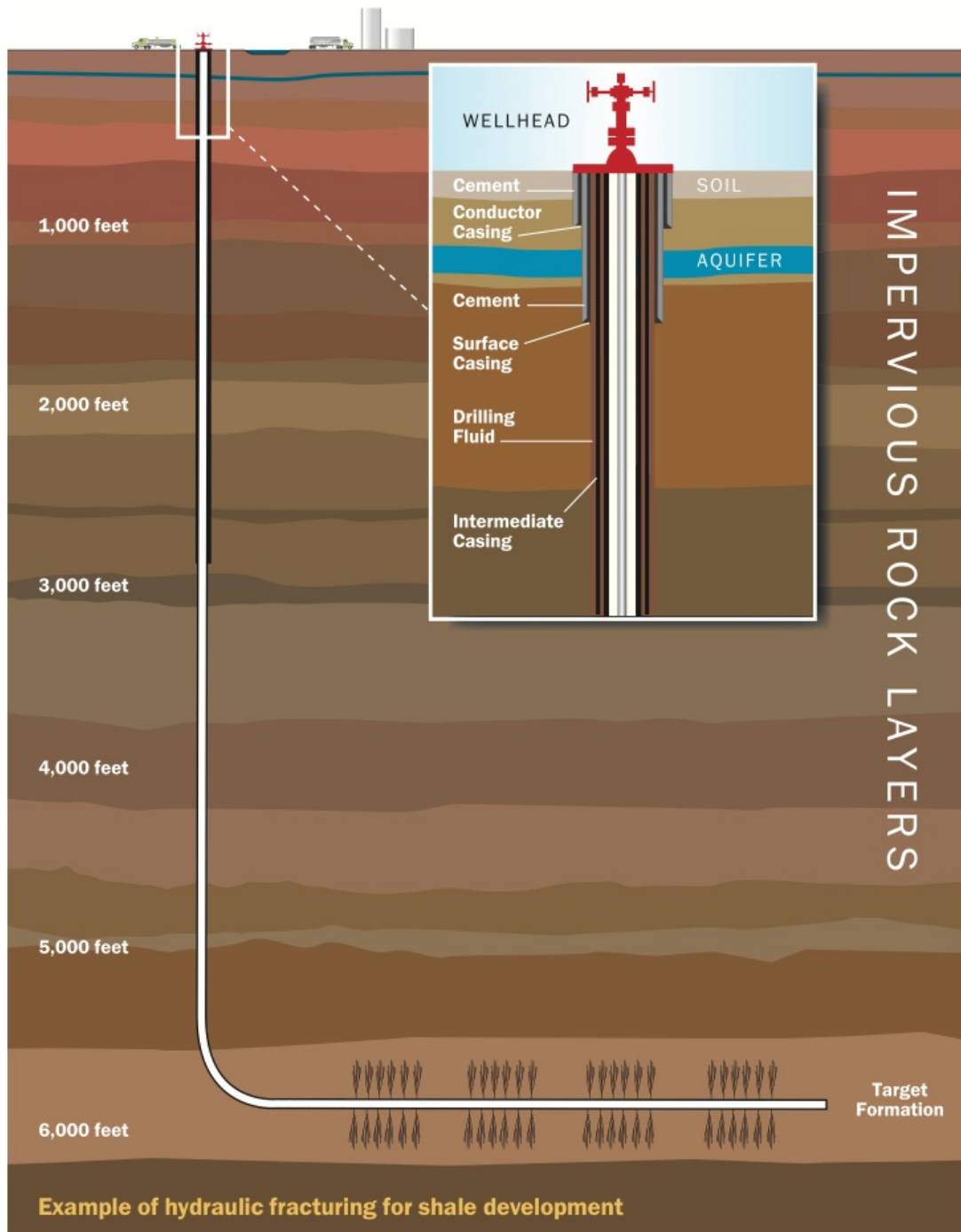


Figure 2: Cross-section of a horizontal well, showing hydraulically fractured fissures within the target formation [26].

The use of hydraulic fracturing in the production process has raised serious environmental concerns, pushing the boundaries of the existing regulatory framework for this industry. However, best practices applied to production, through effective regulation and

monitoring, can mitigate potential environmental risks such as excessive water use, contamination, and disposal. Development of other unconventional gas resources, such as coal-bed methane, is growing in Australia, while unconventional gas projects in China, India, and Indonesia are in their early stages [24].

All these factors point to a coming era in which natural gas will hold greater dominance as a global fuel of choice, increasingly recognized as the golden age of natural gas. In order to take advantage of this era, primemovers such as turbines and internal combustion engines (ICEs) will be optimized to utilize this fuel and deployed in greater numbers in applications relating to power generation and transportation.

1.2 Classification of Internal Combustion Engines

Owing to their efficiency, robustness, and power density, stationary reciprocating ICEs are the primemover of choice in a variety of applications including distributed power generation, gas transmission, and water pumping (irrigation). Regulatory bodies continue to reduce emissions limits on this class of primemover, requiring development of new technologies for emissions reduction. The type of emission reduction technology deployed in a given situation is closely related to the type of engine used in that situation. Air-Fuel Ratio (AFR) is a key factor influencing engine efficiency, emissions and overall operation. Therefore, an ICE is classified based on the range of AFR within which it is designed to operate: lean-burn engines are optimized to utilize excess air during the combustion process; stoichiometric engines, use chemically balanced measures of air and fuel during combustion; rich-burn engines use (marginally) less air than stoichiometry for combustion. In general, rich-burn engines can operate in a stoichiometric configuration but lean-burn engines are not capable of such flexibility. In the

natural gas industry, rich-burn engines are actually stoichiometric engines [27]. From basic study of combustion chemistry, it is known that the emissions produced during combustion in an excess-oxygen environment are markedly different than those from a fuel-rich environment. Therefore, it follows that the pollutant species, and by extension, the exhaust after-treatment deployed on an engine, is primarily guided by the type of engine being used i.e. lean, stoichiometric, or rich-burn. A common parameter used to monitor and control engine AFR is the real-time equivalence ratio (ϕ), defined as:

$$\phi = \text{AFR}_{\text{stoic}} / \text{AFR}_{\text{act}} , \text{ where}$$

$$\text{AFR}_{\text{stoic}} = \text{mass-based stoichiometric air-fuel ratio}$$

$$\text{AFR}_{\text{act}} = \text{mass-based actual air-fuel ratio.}$$

Figure 3 shows the relationship between concentrations of different exhaust constituents, for varying values of ϕ (known as a ϕ sweep). It can be noticed that engine operation at rich and stoichiometric conditions produces higher amounts of NO_x, CO, and HC as compared to that during lean operation. However, it can also be seen that, for constant values of pressure and temperature in the intake manifold, peak engine power occurs in a region of rich operation. Therefore, for a given application, considerations between engine power versus emissions determine the type of engine that is selected. It is worth noting that since NO_x formation is exponentially linked to in-cylinder temperature [17], the NO_x curve in Figure 3 can also be interpreted as representative of engine temperature across the λ sweep.

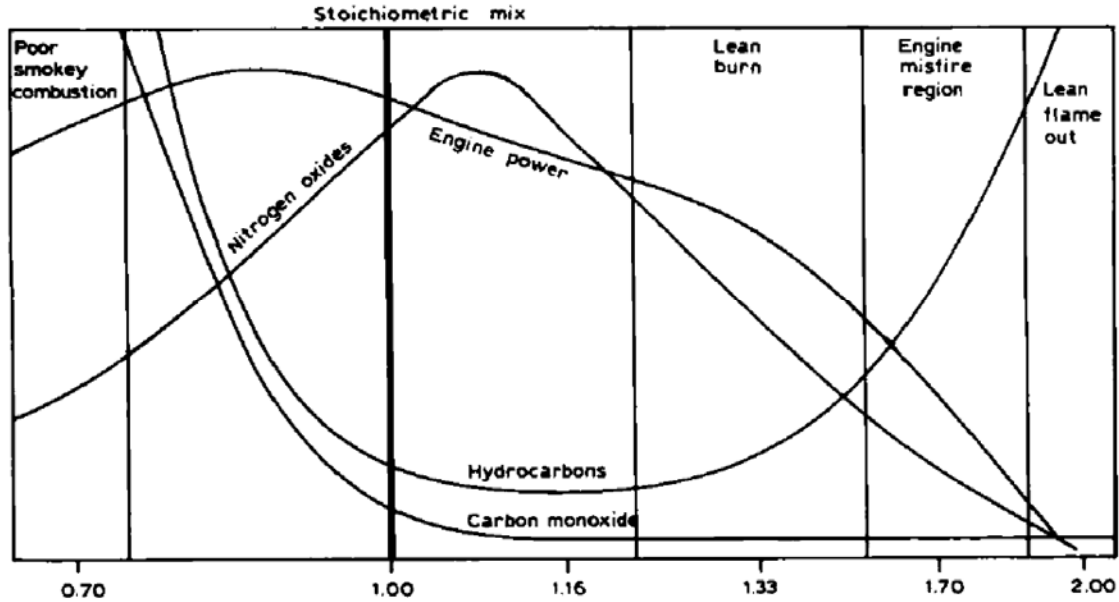


Figure 3: Engine-out emissions of various constituents and engine power output (on y-axis) produced during a λ sweep (on x-axis) [Reprinted from 10].

Using improved component designs, advanced system topology, and sophisticated control techniques, great strides have been made in improving the combustion efficiency of an ICE, leading to very impressive reductions in the emissions footprint of these primemovers. However, ever-tightening air quality regulations require the use of exhaust after-treatment systems to meet these stringent norms.

1.3 Exhaust After-Treatment Systems

Appropriate selection of an exhaust after-treatment system is primarily dependent on the type of engine (CI, SI, lean, rich) and whether it is for a mobile or stationary application. Table 1 provides an overview of commercially available exhaust after-treatment technologies.

1.3.1 Catalytic Considerations

When designing an exhaust after-treatment system, two additional parameters need to be considered if a catalyst is used, namely: Light-off Temperature and Space Velocity.

Since catalysts are designed to operate within a specified temperature range, the light-off temperature of a catalyst, which is the minimum temperature at which reduction efficiency is at least 50%, is critical when designing a catalytic treatment system [27].

Space Velocity is the ratio of the volumetric flow rate of the exhaust gas stream at the inlet of the catalyst housing to the volume of the catalyst bed. It can be calculated either based on standard conditions (STP), referred to as Standard Space Velocity, or actual gas stream temperature and pressure, and referred to as the Actual Space Velocity. It is equivalent to the reciprocal of gas stream residence time in the catalyst-bed and is commonly denoted using units of hr^{-1} . In addition to gas flow rate and reactor volume, cell density of the catalyst substrate (which is a commonly used metric for designating the amount of catalyst material in an element) influences pressure drop across the catalyst element and its space velocity [27].

Long-term durability of catalyst reduction efficiency is influenced by the thermal and chemical environments within which a given catalyst element operates. Degradation due to thermal aging is typically associated with sintering, which causes wash coat destruction, in turn encapsulating active catalyst material, thereby decreasing catalytic activity of the precious metal coat. Chemical aging is brought about two phenomena: fouling and poisoning. The former occurs when particulates in the exhaust stream accumulate within the substrate channels, effectively blocking the channels and restricting the reaction of constituents in the exhaust gas stream at active catalyst sites. The latter is primarily associated with sulphur and phosphorus compounds, originating in the fuel or lubrication oil, that become reactive during combustion and proceed to chemically bond with catalyst precious metals, causing a reduction in the number of active sites available for catalysis [20, 21, 22, 23].

Table 1: Overview of currently available exhaust after-treatment systems [7, 16, 17, 18, 19].

<p>Oxidation Catalyst [17]</p>	<ul style="list-style-type: none"> • Used on SI or CI lean-burn and stoichiometric engines • Oxidizes THC and CO into CO₂ and H₂O, using O₂ available from lean operation. In the case of stoichiometric operation, additional O₂ is introduced to the exhaust stream using an external blower/compressor • Catalyst bed is constructed of noble metals (Platinum and Palladium)
<p>Selective Catalytic Reduction [18]</p>	<ul style="list-style-type: none"> • Designed for operation with CI and SI lean-burn engines • A reagent (urea, NH₃) is injected into the exhaust manifold, upstream of the catalyst, facilitating reduction of NO_x into chemically benign N₂ and H₂O
<p>Lean NOx Traps [16]</p>	<ul style="list-style-type: none"> • Designed to reduce NO_x on lean-burn SI and CI engines • Catalyst bed comprises of materials for oxidation (Platinum), adsorption (Barium), and reduction (Rhodium) • Requires periodic regeneration
<p>Non-Selective Catalytic Reduction [7]</p>	<ul style="list-style-type: none"> • Designed to simultaneously reduce NO_x while oxidizing THC and CO on stoichiometric SI engines • High reduction efficiencies require operation within a narrow range of AFRs, near stoichiometry. Cyclic variation (~1 Hz) of AFR (dithering) widens this operational range • Closed loop control via an O₂ or NO_x sensor is required

	<ul style="list-style-type: none"> • Rich operation produces NH_3 across catalyst • Catalyst bed is constructed of Rhodium and Platinum
Exhaust Gas Recirculation [17]	<ul style="list-style-type: none"> • Designed for reduction of NO_x emissions by recirculating exhaust gases containing inerts into the intake manifold, effectively reducing peak combustion temperature, which is a key factor in NO_x formation.
Thermal Reactors [19]	<ul style="list-style-type: none"> • Designed for operation on rich-burn engines coupled with auxiliary air injection into the exhaust stream • Oxidizes CO and THC, typically in an enlarged exhaust manifold • Efficacy is dependent on temperature, oxygen availability, and residence time in the reactor
Particulate Filters [19]	<ul style="list-style-type: none"> • Designed to reduce particulate emissions from CI engine exhaust stream • Demonstrated removal efficiencies of 60-90% • Filter element, constructed from ceramic in a mat or mesh structure, requires periodic regeneration

1.3.2 Oxidation Catalysts

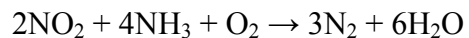
Oxidation catalysts are typically employed on lean-burn engines, such as diesels, to control emissions of HC, CO, and PM. These catalysts, deployed in the exhaust stream, contain precious metals impregnated onto a carrier having a high geometric surface area.

Oxidation catalysts can achieve greater than 98% reduction of CO and over 90% of THC, depending on engine type and fuel. For example, oxidation catalysts are ineffective at reducing CH₄, which is the primary species in THC emissions from natural gas engines. They can also reduce particulate emissions from diesel engines by oxidizing the soluble organic fraction of the particulate – reductions of over 30% have been reported [12] – serving the dual purpose of also eliminating the characteristic odor associated with diesel exhaust (through oxidation of aldehyde and acrolein).

1.3.3 Selective Catalytic Reduction (SCR)

SCR is an effective method for controlling NO_x emissions from lean-burn stationary ICEs and is termed as such because in the presence of a reducing agent, the catalyst selectively reduces NO_x, typically achieving reduction efficiencies greater than 90%. Since its introduction in 1959, this technology has been successfully applied at hundreds of NO_x generating sources worldwide, some of which have been stationary ICEs.

This process reduces NO_x emissions to N₂ in the presence of a reducing agent such as anhydrous NH₃, aqueous NH₃, or aqueous urea [13]. In all cases of practical significance, the chemically active reagent species is NH₃. Lean-burn engines are characterized by an oxygen-rich exhaust, thereby making the reduction of NO_x virtually impossible using NSCR catalyst technology. However, introduction of NH₃ facilitates the necessary chemical reactions [14], as shown below:



1.3.4 Lean NOx Trap (LNT)

Another technology designed for exhaust stream NO_x control from lean burn ICEs is LNT, also referred to as a NO_x storage reduction catalyst. In this process, the first step occurs during lean operation, when NO_x is removed from the exhaust stream and stored (adsorbed) on an alkaline-earth metal oxide bed in the form of nitrites and nitrates. When this storage bed is saturated, a NO_x sensor, installed downstream of the catalyst bed will switch the engine to rich operation (or activate fuel injection into the exhaust stream) in order to generate reductants such as CO, H₂, and HCs, which stimulate NO_x release (desorption) from the storage bed, followed by catalytic reduction to N₂, CO₂, H₂O, and in some cases, NH₃ [15].

1.3.5 Non-Selective Catalytic Reduction (NSCR)

NSCR, or three-way catalytic (TWC) after-treatment is effective at simultaneously reducing NO_x, CO, volatile organic compounds (VOCs), and formaldehyde (CH₂O) emitted from rich-burn natural gas engines. To accomplish this, ϕ must be precisely controlled within a narrow range near stoichiometric conditions, as depicted in Figure 4. Due to this, it cannot operate in conjunction with CI, 2-stroke, or other types of lean-burn ICEs.

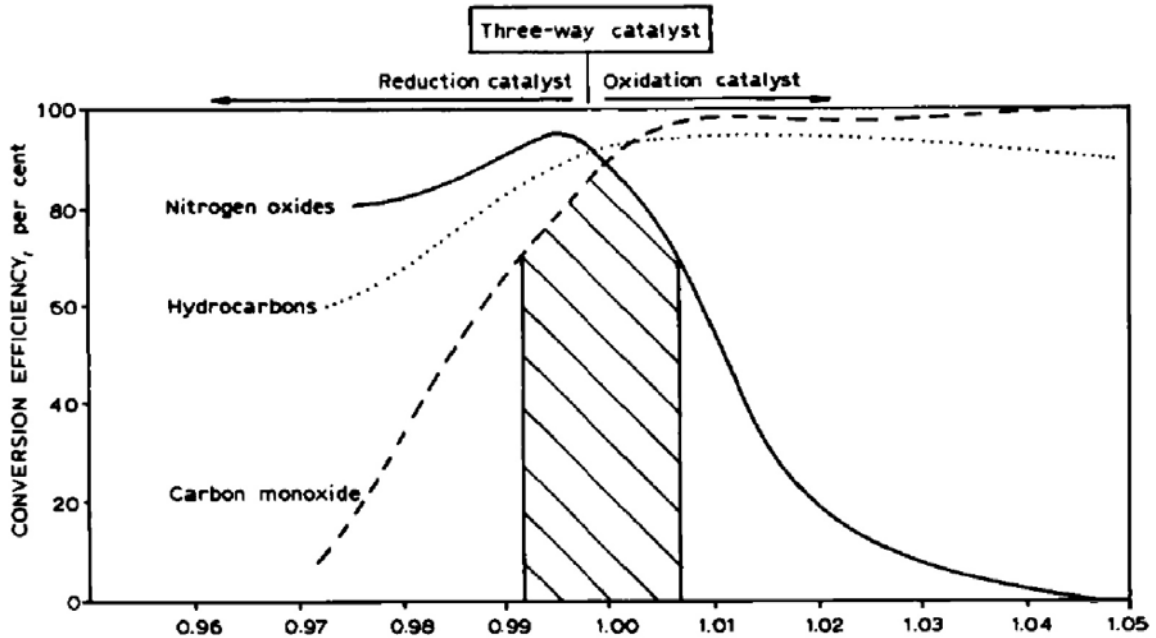


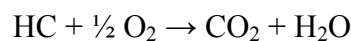
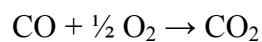
Figure 4: NSCR (or TWC) conversion efficiencies (on y-axis) for various constituents over a range of operational ϕ (on x-axis) [Reprinted from 11].

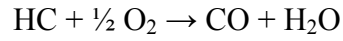
Studies [1, 2] have shown that NSCR after-treatment of exhaust gas streams from natural-gas fueled industrial engines require engine operation within a tightly controlled range of equivalence ratios for effective reduction of NO_x , CO, and non-methane hydrocarbons (NMHCs). It should be noted that conversion efficiency of a catalyst, denoted by η_{catalyst} , is defined as:

$$\eta_{\text{catalyst}} = \frac{(\text{Pre-catalyst Emissions} - \text{Post-catalyst Emissions}) \times 100}{\text{Pre-catalyst Emissions}}$$

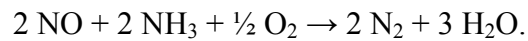
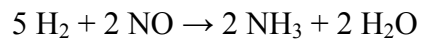
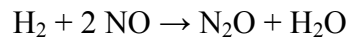
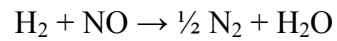
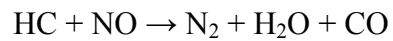
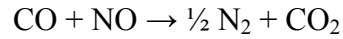
The global chemical reactions that occur within a NSCR catalyst are as follows [7]:

Oxidation reactions (using O_2 as the reagent)

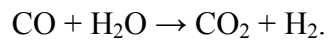




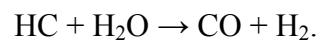
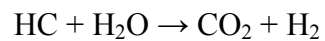
Oxidation and reduction reactions (using NO as reagent)



Water-gas shift reaction

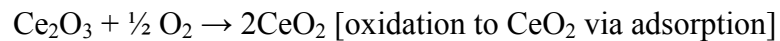


Reforming reactions



DeFoort et al. showed, on a Superior 6G-825 industrial natural gas engine, that the equivalence ratio range from 1.015 to 1.020, representing a ϕ control range of $\pm 0.5\%$, produced a catalyst reduction efficiency of 90% for NO_x and CO. In field operations however, it is challenging to consistently achieve a ϕ control range of $\pm 0.5\%$ over an extended duration, owing primarily to drift in the output signal from the oxygen sensor. Also, it should be noted that there is an inverse relationship between the ϕ control window and the magnitude of reduction efficiency being sought. Other parameters that impact the ϕ control window and maximum achievable catalyst efficiency are (i) space velocity, which is inversely proportional to the volume of NSCR catalyst used and (ii) catalyst operating temperature. It has been shown by Amadu et al. that lower space velocity and higher catalyst temperature widens the ϕ compliance window of an NSCR catalyst.

The work by DeFoort et al. also examines the benefits of equivalence ratio dithering. Dithering has been shown to widen the control window of a catalyst, effectively increasing the equivalence ratio range of operation. DeFoort et al. found that a 1% variation in equivalence ratio at 0.2 Hz (dithering) widened, by approximately 20%, the catalyst window for 80% reduction efficiency. This phenomenon can be ascribed to the oxygen storage capacity of a catalyst, which regulates the available O₂ present on the catalyst bed. A common material used for this application is ceria (CeO₂), owing to its excellent oxygen adsorption and desorption properties, explained by the following reactions [4]:



The ability of AFR control systems to consistently maintain engine equivalence ratio in the required narrow operating range over the long-term, under field conditions has not been

established. Another study [3] which sought to better understand the limitations of current commercially available AFR control systems for rich-burn engines with NSCR catalysts concluded that the AFR controller evaluated during that study exhibited poor control for NSCR operation, owing primarily to drift in oxygen sensor calibration.

In response to these issues faced by the natural gas industry, Woodward, Inc. developed and commercialized a new Heated Exhaust Gas Oxygen (HEGO) sensor (commercially referred to as StableSense™), tailored for the rigors of industrial gas engine applications. Compared against automotive-grade O₂ sensors that were traditionally used on AFR control systems for industrial gas engines, the StableSense™ HEGOs exhibited drastic reductions in signal drift, even when operated in environments containing unburned CH₄ and H₂ [4]. Signal response of the StableSense™ HEGO sensor is similar to that of the upstream sensor described in the work by Mizutani et al. The primary difference between HEGO sensors for automotive applications versus the StableSense™ HEGO for industrial gas engines is that the design for the latter application utilizes special sensor packaging features that accommodate the operational requirements of high vibration and near-100% duty cycle [6].

Coupling this advanced sensor capability with 32-bit microprocessor functionality, a very robust control architecture was developed that enabled optimal NSCR operation. This control system, commercialized by Woodward, Inc. is known as the E3 Rich-Bun Air-Fuel Ratio Control with StableSense™. In this report, it is referred to as the E3RB. It should be noted that the E3RB must utilize StableSense™ HEGOs; alternate types or brands of HEGO sensors are not acceptable substitutes in the E3RB system.

Following on the heels of very recent work [4], this thesis elucidates on the results of a long-term study (6-months) conducted on the E3RB AFR control system. In particular, this

project was intended to evaluate performance of the E3RB while maintaining optimal NSCR operation and durability of StableSense™ HEGOs over a wide range of ambient and engine load conditions. Existing literature does not contain performance data on the E3RB or the StableSense™ HEGO sensors.

2. Site Overview

This field study was conducted on a Waukesha VHF-series L7044GSI engine, sited at Encana Corporation's Frenchie Draw operation, in Wyoming's Wind River Basin, located 6,000 feet above sea level. This engine, deployed at a compressor station, powers a gas compressor for a gas gathering application (Figure 5, Figure 6, Figure 7, and Figure 8).



Figure 5: Compressor station external view, with engine room (in foreground) and exhaust stack/tailpipe on elevated catwalk (in background)

The Waukesha L7044GSI, designed for operation at a stoichiometric AFR, is categorized as a rich-burn engine. The engine design utilizes a cross-turbo configuration, which flows exhaust gases from the right cylinder bank into the left turbocharger and vice versa. Complete engine specifications are provided in Appendix A. The compressor coupled to this engine is manufactured by Ariel and is a 4-cylinder, 4-throw model having a maximum allowable working pressure of 1500 psig.

The air quality permit issued for this site allows up to 0.7g/bhp-hr of CO and NOx brake-specific emissions from this engine at a nominal speed and load condition of 1150 RPM and 1480 bhp, respectively. This nominal speed/load engine operating point will, in later sections, be referred to as High Speed/High Load (HS/HL) condition. In order to meet these regulatory limits, an NSCR exhaust after-treatment system is deployed.

The NSCR catalyst elements used on this engine are manufactured by Emit, with physical dimensions of $\Phi 33.5'' \times 3.5''$ thickness (Figure 9). Two such elements, placed back-to-back, providing a total space velocity of $\sim 141,000 \text{ hr}^{-1}$, were deployed to obtain adequate engine-out exhaust after-treatment (Figure 10). The Space Velocity was calculated at an engine operating load of 1480 bhp.

The AFR controller under evaluation at this site (the E3RB) can control speed/load, AFR, and ignition timing, for a wide variety of rich-burn gas-engines in many different applications. It can be deployed on carbureted four-stroke, mono-bank (or stereo-bank), naturally aspirated (or turbo-charged engines) over a wide band of power outputs.

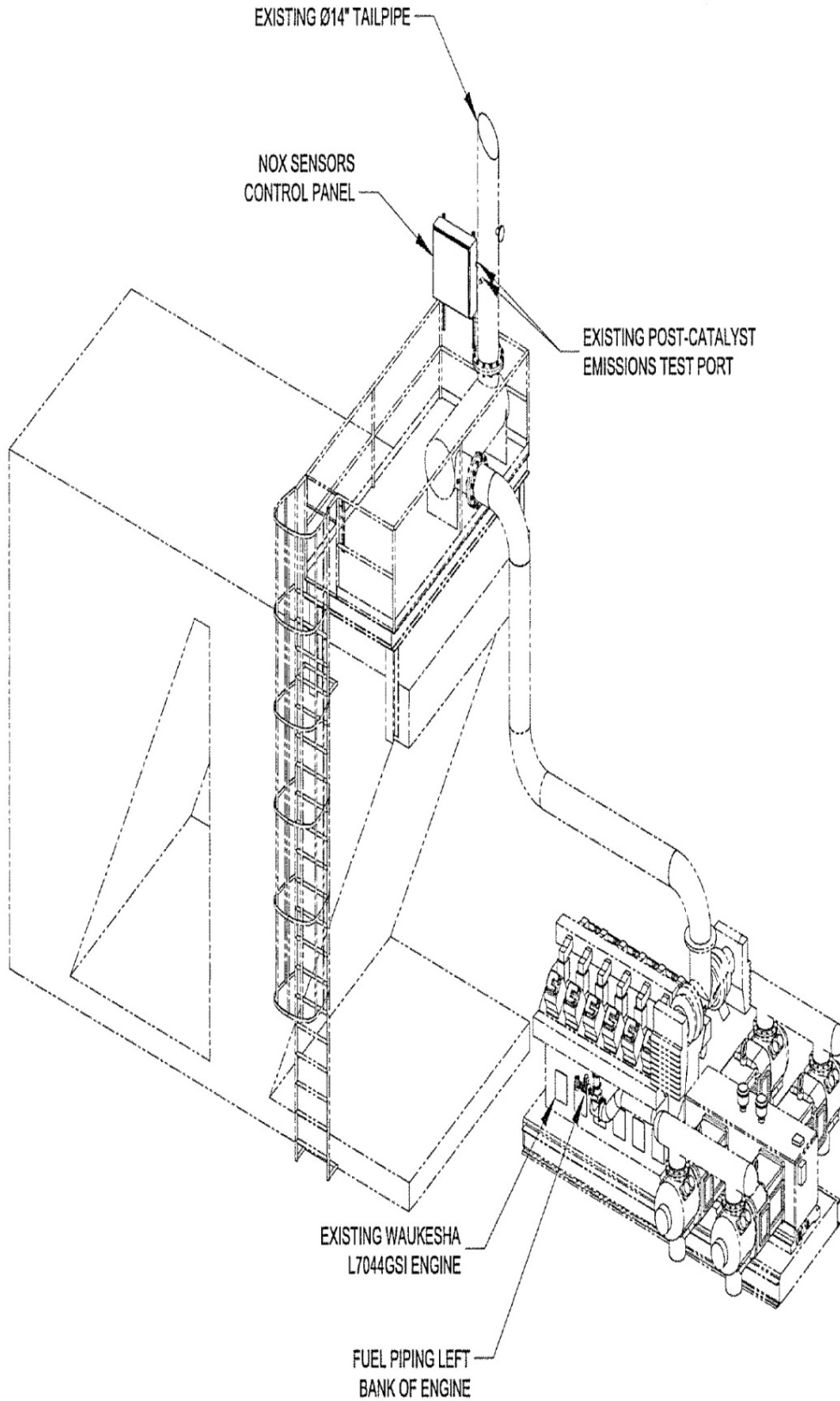


Figure 6: Schematic of compressor station layout, comprising engine, compressor, piping from exhaust manifold to catalyst housing, and stack. The catwalk is mounted atop the cooling fan housing structure

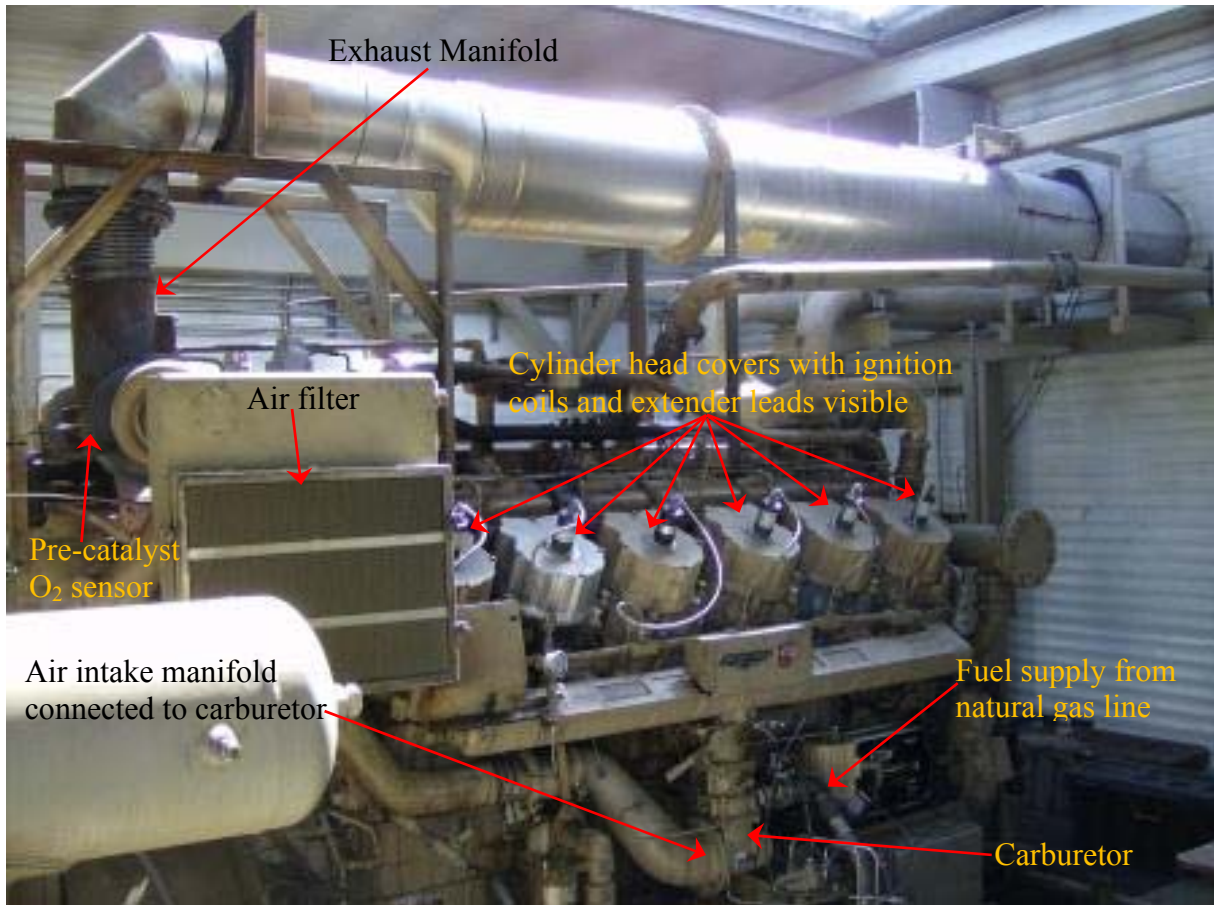


Figure 7: Profile view of the Waukesha L7044GSI engine inside the compressor station with left bank components labeled.

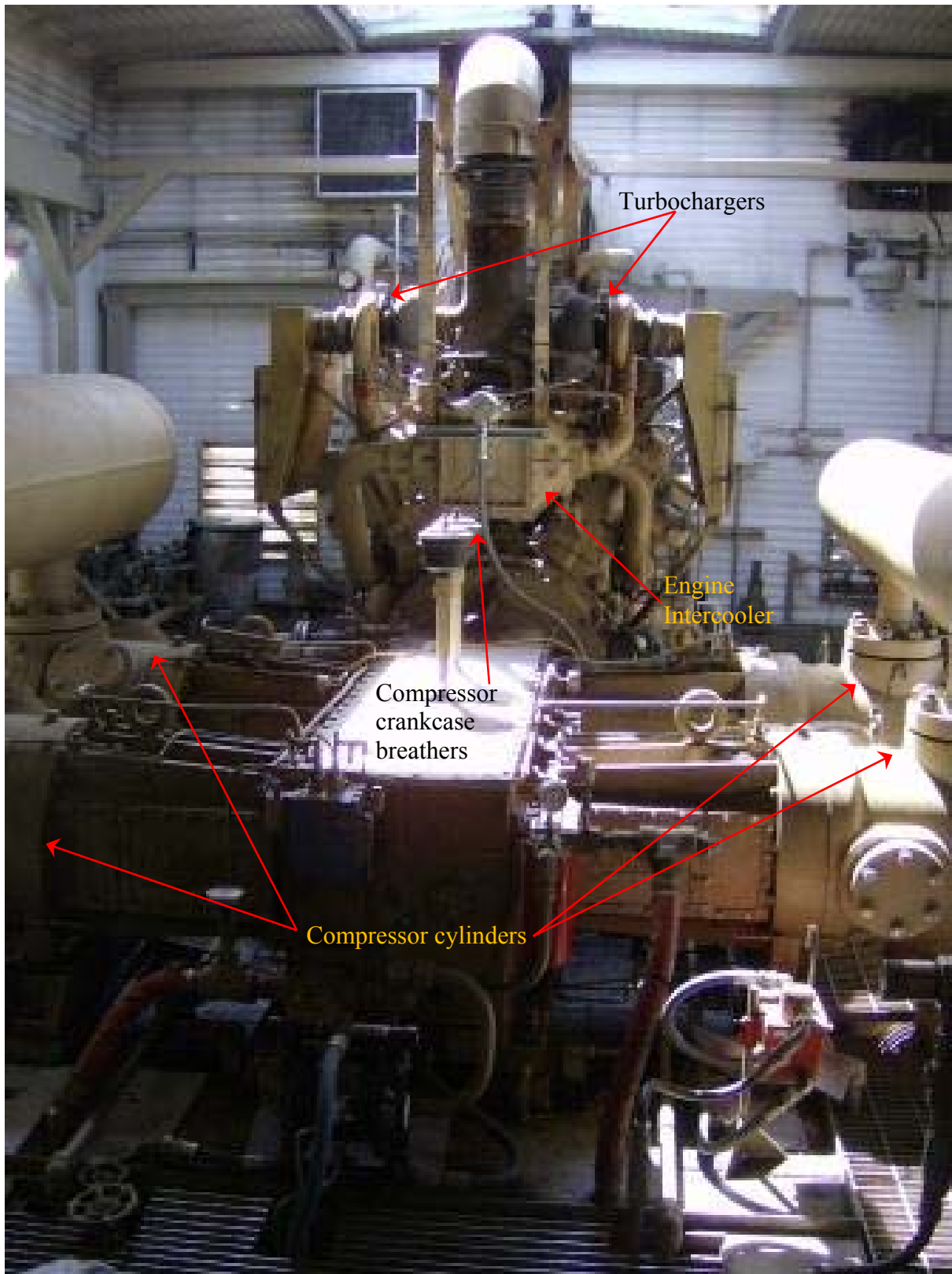


Figure 8: Gas compressor (in foreground) coupled to the engine (in background)



Figure 9: Lagging catalyst element (with ash on front face) being removed from the housing for cleaning.



Figure 10: Emit elements in the catalyst housing (leading element is on the right), with thermal-wrap around the frame for proper sealing. Direction of exhaust gas flow is from right to left.

2.1 Control Architecture

The E3RB was installed at this site (Figure 11) per guidelines obtained from Dresser-Rand Engineering and Woodward, Inc.; personnel from both these organizations participated in the installation process. A schematic of the sensors required to facilitate E3RB operation is shown in Figure 12; complete installation specifications for this site are provided in Appendix F. An overview of the E3RB's control architecture is provided below [8].

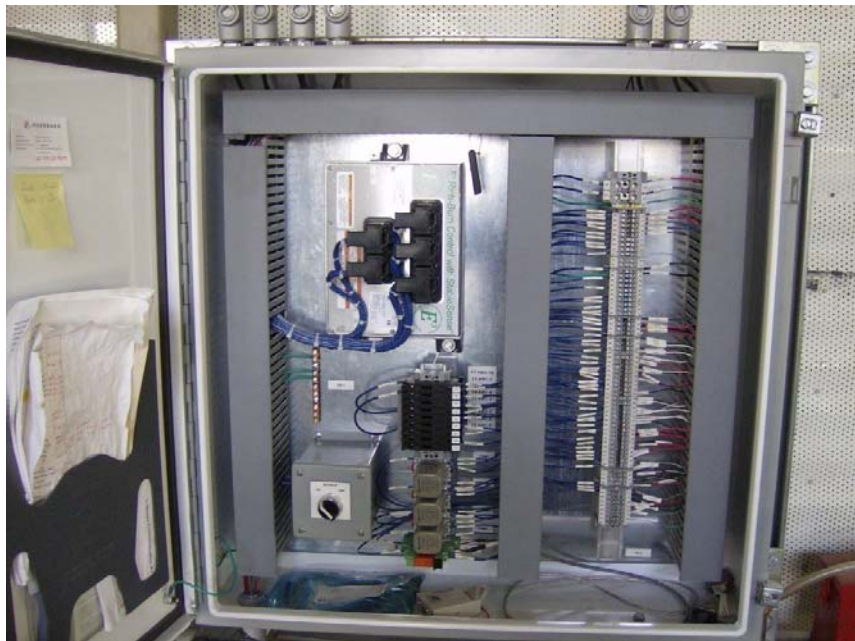


Figure 11: The E3RB control module installed inside the compressor station at the test site.

The E3RB is a microprocessor-based control for carbureted, four-stroke, gaseous-fueled engines operating at a near-stoichiometric AFR. It is designed to work in conjunction with a NSCR catalyst – one that simultaneously eliminates hydrocarbons (HC), carbon monoxide (CO), and oxides of nitrogen (NO_x) – to effectively treat exhaust emissions from rich-burn engines.

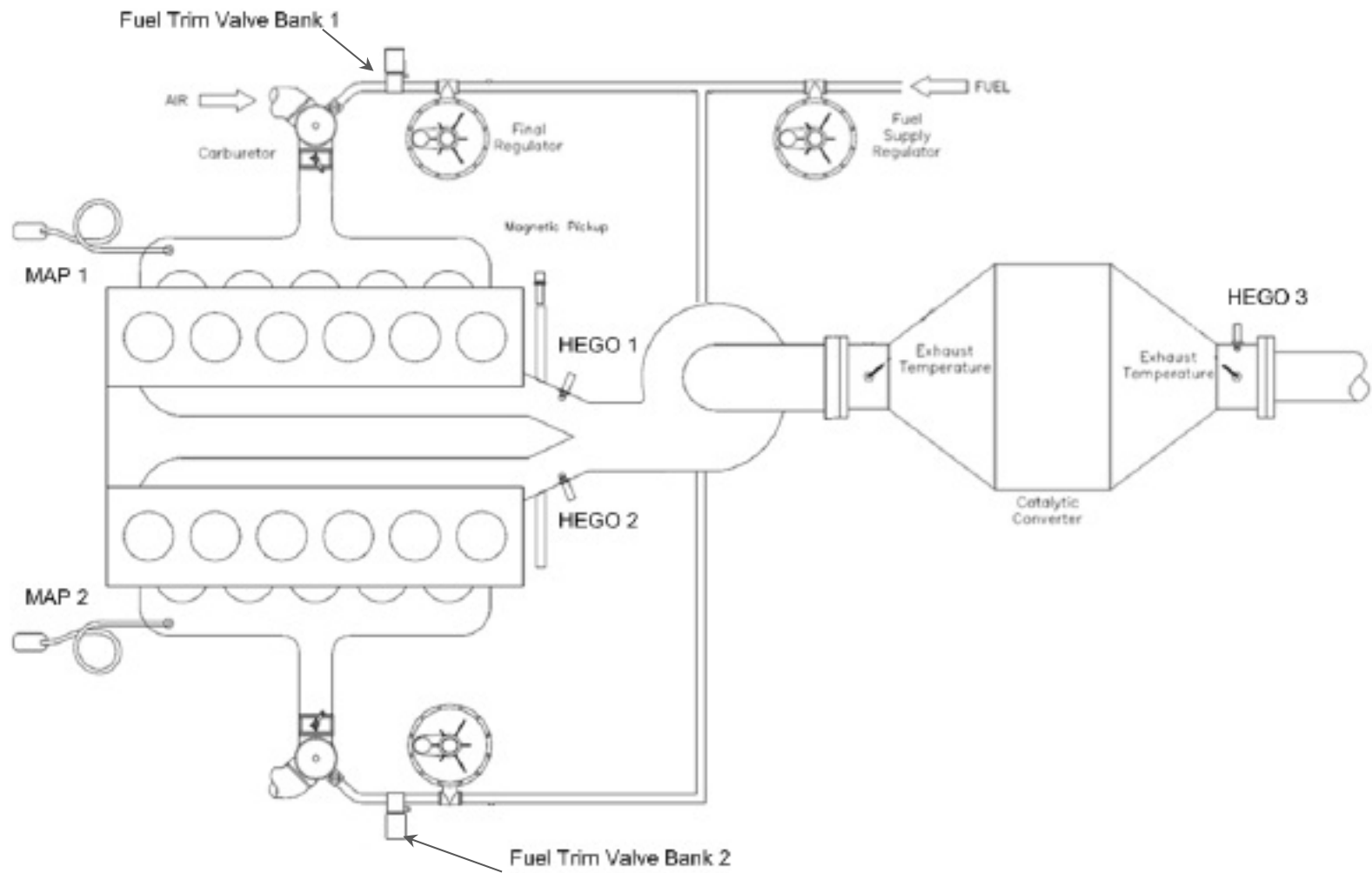


Figure 12: Layout of sensors and actuators for E3RB operation of a dual-bank engine (stereo control) [8].

By continuously adjusting for optimal air/fuel mixtures, emissions compliance can be achieved while simultaneously maximizing catalyst life and minimizing supervisory oversight by operations staff. For optimal performance and to protect the catalyst element from premature aging or damage, precise control is required of the AFR window of operation. When an engine consistently operates within this control window, optimal exhaust after-treatment can be achieved.

In the E3RB, the StableSense™ HEGO sensors generate a voltage signal that is characteristic of this ideal control window, with the controller utilizing this voltage value to keep the engine at the desired air/fuel ratio. It should again be noted that the E3RB must utilize StableSense™ HEGOs – alternate brands are not acceptable substitutes for the E3RB system. Optimized for Full-Flow Trim operation, the carburetor remains in place on the engine, the base AFR is adjusted slightly rich, and the trim valve restricts fuel flow to the carburetor so as to adjust the air/fuel mixture to the precise value that will maximize catalyst efficiency. The given engine being a dual bank design, optimal inlet conditions to the NSCR catalyst are maintained by way of stereo control, which uses two pre-catalyst HEGO sensors (one in each bank) for closed loop, exhaust oxygen feedback control and one post-catalyst HEGO sensor for post-catalyst, exhaust oxygen cascade feedback control (Figure 13). Fluctuations in engine load are managed by varying the post-catalyst HEGO sensor's base setpoint value, as tabulated in the post-catalyst setpoint table. The operational range of the feedback algorithm and HEGO sensors cover a wide spectrum of gas compositions, including LPG, pipeline natural gas, and coal-bed gas. In addition, the algorithm incorporates fuel valve dithering in order to maximize flexibility of catalyst operation. Changes in gas quality and the ambient environment during normal engine operation are compensated by post-catalyst closed loop HEGO control. In the event of a critical oxygen

sensor malfunction, the control reverts to an open loop strategy, during which time the valve position is determined using pre-assigned values from an open loop table. The fuel metering subsystem consists of a carburetor combined with an in-line fuel trim valve. Additional details follow on control terminology used in the above overview.

Stereo Control

Stereo AFR control systems are used on dual bank engines and utilize two Pre-Cat HEGO sensors (one on each bank) and two Fuel Trim Valves (one on each bank). Stereo control poses more challenges owing to twice the number of components deployed but does present the opportunity to improve the catalyst efficiency by dithering the AFR in each bank to be out of phase with each other, thereby simultaneously providing the NSCR catalyst with exhaust gas constituents required for both oxidation and reduction reactions.

Pre-Catalyst Exhaust Oxygen Control

Primary AFR control is achieved using the pre-catalyst oxygen sensors, via the Fuel Trim Valves, which increase or decrease fuel flow to the engine, so as to hold the average voltage signal of the pre-catalyst sensors at a preset target.

Post-Catalyst Exhaust Oxygen Control

As ambient conditions vary and the catalyst element ages, optimal catalyst performance is assured by means of a “Cascade” control loop that uses feedback from a second oxygen sensor in the exhaust, downstream of the catalyst element. This post-catalyst control loop adjusts the primary pre-catalyst control setpoint to changes in fuel composition, catalyst efficiency, and environmental conditions that are detected in the post-catalyst oxygen concentration.

Post-Catalyst Setpoint Table

The Post-Catalyst Setpoint Base value may vary several millivolts from engine to engine, catalyst to catalyst, and load to load. Additionally, as some engines operate with varying loads, optimum catalyst performance is obtained by adjusting the Post-Catalyst Setpoint. During initial tuning and system commissioning activities, the required setpoints are entered into the Post-Catalyst Setpoint table so that the pre-catalyst setpoint target can be changed at different loads to ensure compliance throughout the engine load range. The E3RB tracks engine load by monitoring engine speed, intake manifold pressures, and temperatures (MAP and MAT, respectively). Combining these parameters with an assumed volumetric efficiency (which varies as a function of speed), an approximate engine charge flow (Q_{mix}) is calculated and used as the indicator of engine load. The load range of the engine is divided into eight segments and a Post-Catalyst Setpoint value can be manually assigned for each of these levels.

Fuel Valve Dithering

As discussed earlier, dithering the AFR into the engine enhances catalyst performance. The E3RB system includes parameters to adjust the dither amplitude and frequency so as to optimize the oxygen storage capacity of the catalyst. This strategy widens the window of operation and permits greater drift tolerance whilst maintaining acceptable reduction efficiencies.

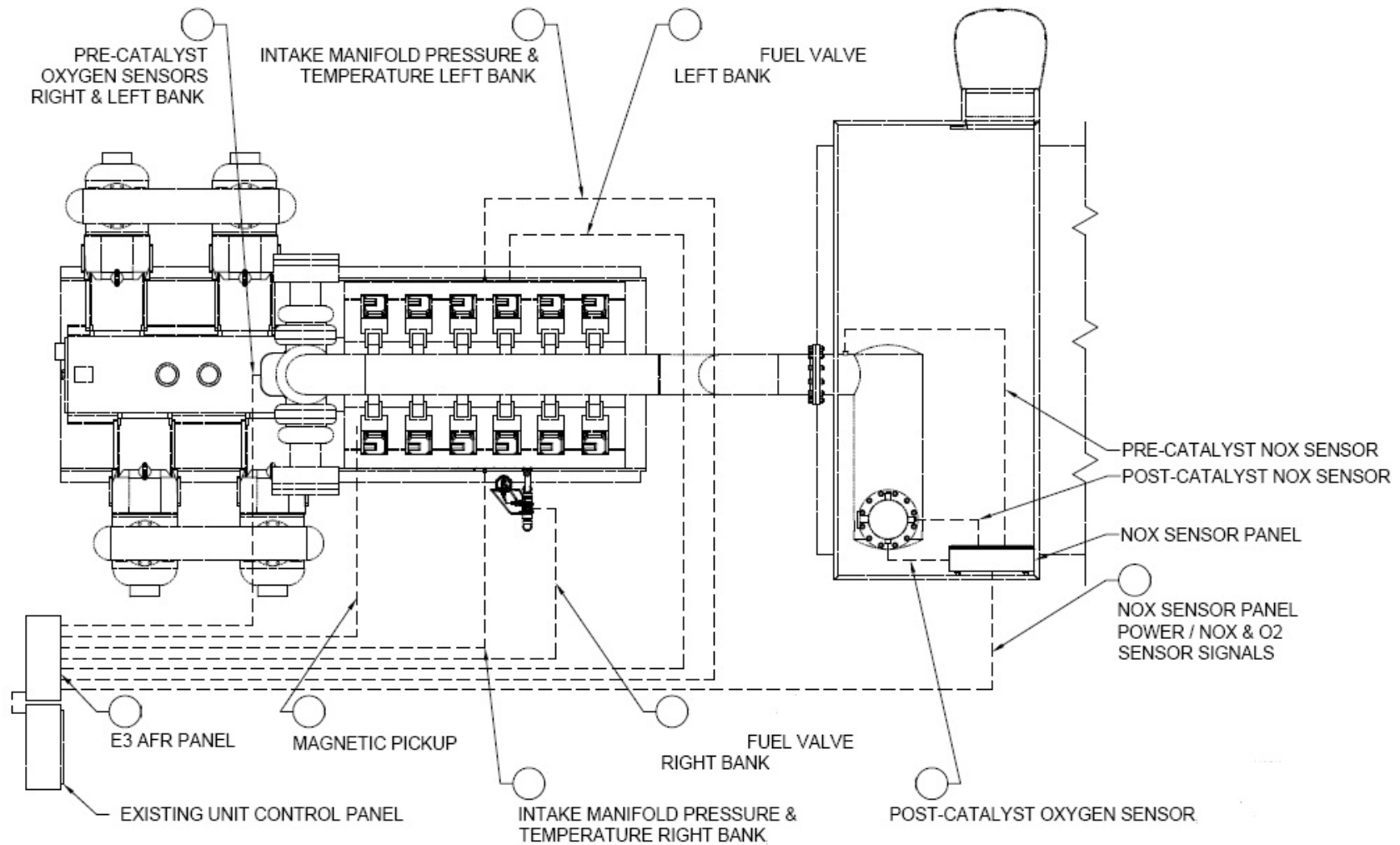


Figure 13: Schematic of valves and sensors installed on the field engine to facilitate E3RB operation. NO_x sensors, coupled to onsite SCADA, provided remote emissions monitoring capability (not required by the E3RB system).

Open Loop Control Mode

The open loop mode will control the coarse air/fuel ratio of the engine without the closed loop pre and post-catalyst sensor measurement; it is less accurate than the closed loop mode but is more accurate than using a stand-alone carburetor. This mode draws from the Open Loop Table, which correlates Fuel Trim Valve Position to the engine load parameter, Q_{mix} . This table contains valve operating positions for eight (8) load points over the engine's entire load range; valve position for other load points are determined by interpolation. If either of the pre-catalyst sensors fail, the control automatically defaults to the open loop mode using values from this table that were manually entered during initial control calibration.

2.2 Emissions Sampling System

The emissions sampling system at this site comprised the following arrangement:

1. Pre and post-catalyst sampling probes for $\Phi 14''$ exhaust pipe, prepared using guidelines in EPA Method 1.
2. Filter (for particulates in the exhaust gas stream)
3. 3-way valve (to allow switching between pre and post-catalyst samples)
4. Heated sample line, maintained at 220°F , using a temperature controller
5. Heated head sample pump
6. Portable emissions analyzer

The above listed items are shown in Figure 14, Figure 15, Figure 16, Figure 17, and Figure 18. All the lines connecting sample probes to the filter were wrapped in exhaust header tape to minimize heat dissipation; these lines were also routed in close proximity to the catalyst housing, providing a localized elevated-temperature environment. Both these measures

prevented water condensation in the lines, thereby eliminating any reduction in output levels of emission species by way of aqueous phase absorption.

An alternate setup, shown in Figure 18 (right), was also used to draw exhaust into the analyzer. In this arrangement, the exhaust gas stream was drawn through the heated sample line directly into the analyzer using the analyzer's internal pump, bypassing the heated head pump. Utilization of this setup did not alter the flow rate of exhaust gas into the analyzer and was the preferred configuration for emissions sampling.

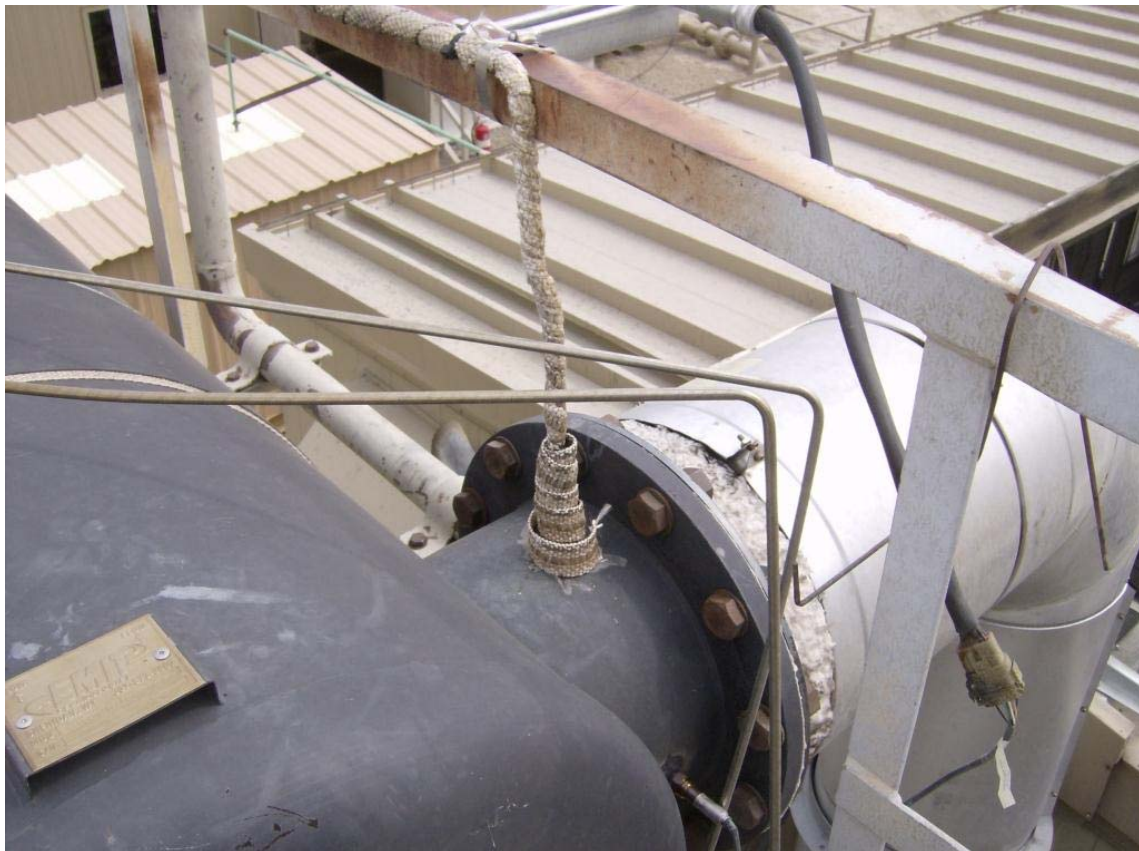


Figure 14: Pre-catalyst emissions sampling probe in exhaust manifold.



Figure 15: Post-catalyst emissions sampling probe in exhaust manifold.

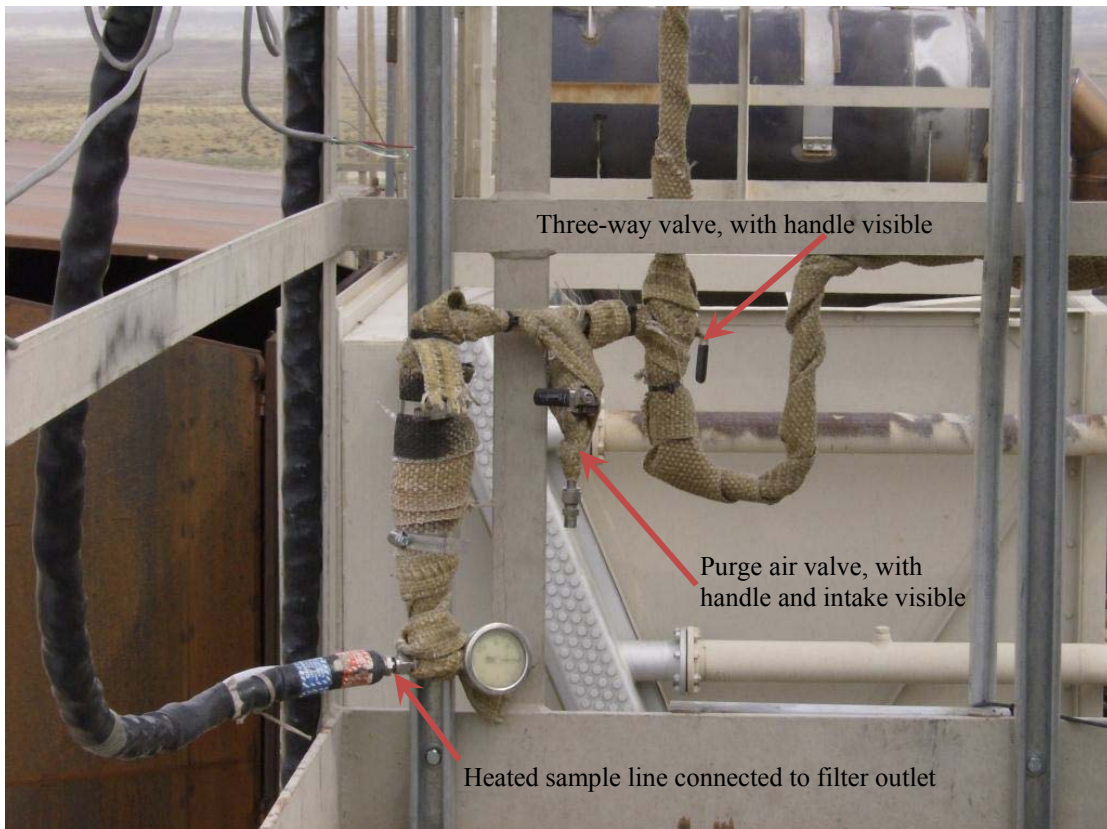


Figure 16: Heated sample line (bottom left) connected to filter outlet, shrouded in thermal wrap. Handle of three-way valve is on the far right, with handle of purge air valve visible in the middle.



Figure 17: Heated sample line is routed from the sampling port on the elevated catwalk (left), through a ground level window in the engine room (middle), to the inlet of the heated head pump (right).



Figure 18: (Left) Portable emissions analyzer setup inside the engine room. (Right) Alternate arrangement for exhaust sampling: heated sample line (hanging in foreground) ready for direct connection to the sampling port on the analyzer.

2.2.1 Portable Emissions Analyzer

The portable emissions analyzer used during field site visits was donated by ECOM America, model J2KN-IND. Among its many features, this model has an internal pump with bypass plumbing for fresh air purge, a thermo-electric gas cooler and moisture trap with automatic moisture dump, wireless handheld remote control with Bluetooth™ radio connectivity to a laptop or workstation, an on-board flowmeter, and automatic switch over between high and

low-range CO sensors. The unit used for the field test was fitted with sensors for measurement of CO (low range), CO (high range), NO, NO₂, and CH₄. Sensor resolution and measurement accuracies are shown in Table 2.

Table 2: Specifications of sensors fitted on ECOM J2KN portable emissions analyzer

Species	Range	Resolution	Accuracy	Sensor Type
O ₂	0 – 21 %	0.1% vol.	± 2% measured	Electrochemical
CO (low)	0 – 4000 ppm	1 ppm	± 2% measured	Electrochemical
CO (high)	0 – 40,000 ppm	1 ppm	± 2% measured	Electrochemical
NO	0 – 4000 ppm	1 ppm	± 2% measured	Electrochemical
NO ₂	0 – 500 ppm	1 ppm	± 2% measured	Electrochemical
CH ₄	0 – 30,000 ppm	10 ppm	± 5% measured	Infra-Red
CO ₂	0 – max. of fuel	N.A.	N.A.	Calculated

As the primary species of interest for this study were CO and NO, these were the calibration gases acquired for this field test. Prior to the start of emissions monitoring on each test day, the ECOM analyzer was calibrated using the gases listed in Table 3. At the end of the test day, a calibration check was conducted to quantify the sensor drift that occurred over the course of the day. For this field study, the established limit for sensor drift was ± 5% of the calibration standard. If, over the course of a test, the sensor temperature drifted beyond 10°F from the temperature at which initial calibration was performed, the analyzer was recalibrated at

the new sensor temperature. Details of calibrations conducted during each test day are provided in Appendix B.

Table 3: Calibration gases used for the portable emissions analyzer during field site visits

Species	Cal gas conc.	Grade/Accuracy	Expiration
O ₂	Ambient (21%)	N.A.	N.A.
CO (low)	401 ppm	Certif. Master Class	28-Nov-2013
CO (high)	6891 ppm	± 2%	20-Aug-2013
NO	201 ppm	Certif. Master Class	28-Nov-2013

When using this portable analyzer in continuous mode, it was necessary to purge the cells with air between measurements to prevent cell poisoning and drift. A 50% duty cycle (15 minute measurement cycle; 15 minute purge cycle) was used to maintain measurement quality. During periods between site visits, engine operation was monitored remotely using SCADA data from existing compressor station instrumentation (Figure 19 and Figure 20). Emissions trends were similarly developed using SCADA information from CSU-installed pre and post-catalyst NO_x sensors (Figure 21 and Figure 22). The output range of these NO_x sensors is from 0 – 5V and the scale applied to the voltage output was as follows:

Pre-catalyst: 0V = 0 ppm ; 5V = 5000 ppm

Post-catalyst: 0V = -50 ppm ; 5V = 200 ppm



Figure 19: Screenshot of SCADA page for Engine Data

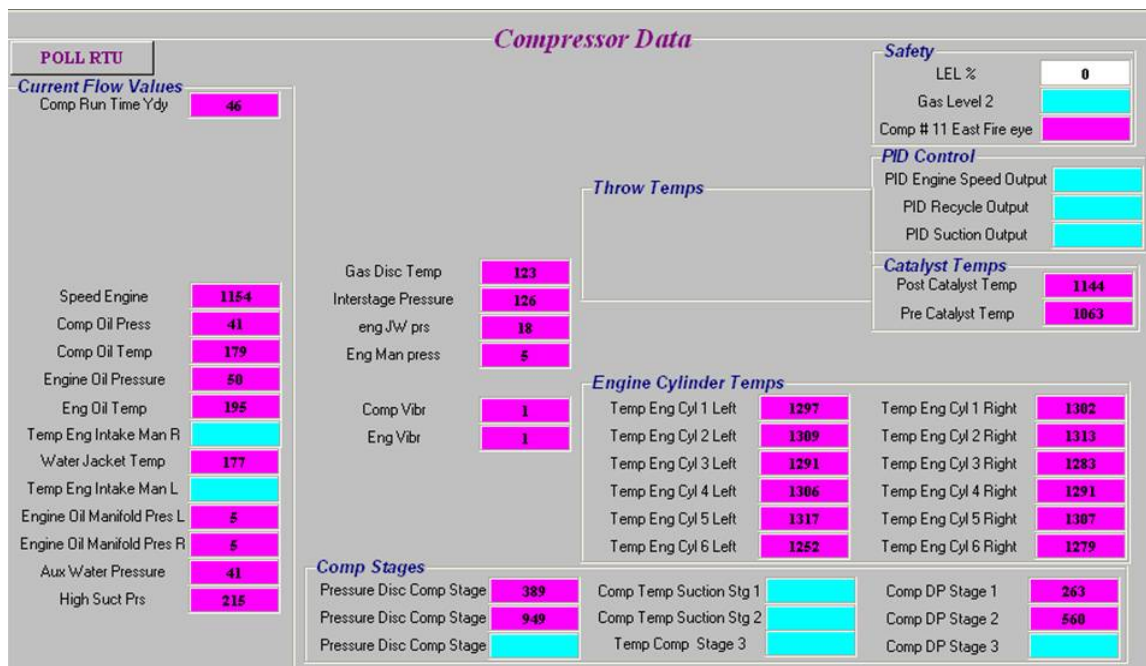


Figure 20: Screenshot of SCADA page for Compressor Data

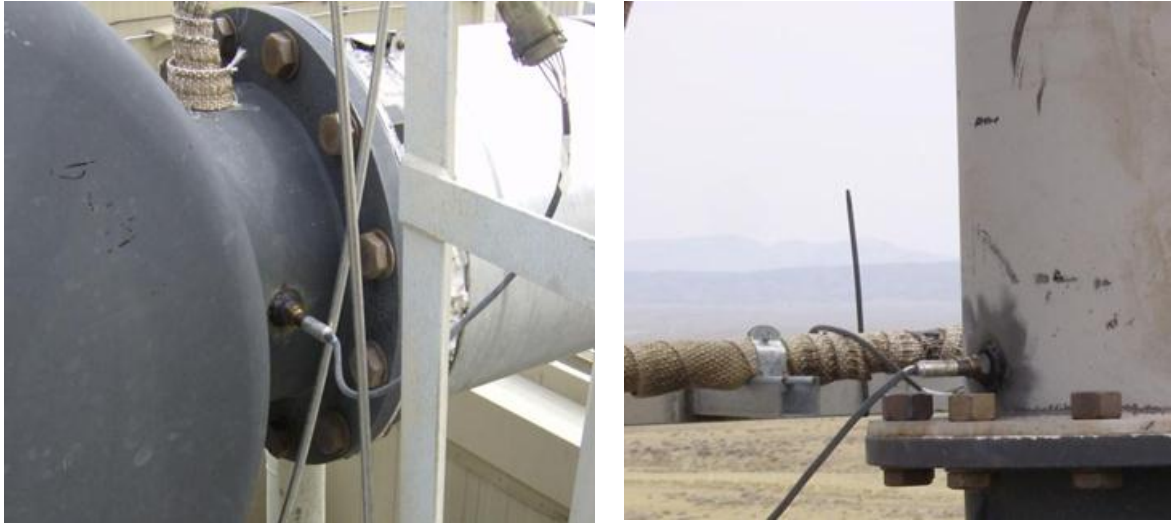


Figure 21: (Left) Pre-catalyst NOx sensor. (Right) Post-catalyst NOx sensor.



Figure 22: NOx sensor control module installed inside sealed enclosure on elevated catwalk.

2.2.2 Portable Gas Chromatograph

A portable gas chromatograph (GC) was used to characterize fuel gas variations at the field site over a 24 hour period. The model used was the Varian CP-4900 Micro GC (Figure 23). This instrument has built-in Micro Electronic Gas Control regulators that can be adjusted to obtain constant or programmed pressure control, resulting in constant or programmed flow through the injector, column and detector. When a run is initiated, a gas sample is drawn through a sample loop inside the injector, using an onboard vacuum pump, and is then injected into the carrier gas stream. A typical injection time is 40 milliseconds (ms), which corresponds to an injection volume of 200 nL.

This model is also equipped with a Thermal Conductivity Detector (TCD) and a Differential Mobility Detector (DMD). The former responds to differences in thermal conductivity between the carrier gas and the gas sample constituents while the latter deploys an advanced form of Ion Mobility Spectroscopy (IMS).

CSU's GC is configured for use with Helium (He) as a carrier gas, having a minimum purity of 99.995% and limited to 80 ± 2 psi on the main gas supply.

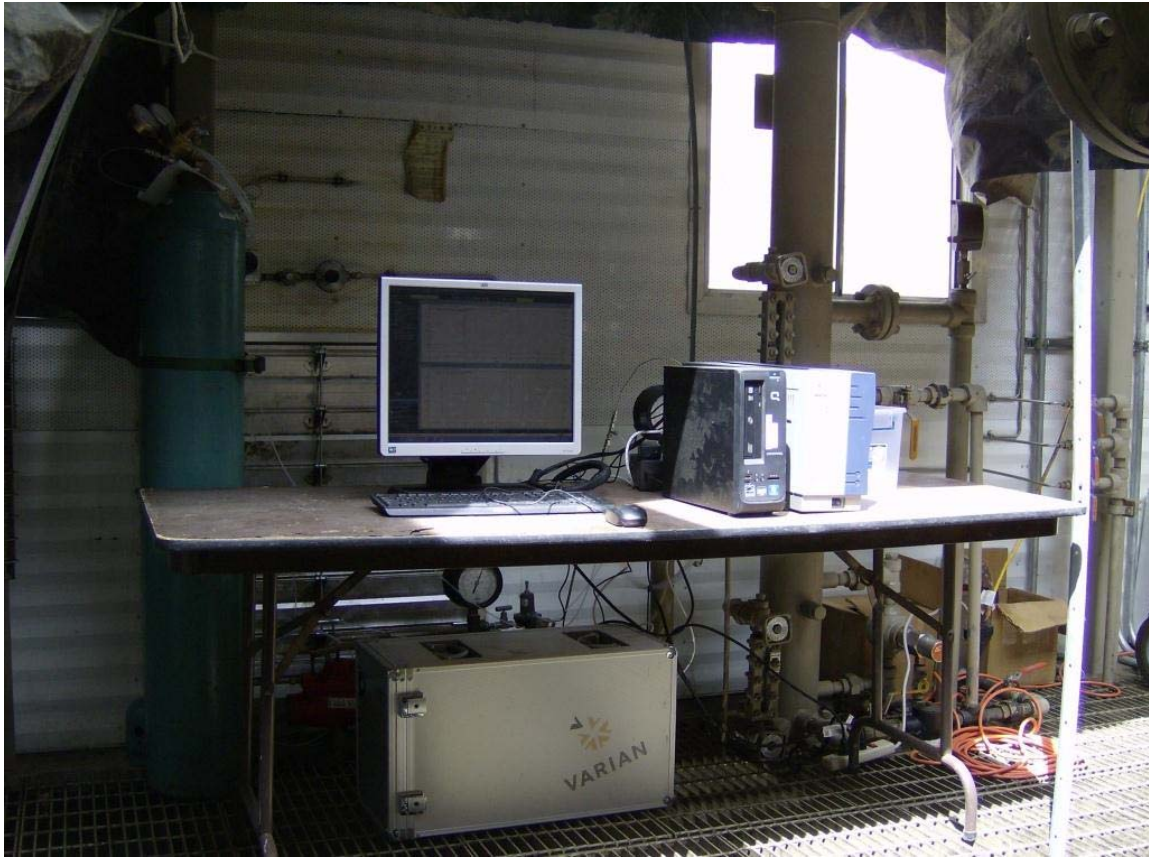


Figure 23: Portable fuel gas chromatograph station inside the engine room.

2.3 Project Timeline and Milestones

July 2011 – Site visit to Frenchie Draw (WY), hosted by Justin Lisowski (Encana). Visitors: Daniel Olsen, Chris Hagen (CSU) ; Chris DeFoor (Woodward) ; Earl Glover (Dresser-Rand Enginuity).

September 26, 2011: E3RB control box delivered to Encana office in Riverton, WY.

November 7 – 13, 2011: Installation of E3RB, followed by first commissioning attempt. Tuning could not be completed owing to wastegate malfunction therefore, commissioning was postponed. Engine hours on November 13 = 45,292.

January 2 – 4, 2012: Second commissioning attempt. Tuning could not be completed owing to exhaust leaks therefore, commissioning was postponed.

February 13 – 20, 2012: Third commissioning attempt. Single EmeraChem catalyst element deemed as insufficient for adequate NSCR exhaust after-treatment. Therefore, two (2) new Emit NSCR elements were installed in catalyst housing. Fuel pressure oscillations (120↔140 psig over 30 second intervals) were noticed in main supply line, owing to malfunctioning motor valve in liquids drop-out shed. This was corrected by over-pressurizing the fuel supply line to this engine, causing the pressure relief valve to remain open. In this way, a constant pressure of ~140 psig was maintained in the fuel supply line to this engine. All tuning was conducted at fuel pressure of ~140 psig.

February 20, 2012: Tuning and commissioning completed; handover to CSU for monitoring and performance evaluation. No further tuning was performed on the E3RB after system commissioning and handover. Engine hours = 47,434.

February 26 – 28, 2012: Monitoring visit # 1.

February 27, 2012: To overcome erratic engine behavior brought on by fuel pressure fluctuations, the fuel supply line was over-pressurized beyond the cracking pressure of the relief valve. This stabilized fuel pressure to the engine. All emissions data was collected at a constant fuel pressure of ~ 140 psig. Catalyst elements WERE NOT blown out with compressed air prior to evaluating controller performance and collecting emissions data.

March 11 – 13, 2012: Monitoring visit # 2.

March 13, 2012: Catalyst elements were blown out with compressed air prior to evaluating controller performance and collecting emissions data. Fuel pressure fluctuations were rectified – constant fuel pressure of ~140 psig has been restored to main fuel supply line.

April 1 – 3, 2012: Monitoring visit # 3.

April 2, 2012: Catalyst elements were blown out with compressed air prior to evaluating controller performance and collecting emissions data.

May 13 – 16, 2012: Monitoring visit # 4.

May 14, 2012: Catalyst elements were blown out with compressed air prior to evaluating controller performance and collecting emissions data.

May 16, 2012: New spark plugs installed in the engine.

May 30, 2012: Emit elements (2) removed from catalyst housing for washing. Interim NSCR exhaust after-treatment provided by EmeraChem single element.

June 24 – 27, 2012: Monitoring visit # 5.

June 25, 2012: Prior to emissions monitoring on this engine, the following maintenance was conducted: (a) Existing HEGO sensors on E3RB system were replaced with new HEGOs – the new sensors were identical models as those replaced. The old HEGOs, having ~5138 hours of run-time, were returned to Woodward for analysis. (b) The EmeraChem single catalyst element installed on May 30, 2012 was removed from the housing and two (2) freshly washed Emit catalyst elements were reinstalled.

July 18 – August 9, 2012: Engine offline owing to compressor main bearing failure.

August 19 – 24, 2012: Monitoring visit # 6.

August 20, 2012: Catalyst elements WERE NOT blown out with compressed air prior to evaluating controller performance and collecting emissions data. 6 month evaluation has been completed. Engine hours = 51,249.

August 21 – 24, 2012: E3RB tuning (HEGO setpoints, dither frequency/amplitude, PID bias) optimized for this engine based on results of equivalence ratio sweep conducted at high speed/high load condition.

The relevance of blowing out catalyst elements with compressed air prior to monitoring emissions will be discussed in the Results section of this thesis.

2.4 Test Matrix

Based on feedback from Encana field personnel, three distinct engine load conditions were defined, which represented the range of typical operation of the engine at this site; shown in Table 4 as High Speed/High Load (HS/HL), Mid Speed/Mid Load (MS/ML), and Low Speed/Low Load (LS/LL). The Inducted Charge Flow is an E3RB parameter, described in an earlier section as Q_{mix} , which is used by the controller to indirectly ascertain engine load by calculating the volumetric flow rate of fuel/air charge in the intake manifold. It is useful to once again note that Q_{mix} is a calculated parameter that incorporates both engine speed and load in a single metric.

The emissions monitoring protocol consisted of recording post-catalyst engine emissions at all points in the test matrix, followed by a pre-catalyst measurement at the very last point, allowing for evaluation of catalyst performance at that operating condition. During transitions between each load point, E3RB response was monitored and recorded by way of trends

generated through Woodward’s Control Assistant software, which interfaced with the E3RB controller via a laptop USB connection.

Table 4: Engine speed/load test matrix used for emissions monitoring and evaluation of E3RB performance

Operating Condition	Speed (RPM)	Inducted Charge Flow (scfm)
High Speed/High Load (HS/HL)	1150	2100
Load Step: Monitor E3RB transient response		
Mid Speed/Mid Load (MS/ML)	1000	1700
Load Step: Monitor E3RB transient response		
Low Speed/Low Load (LS/LL)	850	1400
Load Step: Monitor E3RB transient response		
High Speed/High Load (HS/HL)	1150	2100

2.4.1 Performance Evaluation Protocol

The following steps were performed during each site visit, as part of the monitoring protocol. It should be noted that the emissions analyzer was configured to operate at 50% duty cycle (15 minutes emission sampling ; 15 minutes fresh air purge).

1. If it is not already running, start and load the engine per standard procedures. Operate the unit under load for several hours until the system achieves equilibrium.
2. Set the unit to HS/HL condition and allow 20 minute equilibration period.

- a. Record two 15 minute data sets of post-catalyst emissions and all relevant engine and catalyst operating parameters.
 - b. Review the data for repeatability and record additional data sets as required.
3. Set the unit to MS/ML condition and allow 20 minute equilibration period.
 - a. During this load step, record 15 minutes of E3RB controller data.
 - b. Record two 15 minute data sets of post-catalyst emissions and all relevant engine and catalyst operating parameters.
 - c. Review the data for repeatability and record additional data sets as required.
4. Set the unit to LS/LL condition and allow 20 minute equilibration period.
 - a. During this load step, record 15 minutes of E3RB controller data.
 - b. Record two 15 minute data sets of post-catalyst emissions and all relevant engine and catalyst operating parameters.
 - c. Review the data for repeatability and record additional data sets as required.
5. Return the unit to HS/HL condition and allow 20 minute equilibration period.
 - a. During this load step, record 15 minutes of E3RB controller data.
 - b. Record two 15 minute data sets of post-catalyst emissions and all relevant engine and catalyst operating parameters.
 - c. Review the data for repeatability compared to step 2 above. Investigate any aberrations.
 - d. Record one 15 minute data set of pre-catalyst emissions and all relevant engine and catalyst operating parameters.

2.4.2 Evaluation of Engine Power Output

Emissions species were measured as raw concentrations in parts per million dry (ppmd). In order to normalize this raw data to brake specific values, engine power output was required to be known. Direct measurement of engine power was not available at this site and neither was fuel flow, owing to a malfunctioning orifice meter. So, instead three alternate approaches, outlined below, were devised to determine engine horsepower and by extension brake specific emissions. A side-by-side comparison of the engine power output obtained using each method is presented in Figure 24.

Method 1 (Calculated)

Shaft power is calculated using known values of total inducted charge (Q_{mix}), and fuel gas composition, as well as OEM engine specifications for brake specific fuel consumption at various engine speeds.

Method 2 (ESM Load)

The ESM (Engine System Manager) is Waukesha's engine management system, which integrates spark timing control, speed governance, detonation detection, start-stop control, diagnostic tools, fault logging, and engine safeties. At this site, the ESM load rating displayed on the PLC for each operating condition was converted to a proportionate power output, based on the engine speed at that particular load rating.

Method 3 (Ariel Model)

Using recorded values of engine speed, suction and discharge pressures/temperatures for a given loading condition, the engine output was calculated using Ariel Corporation's proprietary

compressor sizing program. A parasitic loss of 5% was assumed for auxiliary loads such as cooling fans.

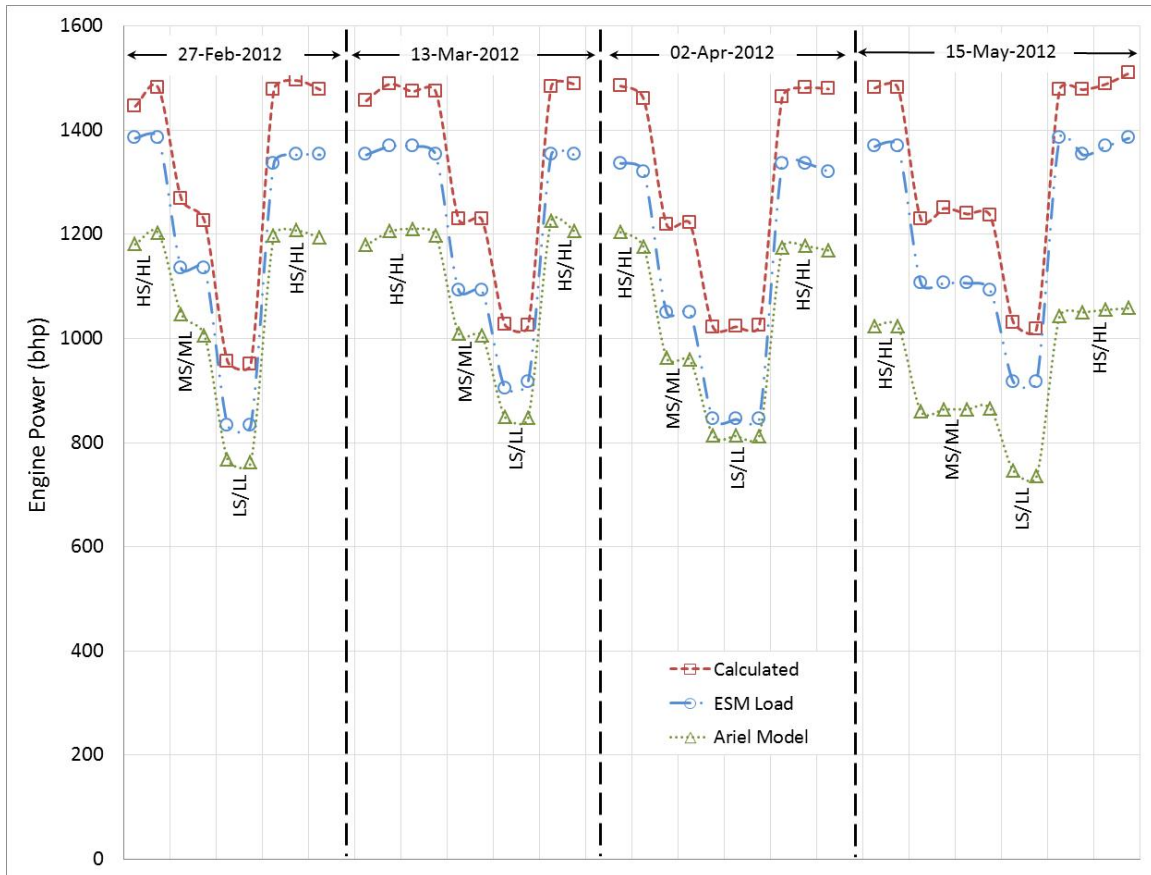


Figure 24: Comparison of engine power output obtained using three different methods.

From Figure 24, it can be seen that variation between the three methods is significant. Torque measurements for compressor and auxiliary shafts would need to have been made in order to reliably measure engine power output and use it to identify the most accurate of the three methods. However, since resources were not at hand to measure shaft torque, for the purposes of reporting brake specific emissions, it was decided to calculate engine power using Method 1.

3. Results

3.1 Engine Tuning

The E3RB was tuned by Woodward across the entire range of site operating conditions anticipated by Encana field personnel. Figure 25 shows the post-catalyst emissions levels of CO and NO_x obtained at various engine load points on February 20, 2012. Taking into consideration the sharp rise in NO_x emissions if an engine operates outside of the lean-limit of the NSCR control window as compared to the gradual increase in CO emissions for an engine operating beyond the rich-limit, conventional wisdom suggests that the target post-catalyst CO:NO_x ratio for optimal NSCR performance be ~2:1 [9].

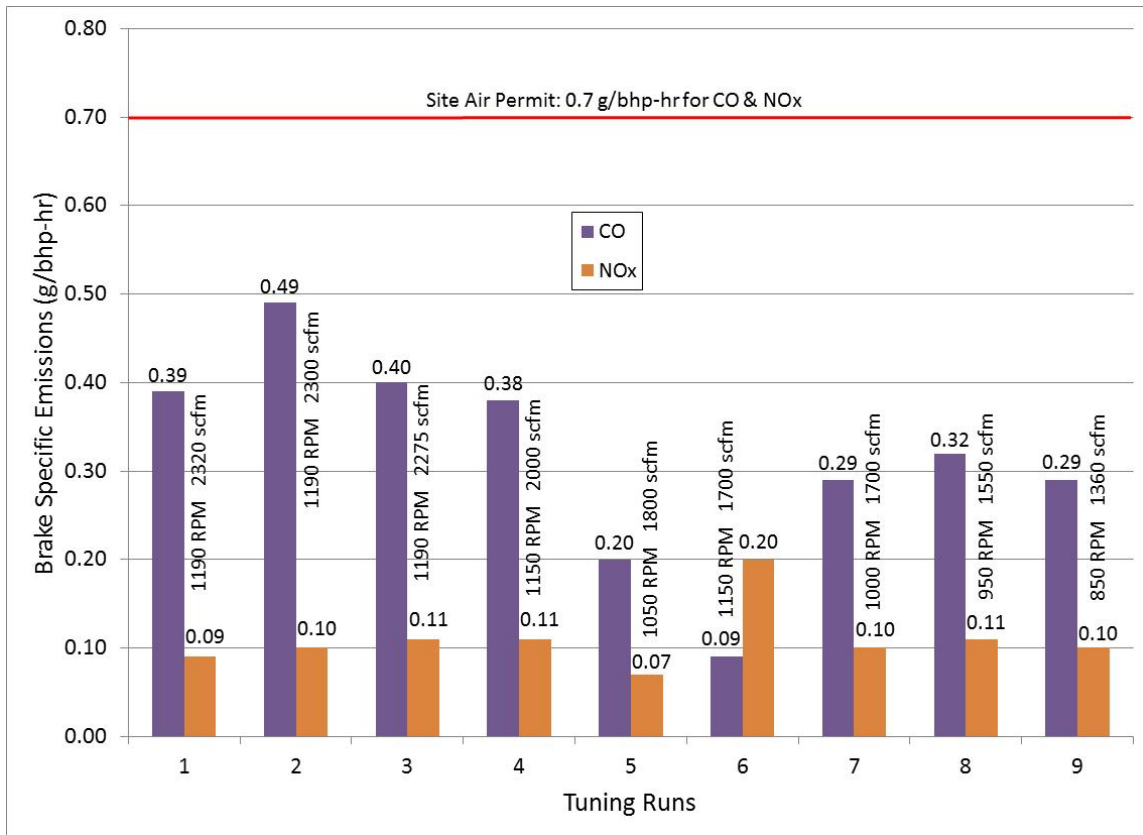


Figure 25: Tuned emissions level across the engine operating load range.

In this case, CO:NO_x at high load conditions is ~4:1, tapering off to ~3:1 at mid and low loads, with an inversion at Run 6, where CO:NO_x is ~1:2. High levels of engine-out CO emissions were observed (> 20 g/bhp-hr); the prime suspect behind this is most likely poor engine health, which is discussed in a following section. It is assumed that appropriate tuning adjustments would have been made to the AFR control, if this issue was discovered during pre-commissioning activities.

3.2 Alarms/Faults

The following system fault/alarm settings were demonstrated to showcase the features of this controller:

1. Misfire
2. System lean/rich
3. Post-catalyst HEGO sensor failure
4. Post-catalyst high temperature
5. Pre-catalyst high/low temperature
6. Bank 1 and 2 HEGO sensor (pre-catalyst) failure

E3RB response trends for each of these alarms can be viewed in Appendix C.

3.3 Engine Health

During the initial screening conducted to identify a suitable unit for this field evaluation, the primary criteria used were low engine hours and reduced catalyst age, with no attention given to other attributes of engine health such as consumption rates of engine fluids (oil and coolant). This oversight in assessment of overall engine health proved to be a costly mistake as it was later

discovered that this particular engine used copious amounts – averaging 10 gallons per day (gpd) – of engine oil, which is an order of magnitude greater than that of adjacent engines (similarly configured Waukesha 7044GSI models), having oil consumption rates of around 0.5 gpd. Poor engine condition and the related high oil consumption can be considered a significant factor influencing:

(i) engine-out CO:NO_x ratio

(ii) degradation of HEGO sensors due to ash-masking of the sensor element

(iii) partial combustion of oil, resulting in additional CO emissions, which are independent of AFR control

(iv) catalyst poisoning of reactive/oxygen storage sites by Calcium, Phosphorus, Zinc, and Magnesium, which are all commonly used additives in engine oil

(v) catalyst degradation due to ash-masking which in effect reduces catalyst surface area

Catalyst elements were blown out at the beginning of every monitoring visit, with the exception of first and last visits, in order to clear the ash built-up on the catalyst elements (Figure 26).

Samples of ash collected from the catalyst elements were analyzed using X-ray Photoelectron Spectroscopy (at CSU's CIF in the Department of Chemistry) to understand the elemental composition of the powder. The results of this elemental analysis can be seen in Table 5 and Figure 27. The measured quantities of Calcium, Phosphorus, and Zinc – which are all additives in the engine oil used at this site – was further evidence that the high rate of oil consumption by this engine is responsible for the accelerated rate of catalyst degradation that

was observed. It is assumed that the oil consumption occurs by way of oil ingress into the combustion chamber, owing to poor sealing by the piston rings. However, an opportunity to verify this assumption did not present itself during the field test. The brand of oil used in this engine is Conoco El Mar Low Ash 40, manufactured by ConocoPhillips.



Figure 26: Catalyst elements being blown out with compressed air to clear ash-masking.

Table 5: Elemental composition of catalyst ash

Element	Oxygen	Calcium	Carbon	Phosphorus	Sulphur	Zinc
Weight (%)	37.09	31.68	15.97	5.64	2.36	1.15

Element	Copper	Iron	Aluminum	Silicon	Magnesium
Weight (%)	0.74	0.39	0.08	0.08	0.06

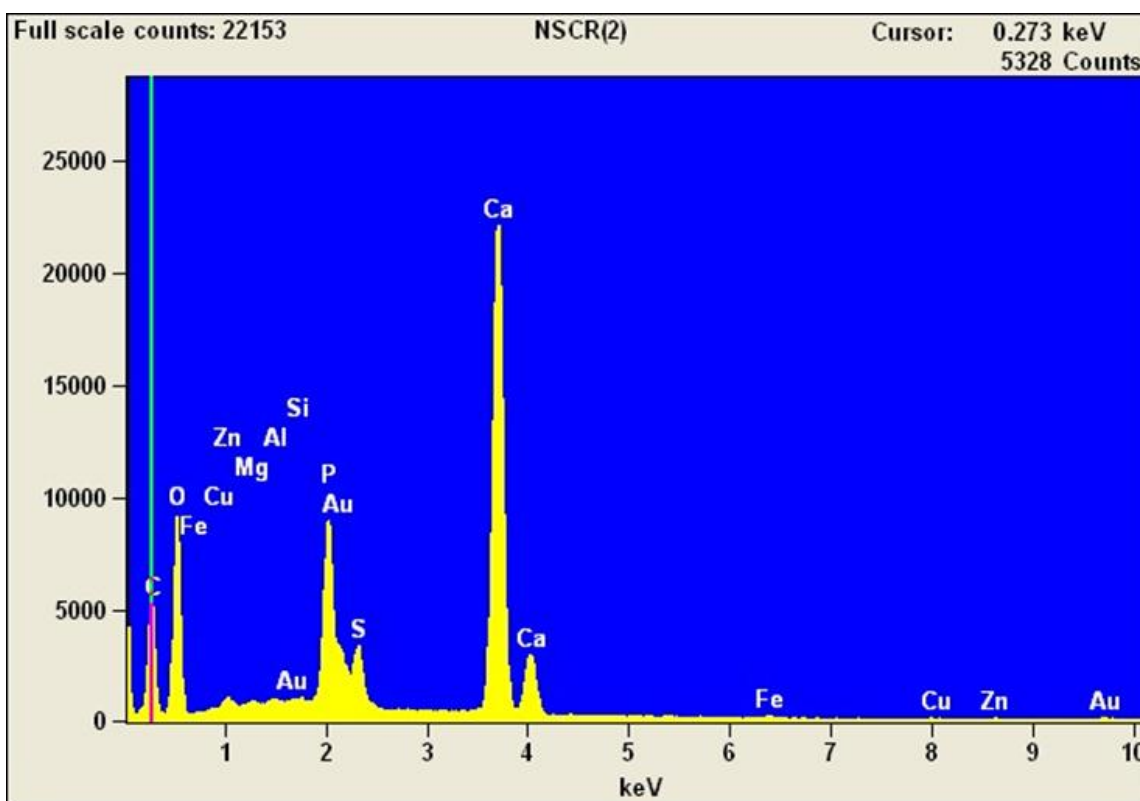


Figure 27: Spectrogram of elemental composition of catalyst ash.

The extent of ash-masking on the catalyst was characterized by correlating it to the pressure differential measured across catalyst elements, using pressure taps affixed to the catalyst housing (Figure 28).



Figure 28: Pre (right) and post (left) catalyst pressure taps affixed atop the catalyst housing.

During the first evaluation visit, conducted on February 27, one week after the E3RB's commissioning on February 20, the catalyst elements were not cleared with compressed air owing to a lack of awareness of the oil consumption issue and therefore, masking not yet being a point of concern. The rationale for foregoing compressed air cleaning of catalyst elements during the last evaluation visit, conducted on August 20, is two-fold:

- (a) During prior update meetings (conference calls) with the project team, the method of employing compressed air to blow out catalyst elements was strongly criticized as a poor practice, having more detriments than benefits, when examined over the life of the catalyst.

(b) From the catalyst pressure differential trend in Figure 29, it can be seen that at the HS/HL operating condition, the rise in pressure between the penultimate data point on June 25 and the following one on August 20 was 0.6” of water. Also noting that between June 25 and August 20, the unit was offline for a period of ~3 weeks, from July 18 to August 9, it was decided that the amount of masking resulting in the observed pressure rise would likely not be sufficient to disrupt catalyst function and by extension, an increase in levels of post-catalyst emissions.

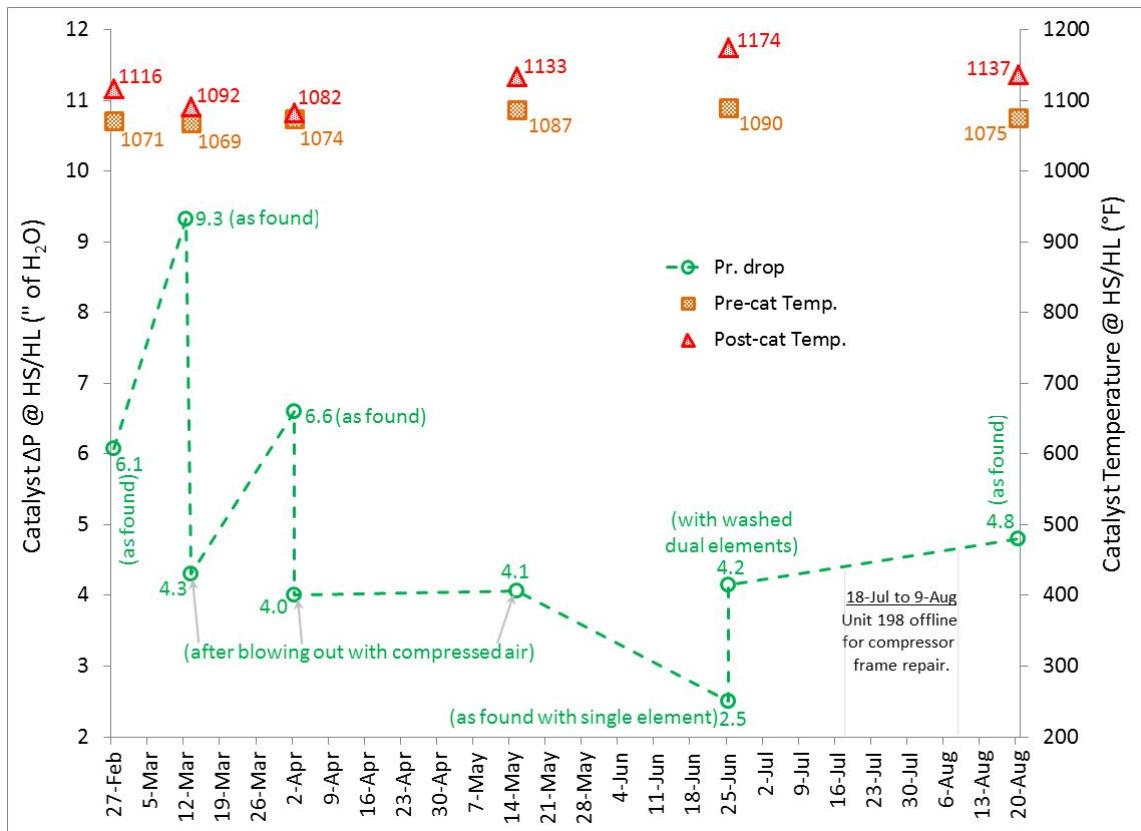


Figure 29: Trend of pressure drop and temperature across catalyst elements at HS/HL operation.

Therefore, the emissions test on August 20 was viewed as an opportunity to examine catalyst performance and emissions levels resulting from not blowing out the catalyst elements with compressed air.

3.4 Steady-State Performance

3.4.1 Engine Condition: High Speed/High Load (HS/HL)

Two key indicators used in this study to qualify the degree of AFR control exerted by the E3RB at the HS/HL condition are the pre and post-catalyst ratios of CO:NO_x. In an ideal AFR control scenario, the first recorded pre and post-catalyst CO:NO_x ratios serve as benchmarks from which subsequent ratios should exhibit minimal deviation. Therefore, any observed increase in post-catalyst emissions can be attributed to catalyst degradation and aging of sensor elements.

Referring to the lower trend in Figure 30 and using the pre-catalyst CO:NO_x ratio of 1.56 from the first site visit on February 27 as a benchmark, during the two subsequent site visits (March 13, April 2), this ratio deviates -10% from the benchmark, which implies AFR has drifted toward lean operation. Beyond that, for the remaining duration of the test, the AFR drifts toward rich operation. A noticeable increase occurs after new HEGO sensors were installed on June 25. The upper trend in the same figure shows a ~24% increase in engine-out emissions of CO after the new HEGO sensors were installed. Comparing the post-catalyst CO:NO_x in Figure 31 to the pre-catalyst CO:NO_x in Figure 30, it is noticed that with the exception of the data point from August 20, the post-catalyst CO:NO_x trend moves opposite to pre-catalyst CO:NO_x. While this is contrary to expectations, a proposed explanation is provided later in this section. From the post-catalyst emissions trend in Figure 31, it can be seen that both CO and NO_x emissions were within air permit limits for this site, during the first three site visits. CO emissions were found to exceed site air permit limits during the monitoring visit on May 15. This can be attributed to two factors, namely:

- (i) poor engine condition that contributed to excessive oil consumption

(ii) excessive NOx margin used during initial tuning

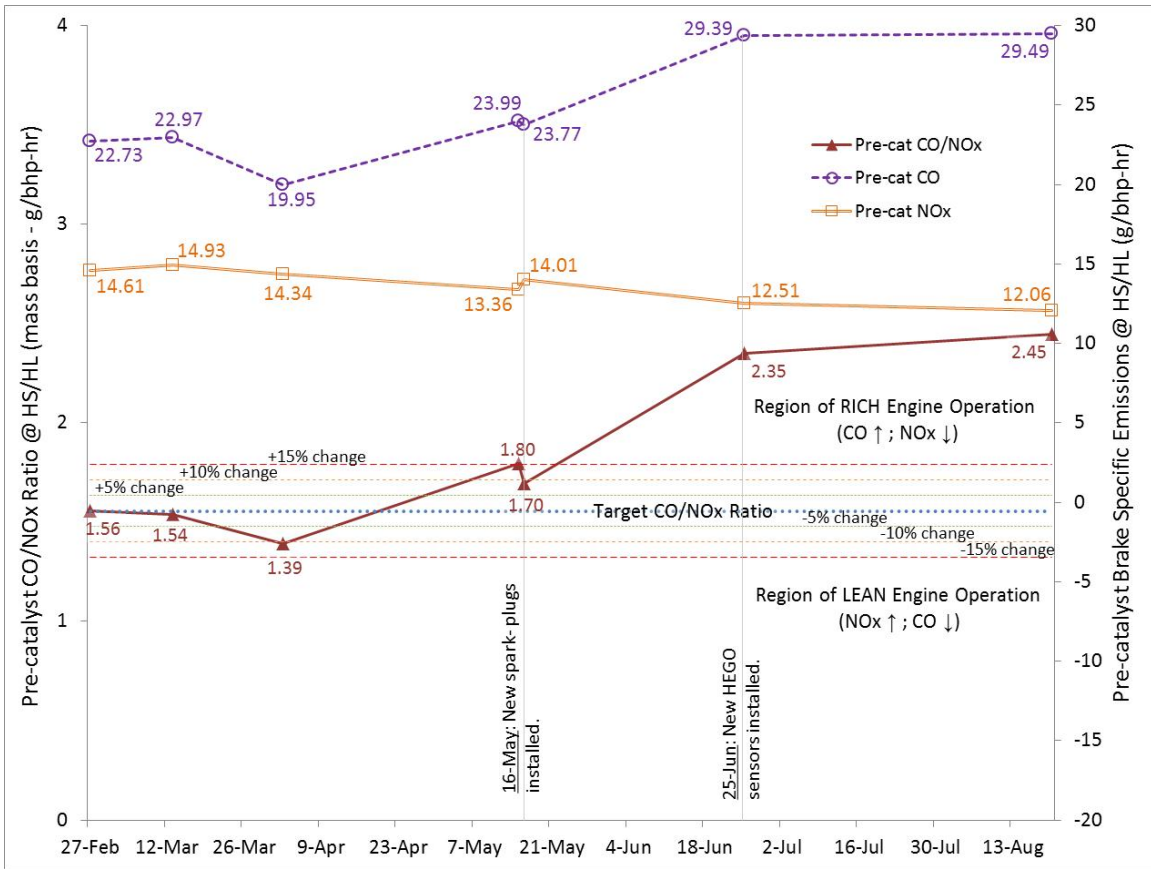


Figure 30: Trends of pre-catalyst emissions and CO:NOx @ HS/HL operation.

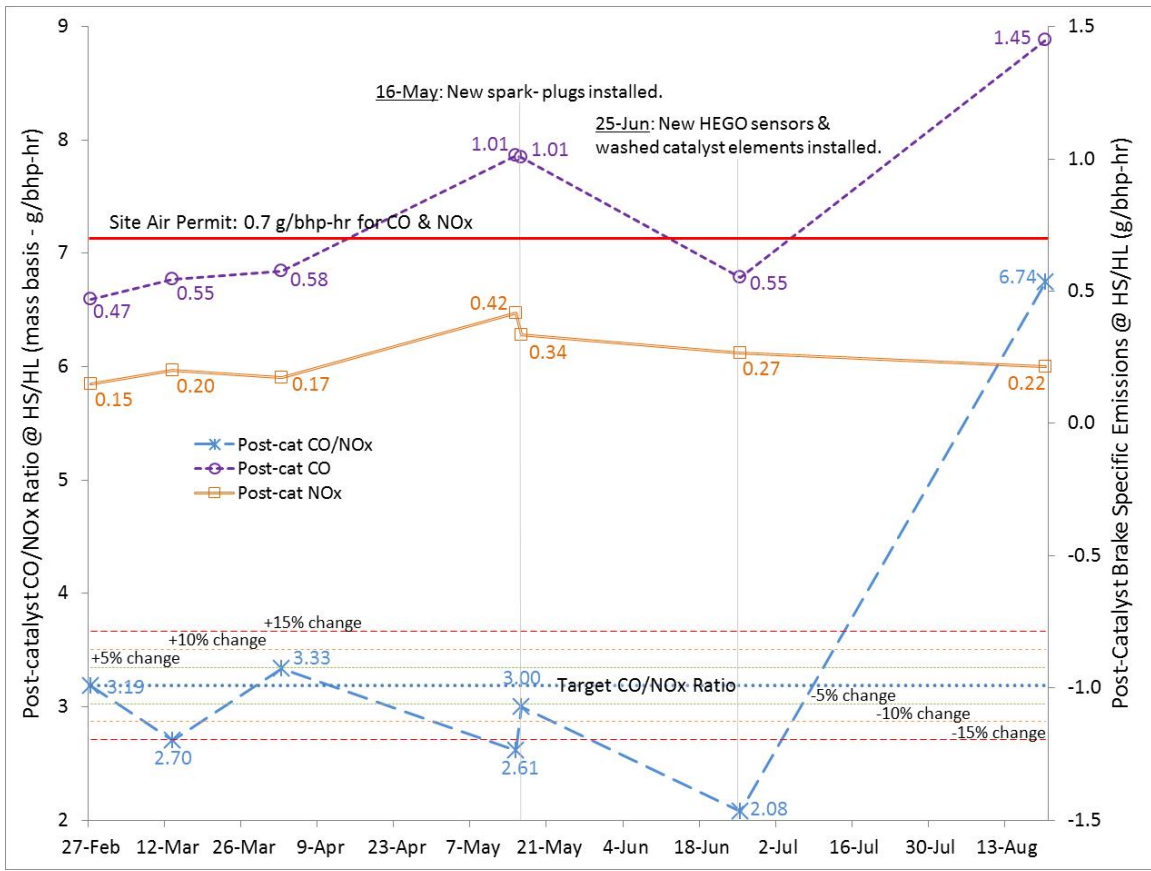


Figure 31: Trends of post-catalyst emissions and CO:NOx at HS/HL operation.

In order to eliminate low ignition energy and incomplete combustion as root causes for the rise in CO, new spark plugs were installed in the engine. After this was completed on May 16, another test was conducted to examine the effect of this change on emissions. Figure 31 shows a noticeable drop in NOx with CO unchanged. This is contrary to expectations because new spark plugs would create higher in-cylinder temperatures resulting from improved combustion. From combustion kinetic considerations, this would be expected to increase engine-out NOx while lowering CO. However, from Figure 32, it can be seen that installation of new spark plugs generated lower in-cylinder temperatures during engine operation (temperatures for cylinders 10-12 were not recorded by the SCADA system). This trend provides a rationale for

the observed increase in NOx emissions (ie. lower in-cylinder temperatures). However, the root cause behind it is still not understood. The old spark plugs removed from the engine did not exhibit any traces of fouling and spark plug gaps were not recorded.

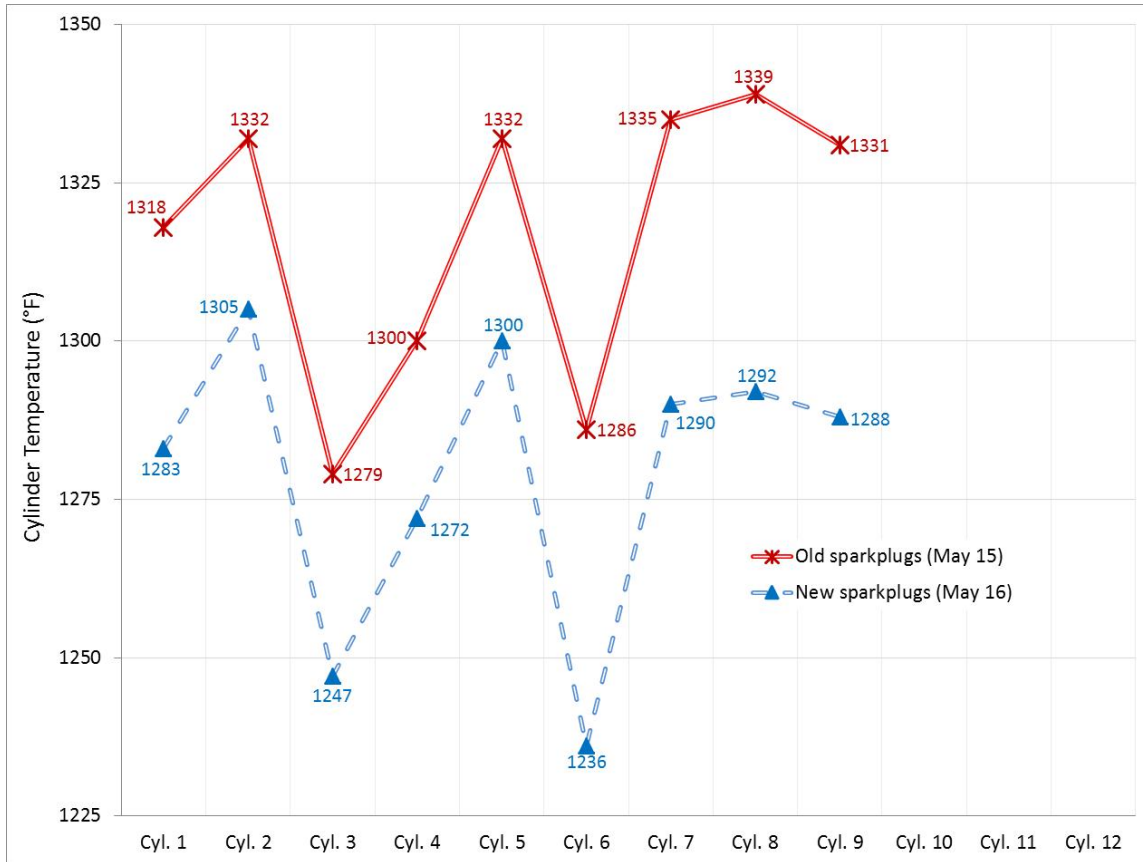


Figure 32: Comparison of in-cylinder temperatures before/after spark plug change.

Since new spark plugs did not resolve the high CO emissions, it was surmised that ash-masking of sensor elements on the HEGOs was feeding improper input signals to the AFR controller. Therefore, on the next monitoring visit, new HEGO sensors were installed on the E3RB. The combination of new HEGO sensors and freshly washed catalyst elements resulted in bringing CO emissions back in compliance during the monitoring visit on June 25.

During the last monitoring visit on August 20, CO emissions were found to be out of compliance, despite a reduction in the NO_x emissions level. The resulting post-catalyst CO:NO_x represented a 112% increase from the benchmark of 3.19, established on February 27.

The catalyst efficiency trends for reduction of CO and NO_x are shown in Figure 33. The trend for CO reduction efficiency is unremarkable until May 16. The decline in CO reduction efficiency during the period between June 25 and August 20 is steeper than during the period from February 27 to May 16. Keeping in mind that (i) ash on the catalyst elements was not cleared with compressed air on February 27 and August 20 (ii) the compressor station was offline for a period of 3 weeks, starting July 18 and ending August 9, the drastic reduction in CO conversion efficiency cannot be explained with the data at hand. For the monitoring visit in May, analyzing the efficiency of NO_x reduction in conjunction with pre and post-catalyst NO_x trends from Figure 30 and Figure 31 (respectively) shows that after the new spark plugs were installed, there was a very apparent increase in pre-catalyst NO_x emissions and mild decrease in CO emissions. Accompanying this increase in engine-out NO_x was a corresponding increase in NO_x reduction efficiency, while that of CO remained almost constant. This increase in catalyst efficiency for NO_x reduction is explained in the discussion linked to Table 6.

Another interesting catalyst efficiency behavior occurs when NO_x reduction efficiency increases during the periods of March 13 – April 2 and June 25 – August 20 while CO reduction efficiency declines over the same period. This observation is explained in the context of dominant NSCR reactions that occur in the catalyst.

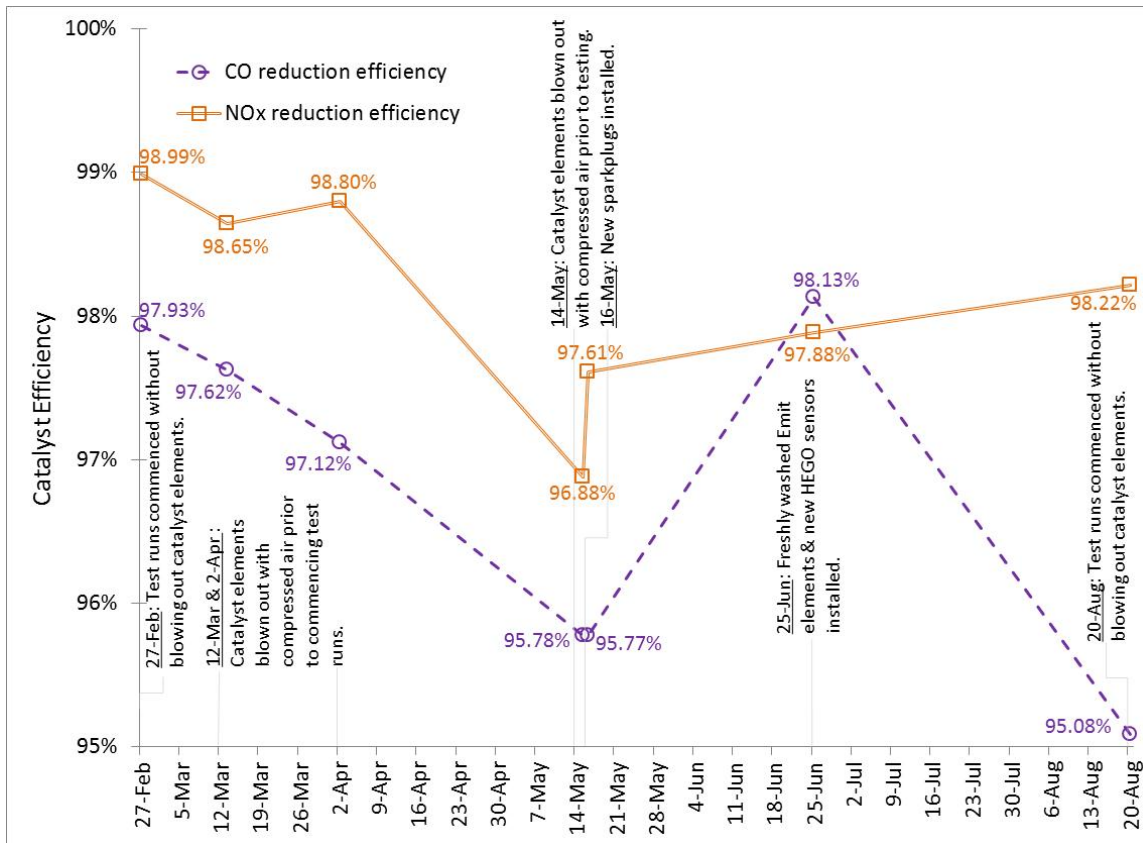


Figure 33: Catalyst efficiency @ HS/HL operation.

Table 6 summarizes the observed trends in various parameters, over the duration of the study; the direction of the arrows indicates the relative movement of a particular trend with respect to the prior recorded value. $(CO:NOx)_{pre}$ and $(CO:NOx)_{post}$ respectively represent the relative motions of pre and post-catalyst CO:NOx ratios; η_{CO} and η_{NOx} respectively represent the relative motion of catalyst reduction efficiencies for CO and NOx. Equations (a) and (b) are two key reactions that occur in an NSCR catalyst for CO oxidation and NO reduction, respectively. The values tabulated in the last column, titled ‘NSCR Rxn.’, are hypotheses as to which of the two NSCR reactions dominated during the monitoring run under consideration.





Of particular interest are the behaviors from April 2, May 16, and August 20, each of which exhibit increases in NO_x reduction efficiency, running counter to the expected degradation trend, similar to that displayed by CO reduction efficiency. A possible explanation for this observation is provided below.

Table 6: Summary of emissions trends @ HS/HL operation

	(CO:NO _x) _{pre}	(CO:NO _x) _{post}	η _{CO}	η _{NO_x}	NSCR Rxn.
Feb 27	Baseline				----
Mar 13	↔	↓	↓	↓	(a) / (b)
Apr 2	↓	↑	↓	↑	(b)
May 15	↑	↓	↓	↓	(a) / (b)
May 16	↓	↑	↓	↑	(b)
Jun 25	↑	↓	↑	↑	(a) / (b)
Aug 20	↑	↑	↓	↑	(b)

On April 2, (CO:NO_x)_{pre} decreases, owing to a drop in engine-out CO, whereas (CO:NO_x)_{post} rises; also η_{CO} decreases while η_{NO_x} increases. The drop in η_{CO} can be attributed to minimal stored oxygen in the catalyst (brought about by ash-masking of oxidation storage sites) whereas the increase in η_{NO_x} is assumed to be due to the dominance of NSCR reaction (b), which takes advantage of the excess CO in the exhaust gas stream that was not oxidized. A similar

trend is noticed on May 16 and the hypothesis extended is the same as that proposed for April 2. On August 20, with the exception of a reversal in $(\text{CO}:\text{NOx})_{\text{pre}}$, the trends are identical to those on April 2 and May 16.

An examination of four E3RB parameters, namely PID Bias and pre-catalyst HEGO signals for each bank (Figure 34), reveals noticeable changes in both PID bias and HEGO setpoints upon installation of the new HEGO sensors on June 25. An abrupt increase in engine-out CO emissions (AFR control shifting rich) is observed once the new setpoints and biases take effect and can likely be correlated to the richer engine operation that commences on June 25. An increase in engine oil consumption did not occur during this time period so, it can be ruled out as a cause for higher CO emissions.

This case demonstrates that if the HEGO sensors are replaced after system commissioning, the E3RB will require retuning in order to continue maintaining optimal AFR control; this is particularly relevant at sites where emission limit margins are tight. Retuning may not be necessary at sites where margins are looser.

It is worth noting that during the period between February 27 and May 15, engine-out CO emissions trend similar to the left bank PID bias, while the right bank PID bias remains stable. There are no conclusions to be drawn from this observed similarity.

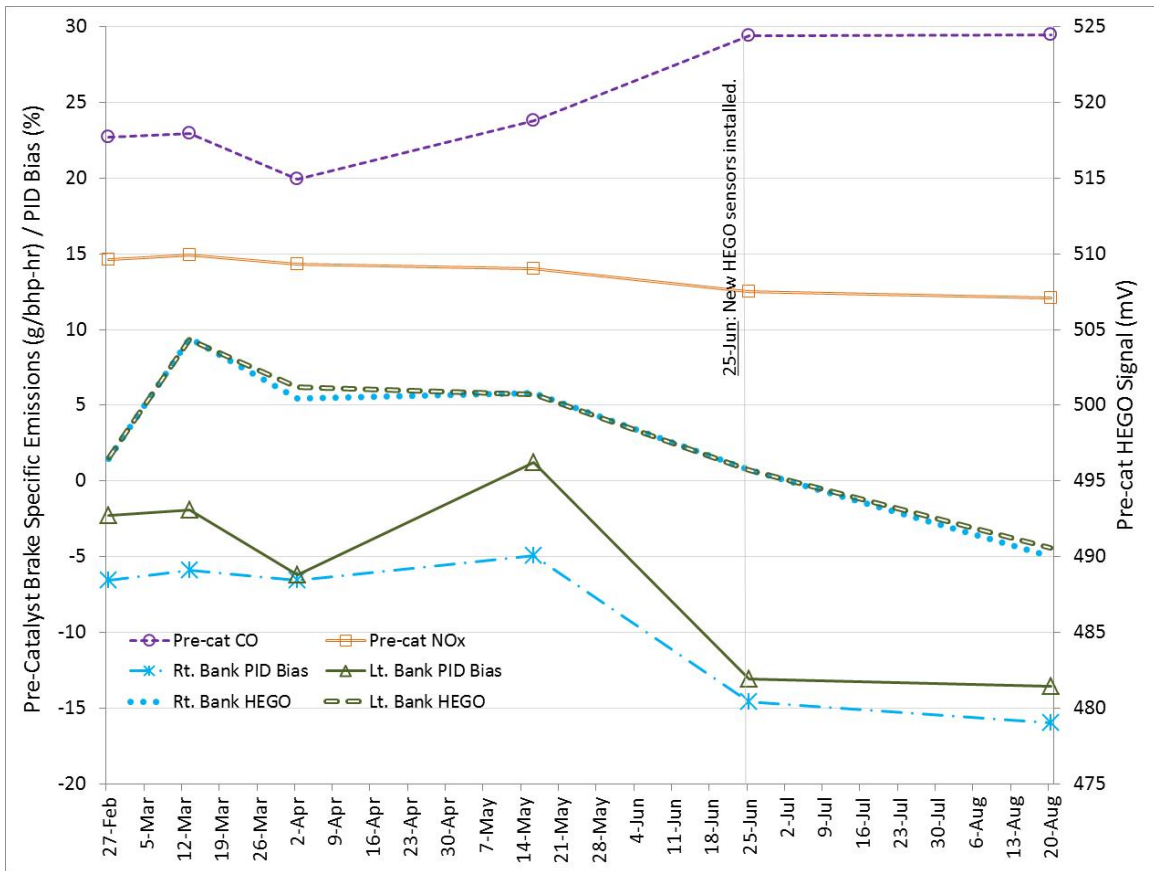


Figure 34: Trends of E3RB parameters and pre-catalyst emissions @ HS/HL operation.

An alternate method to depict the change in AFR operation is with a NOx-CO crossplot, with NOx on the x-axis and CO on the y-axis. When analyzed in conjunction with a CO:NOx trend, these crossplots can be used to characterize the relative contributions of CO and NOx in an exhaust mixture that is either rich or lean.

Figure 35 shows the variation in pre-catalyst CO and NOx at HS/HL operation. From this crossplot, it can be noted that starting from the first data point on February 27, the AFR control initially trended slightly lean in March and April, followed by successively richer operation in May, June and August. Similarly, Figure 36 shows the variation in post-catalyst CO and NOx at HS/HL operation, with an alternating pattern of rich-lean post-catalyst conditions, starting from

February and settling in a rich region at the final data point in August. Other parameters recorded during engine operation at HS/HL are shown in Figure 37. As expected, it can be seen that manifold air temperatures and throttle position follow the ambient air temperature trace. Throttle position data for May 15 and August 20 was unavailable owing to a sensor fault in the PLC. With the exception of April 2, manifold air pressures maintain at 5 psig \pm 0.3psig.

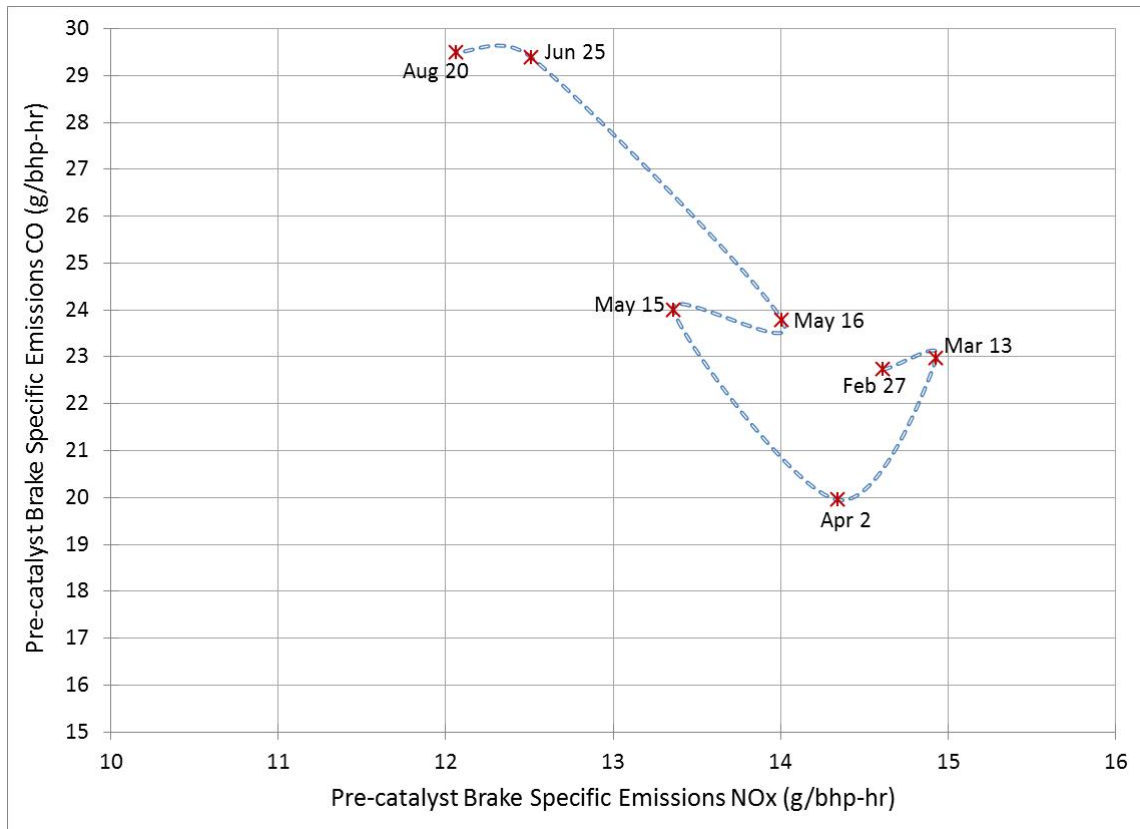


Figure 35: Pre-catalyst NOx-CO crossplot @ HS/HL operation.

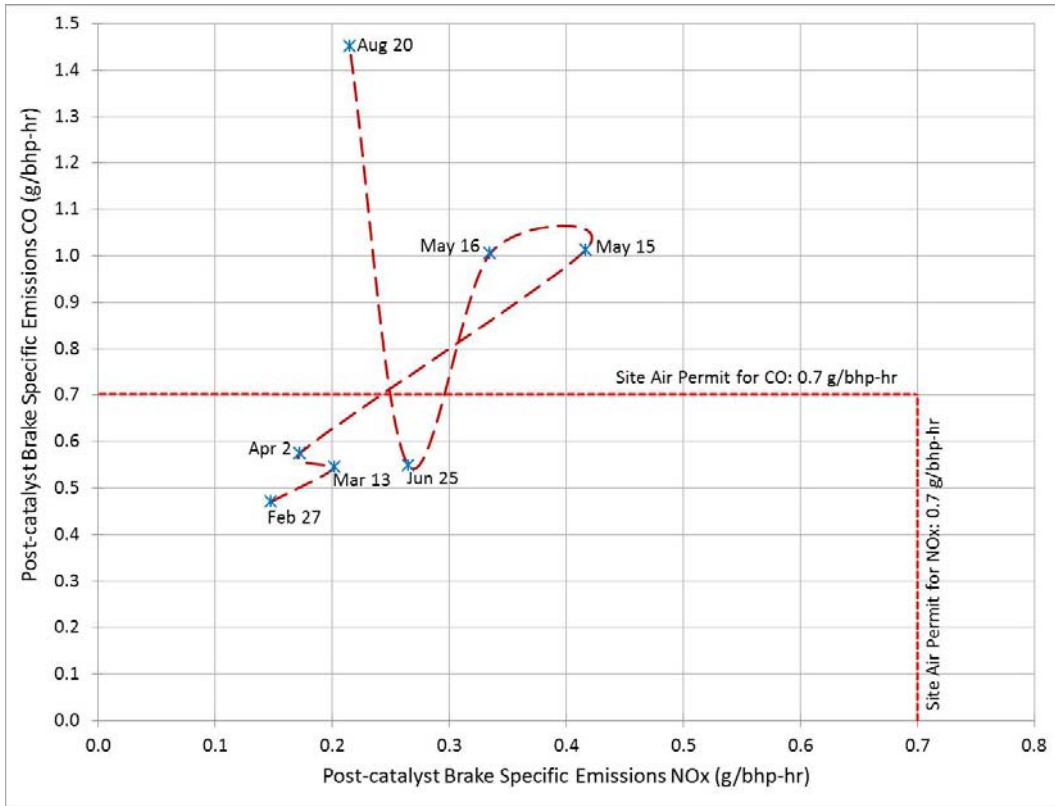


Figure 36: Post-catalyst NOx-CO crossplot @ HS/HL operation.

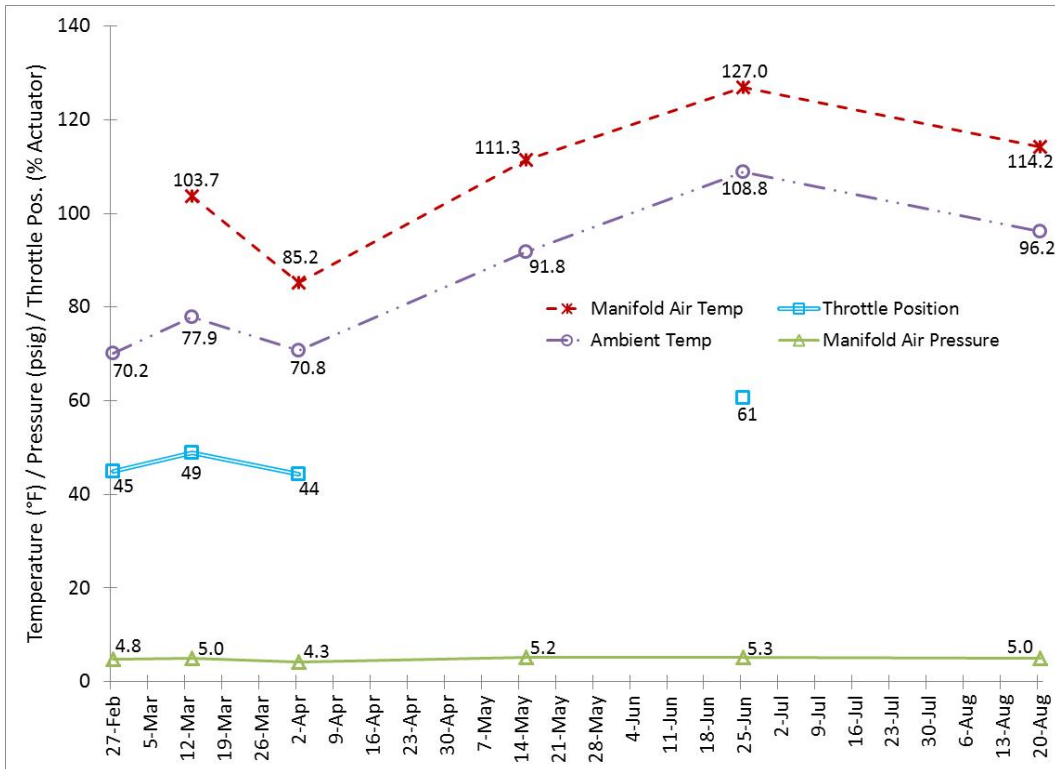


Figure 37: Trends of other engine parameters and ambient temperature @ HS/HL operation.

3.4.2 Engine Condition: Medium Speed/Medium Load (MS/ML)

This section discusses trends in emissions and AFR control at MS/ML operation (Speed: 1000 RPM, Qmix: 1700 scfm). The trend for pressure drop across catalyst elements can be seen in Figure 38. It should be noted that since the ash on catalyst elements was not blown out on February 27 and August 20, the pressure drop recorded on those days is noticeably higher than during the remainder of the monitoring visits.

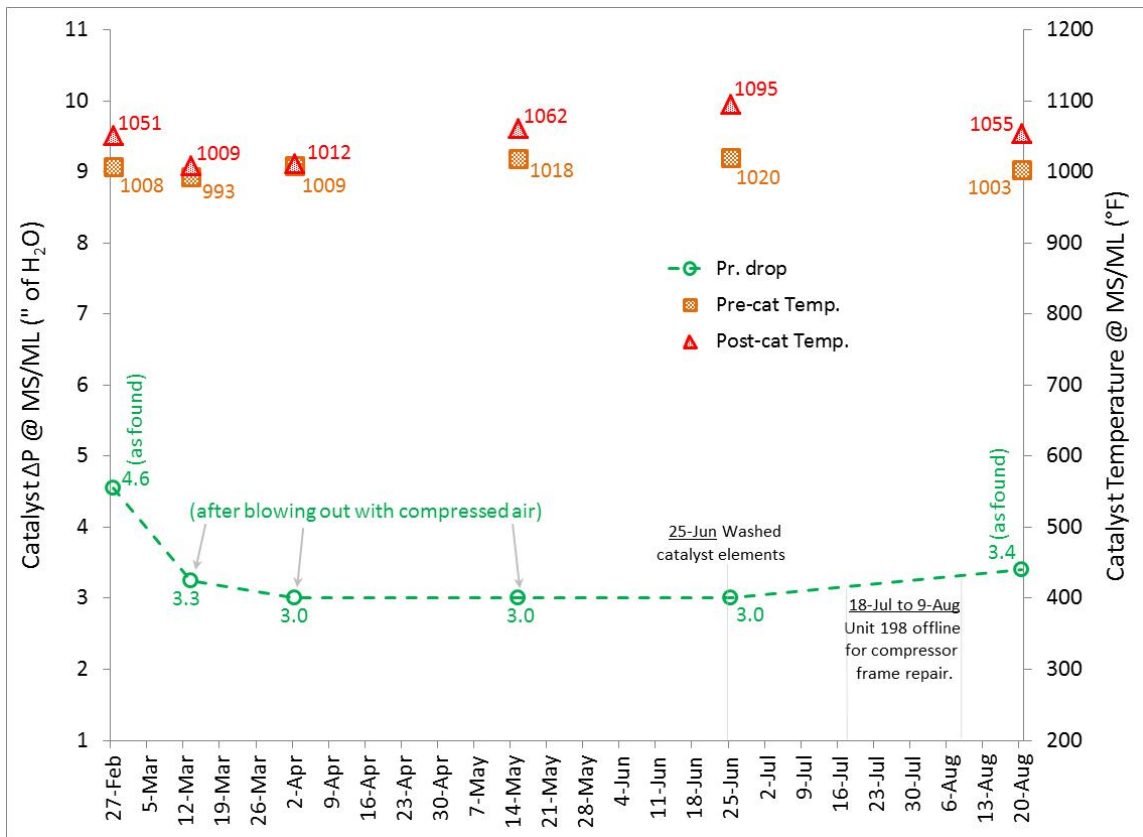


Figure 38: Trend of pressure drop and temperature across catalyst elements at MS/ML operation.

During MS/ML operation, only post-catalyst emissions data was recorded. Therefore, movement of CO:NOx on the post-catalyst side cannot be correlated to engine-out CO:NOx. However, from examining Figure 39 and Figure 40, the following observations can be made:

- (a) During the first four site visits (February 27 – May 15), the engine emissions were within site air quality limits. It should be recalled that the nominal operating condition, defined for purposes of regulatory emissions compliance, is HS/HL.
- (b) The benchmark post-catalyst CO:NO_x ratio of 2.16, recorded on February 27, is in line with expectations. CO:NO_x trend recorded during the three subsequent visits is also within acceptable limits, showing a good CO margin.

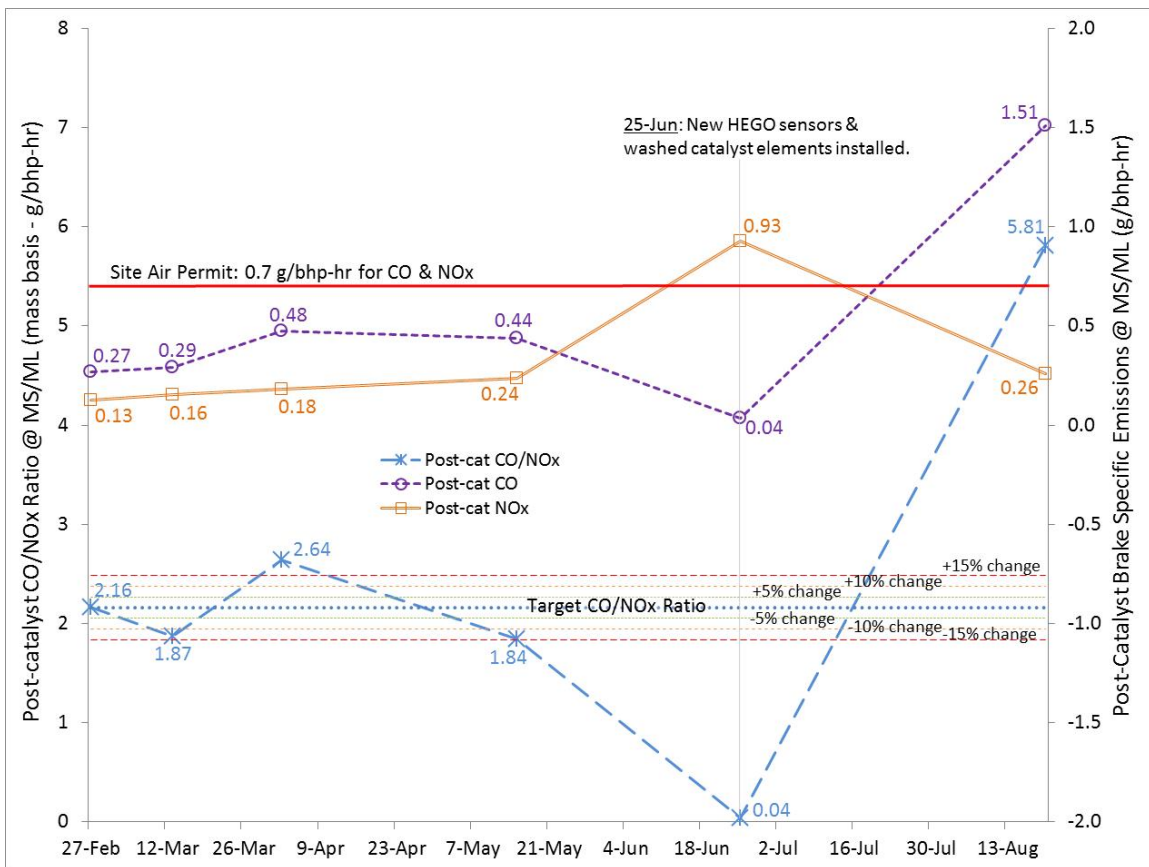


Figure 39: Trends of post-catalyst emissions and CO:NO_x at MS/ML operation.

- (c) On June 25, after new HEGO sensors were installed, a cross-over occurs between CO and NO_x emissions. Assuming that a similar reversal occurred with pre-catalyst engine-out emissions, it would imply that the engine AFR moved toward stoichiometry, causing the

spike in NOx and drop in CO. This change in AFR can be attributed to E3RB control, as evidenced by the sharp declines in both PID bias and HEGO values.

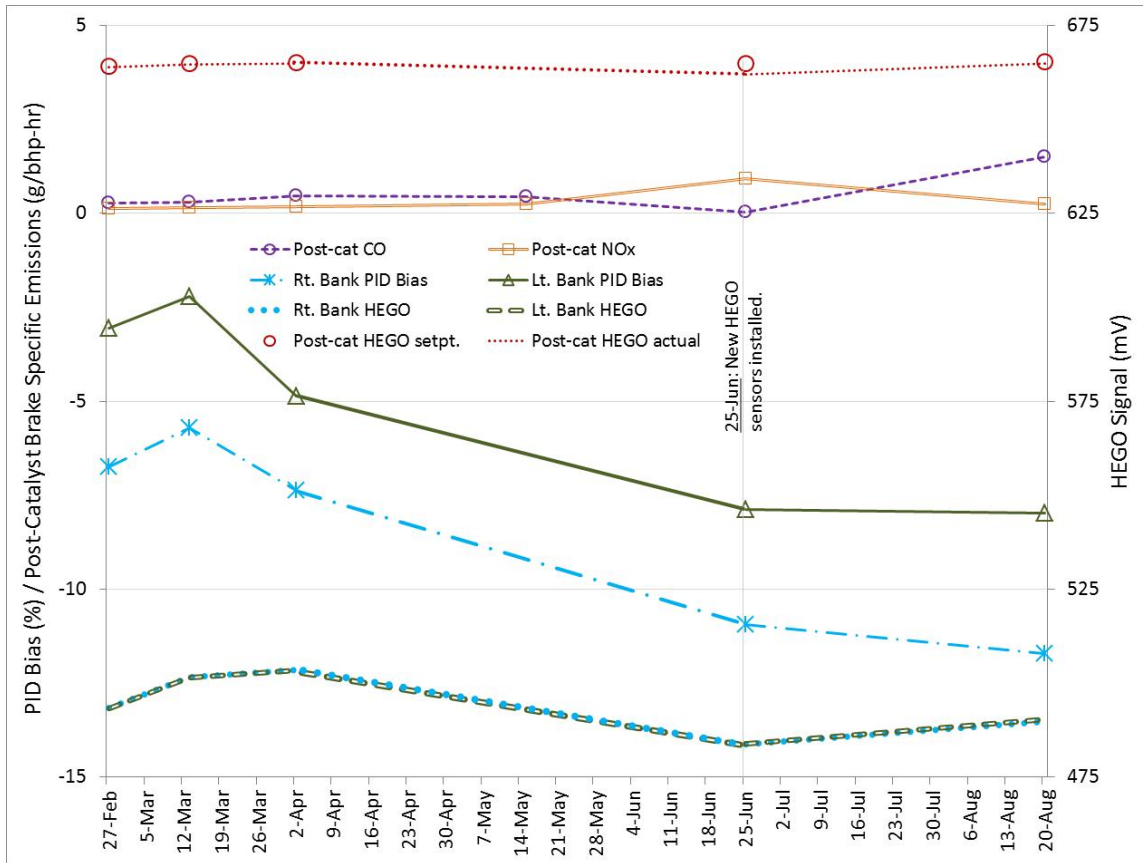


Figure 40: Trends of E3RB parameters and post-catalyst emissions @ MS/ML operation.

(d) On August 20, another emissions cross-over occurs, this time with a rise in CO and dip in NOx, indicating that the AFR has migrated to a rich HEGO. This migration is likely related to the rise in recorded values of the HEGO signal for each bank. The role of catalyst degradation, while undocumented, should not be discounted as a contributing factor in poor CO reduction.

The NOx–CO crossplot in Figure 41 provides further insight about the AFR control deviation that occurred after the HEGO sensor change on June 25. On August 20, the control is

operating in a region that creates NO_x emissions in the same neighborhood as on May 15 but with CO emissions several times higher. During the period from February 27 to May 15, the controller maintains good AFR control, as evidenced by the tight grouping of data points from this period.

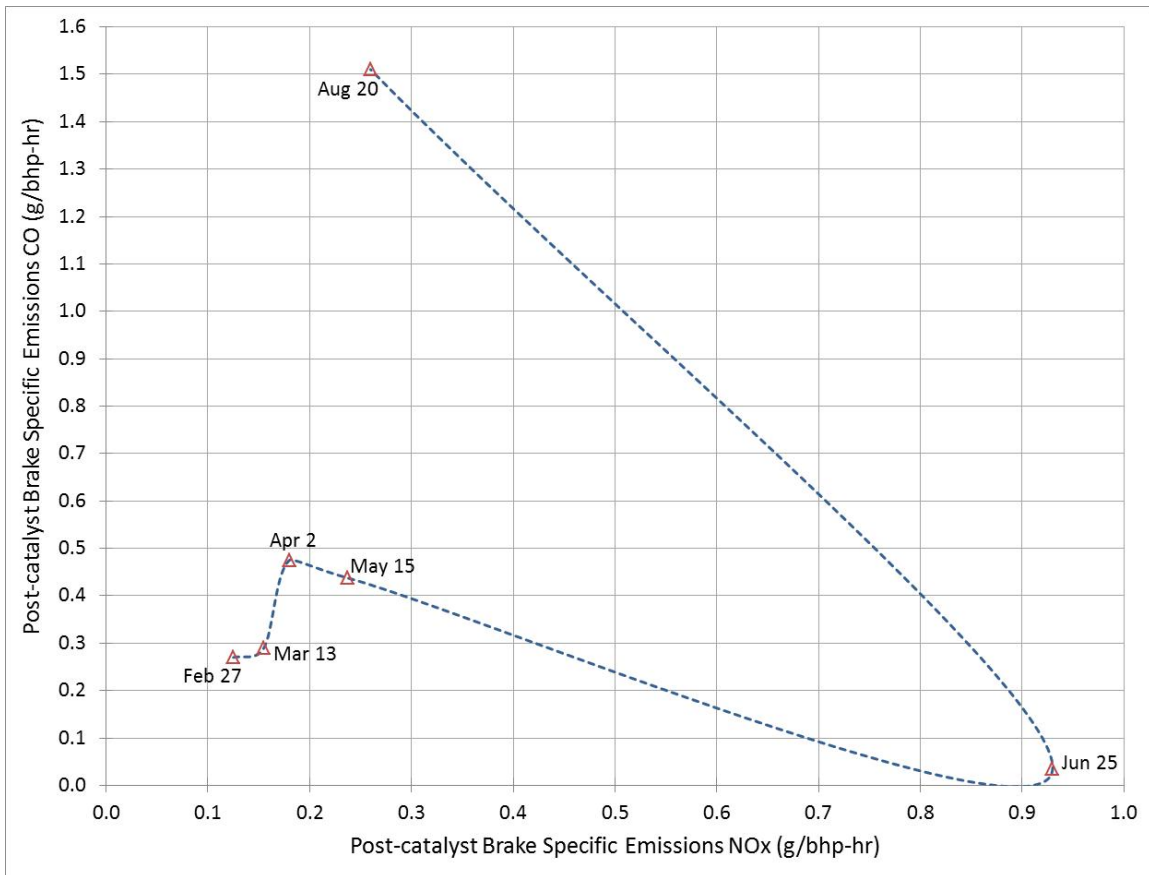


Figure 41: Post-catalyst NO_x-CO crossplot @ MS/ML operation.

3.4.3 Engine Condition: Low Speed/Low Load (LS/LL)

This section discusses trends in emissions and AFR control at LS/LL operation (Speed: 850 RPM, Q_{mix}: 1400 scfm). The trend for pressure drop across catalyst elements can be seen in Figure 42. It should be noted that since the ash on catalyst elements was not blown out on

February 27 and August 20, the pressure differential recorded on those days is noticeably higher than during the remainder of the monitoring visits.

During LS/LL operation, only post-catalyst emissions data was recorded. Therefore, movement of CO:NOx on the post-catalyst side cannot be correlated to engine-out CO:NOx. However, from examining Figure 43 and Figure 44, the following observations can be noted:

- (a) During the first three site visits (February 27 – April 2), the engine emissions were within site air quality limits. It should be recalled that the nominal operating condition, defined for purposes of regulatory emissions compliance, is HS/HL.
- (b) The benchmark post-catalyst CO:NOx ratio of 2.09, recorded on February 27, is in keeping with the recommended value of 2:1. CO:NOx trend during the two subsequent visits is also within acceptable limits.

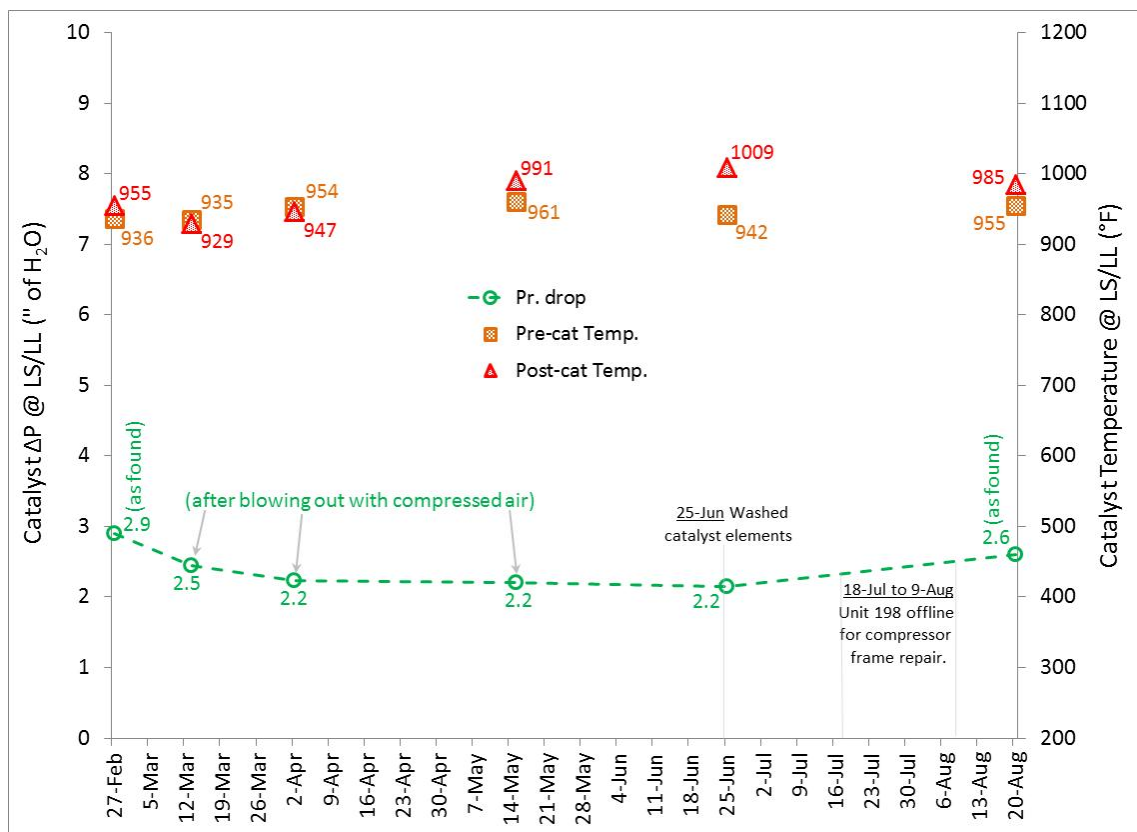


Figure 42: Trend of pressure drop and temperature across catalyst elements at LS/LL operation.

- (c) On May 15, CO emissions increase beyond the site's air permit limit.
- (d) On June 25, after new HEGO sensors were installed, a drastic spike in both CO and NO_x emissions is observed, with levels of both species showing non-compliance with the existing air permit. Correlating this to the change in post-catalyst HEGO value, which is a significant drop from the post-catalyst HEGO setpoint, it indicates that the engine AFR migrated very rich, causing the observed increases in both CO and NO_x.
- (e) On August 20, the emissions are found to have decreased; however, CO is still above the air permit limit while NO_x is now within the acceptable range. At this time, the engine AFR likely moved leaner than where it was on June 25, settling in what would be considered an AFR rich region. The post-catalyst HEGO value is seen to rejoin the setpoint to which it is controlled.

The NO_x-CO crossplot in Figure 45 provides further insight about the AFR control behavior (migration to a very rich region) that occurred after the HEGO sensors were changed on June 25. Compared with this, on August 20, the control is seen to operate in a leaner region. During the period from February 27 to May 15, the controller maintains good AFR control, as evidenced by the tight grouping of data points from this period.

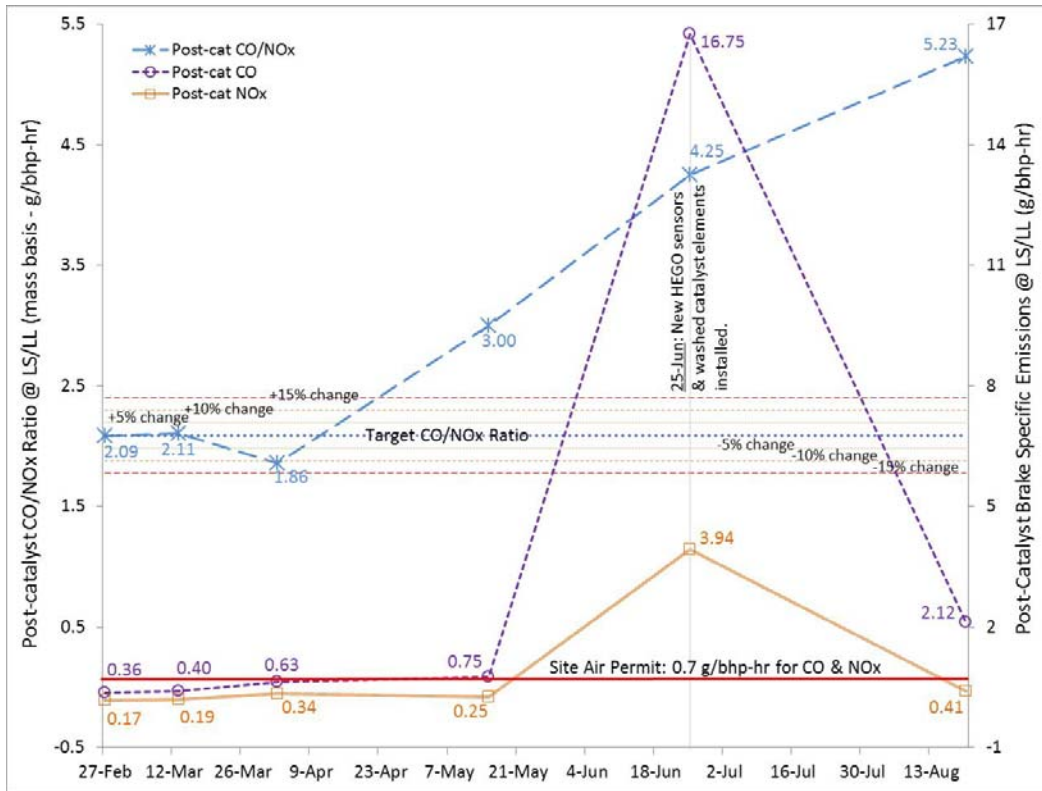


Figure 43: Trends of post-catalyst emissions and CO:NOx at LS/LL operation.

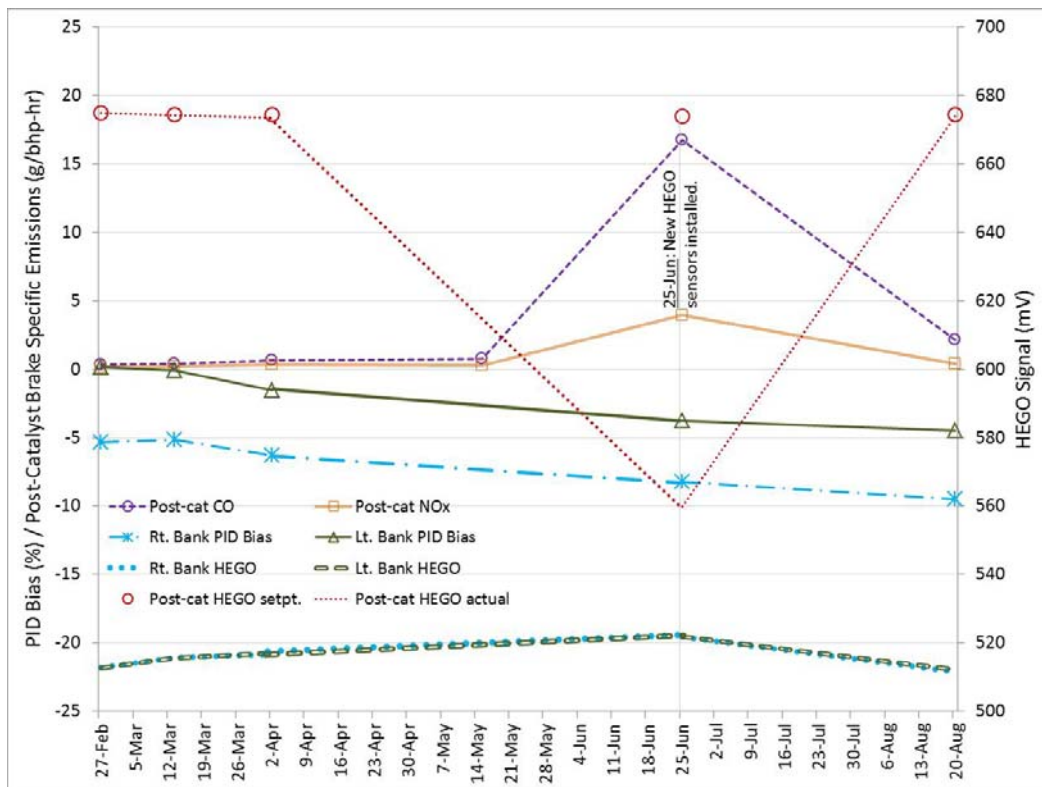


Figure 44: Trends of E3RB parameters and post-catalyst emissions @ LS/LL operation.

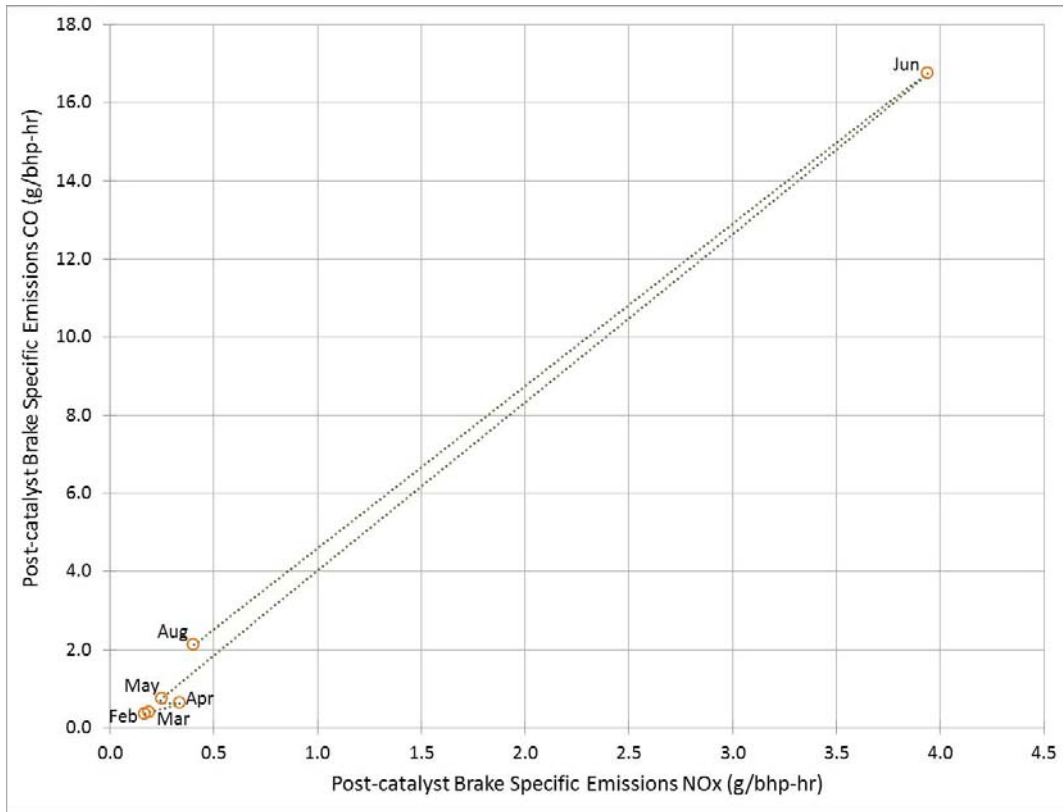


Figure 45: Post-catalyst NOx-CO crossplot @ LS/LL operation.

3.5 Retuned Performance

Upon completion of the 6 month evaluation test, the E3RB was retuned using data from an equivalence ratio (ϕ) sweep that was conducted to determine optimal settings for the post-catalyst setpoint @ HS/HL operation. The results of this ϕ sweep are shown in Figure 46, Figure 47, Figure 48, and Figure 49. A change in ϕ was simulated by altering the post-catalyst HEGO sensor setpoint; this accounts for the independent axis on all the above-mentioned figures being labeled as Post-catalyst HEGO setpoint. Based on the air quality permit limits assigned for this site, the NSCR control window at HS/HL operation was determined to lie between 618 mV for NOx (lower limit) and 646 mV for CO (upper limit).

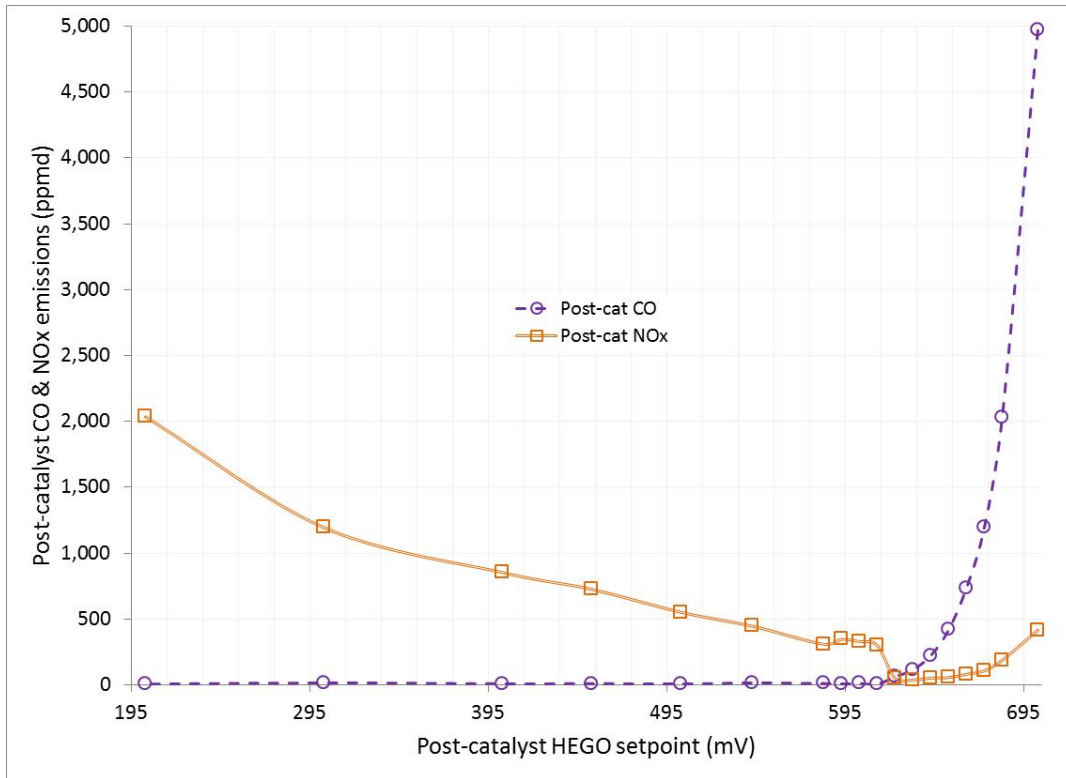


Figure 46: (Coarse scale) Simulated ϕ sweep vs. post-catalyst emissions.

Therefore, the nominal value for the setpoint was readjusted to be 633 mV, which is the midpoint between the upper and lower limits. When operating between these setpoint limits at HS/HL, the corresponding range of expected catalyst efficiencies are 95% \leftrightarrow 99% for NO_x and 97.6% \leftrightarrow 99.7% for CO.

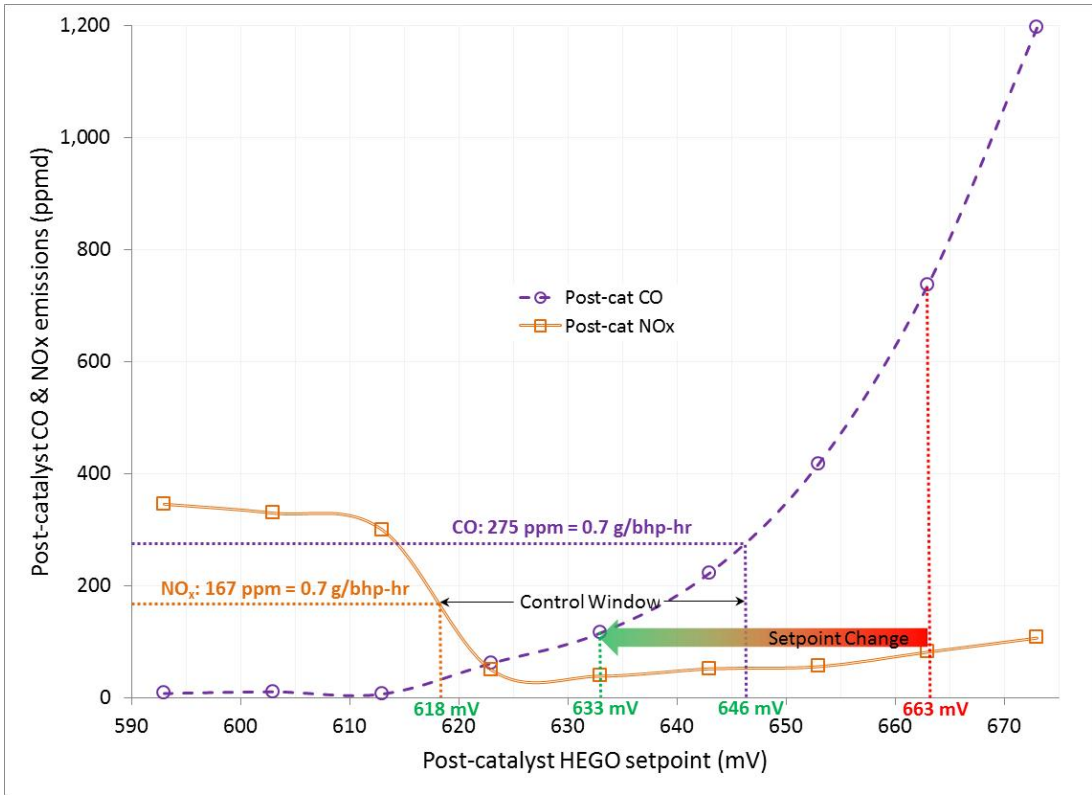


Figure 47: (Fine scale) Simulated ϕ sweep vs. post-catalyst emissions.

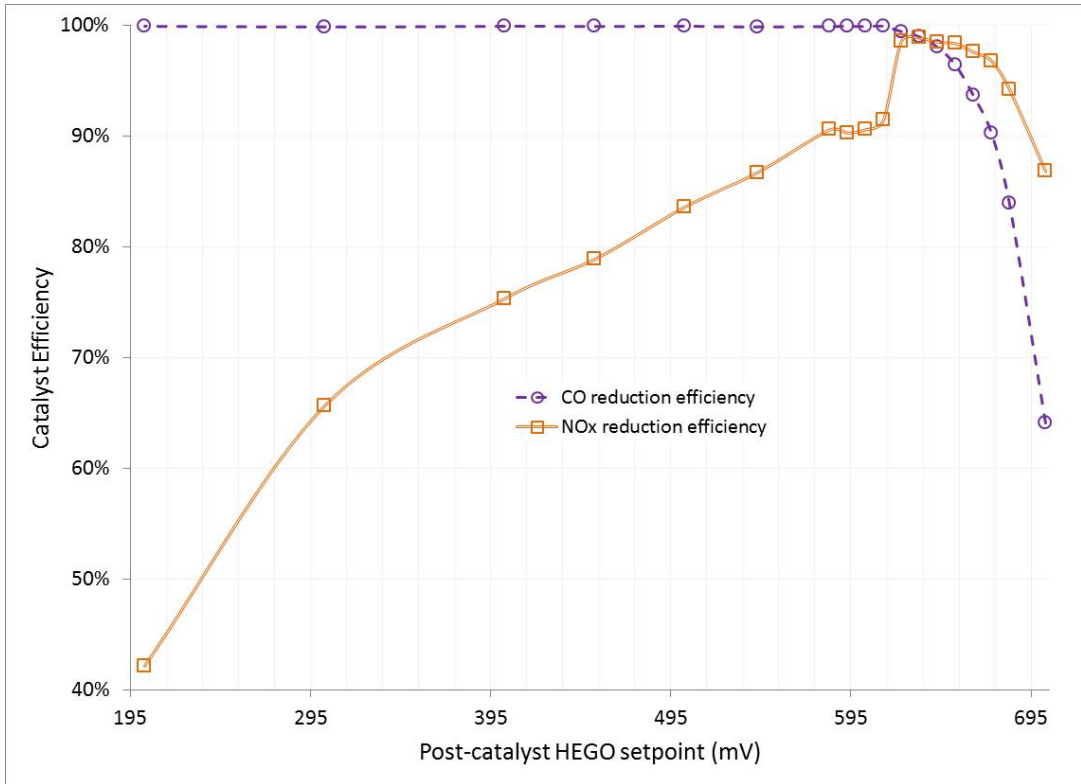


Figure 48: (Coarse scale) Simulated ϕ sweep versus catalyst efficiency.

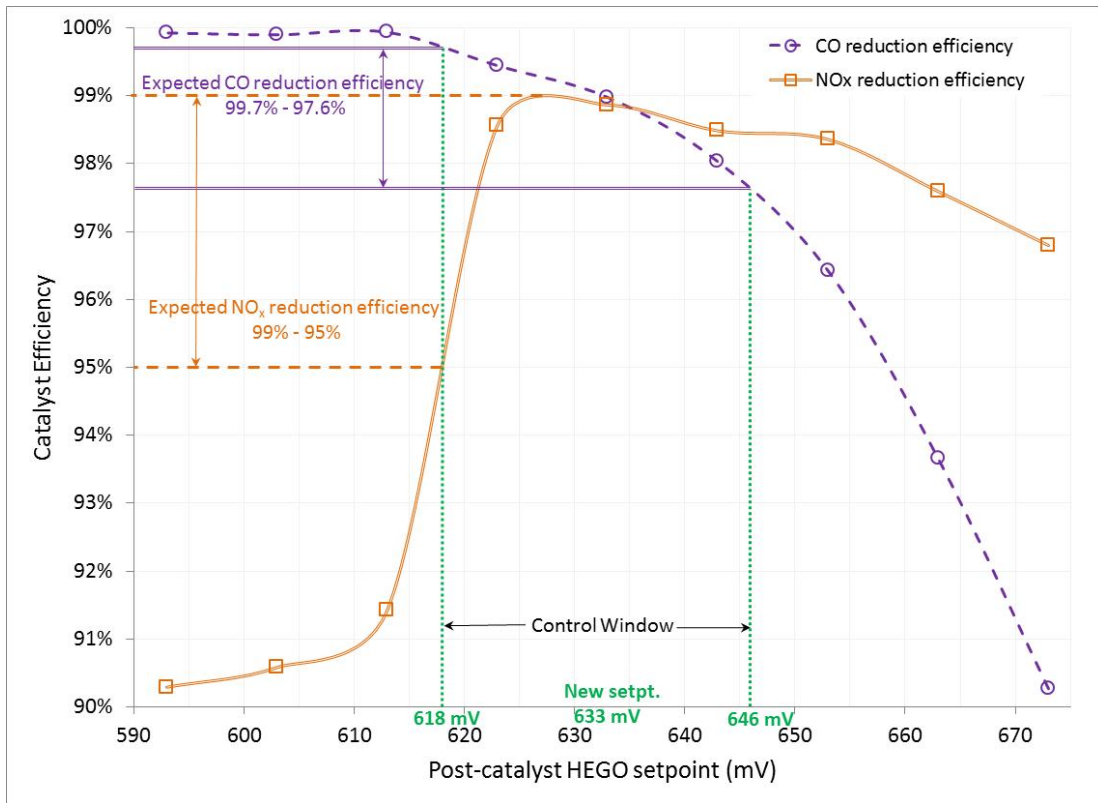


Figure 49: (Fine scale) Simulated ϕ sweep vs. catalyst efficiency.

Using a comparable percentage reduction, post-catalyst HEGO setpoints at MS/ML and LS/LL operation were similarly adjusted. Further fine-tuning was conducted at the HS/HL condition to determine optimal settings for dither frequency/amplitude as well as AFR setpoints (pre-catalyst HEGO setpoints). Upon completion of tuning, emission measurements were recorded at each engine operating condition so as to document any emissions performance enhancements created by this new E3RB settings.

An unexpected plateau in post-catalyst NOx emissions and corresponding reduction efficiency is noticed during the ϕ sweep, occurring between post-catalyst HEGO setpoints between 585 mV and 615 mV. When examining the pre-catalyst emissions trend during the ϕ sweep (Figure 50), it can be seen that between 195 mV & 545 mV, the engine moves toward

richer operation, which is expected as the post-catalyst signal transitions from low mV to high mV. Beginning at 545 mV and lasting until 595 mV, it is observed that the engine unexpectedly begins a lean excursion, as evidenced by the spike in NOx and dip in CO emissions; increasing this signal beyond 595 mV, the engine backtracks to rich operation. When contrasting this engine-out emissions trace against the corresponding post-catalyst emissions, the lean excursion that occurs between 545 mV - 595 mV does not appear to register on the post-catalyst trace. However, when analyzing catalyst efficiency for this same range of post-catalyst HEGO setpoint, the plateau in the NOx trend can be attributed to the lean excursion, which clearly disrupts the expected smooth increase in catalyst efficiency between 545 mV & 645 mV.

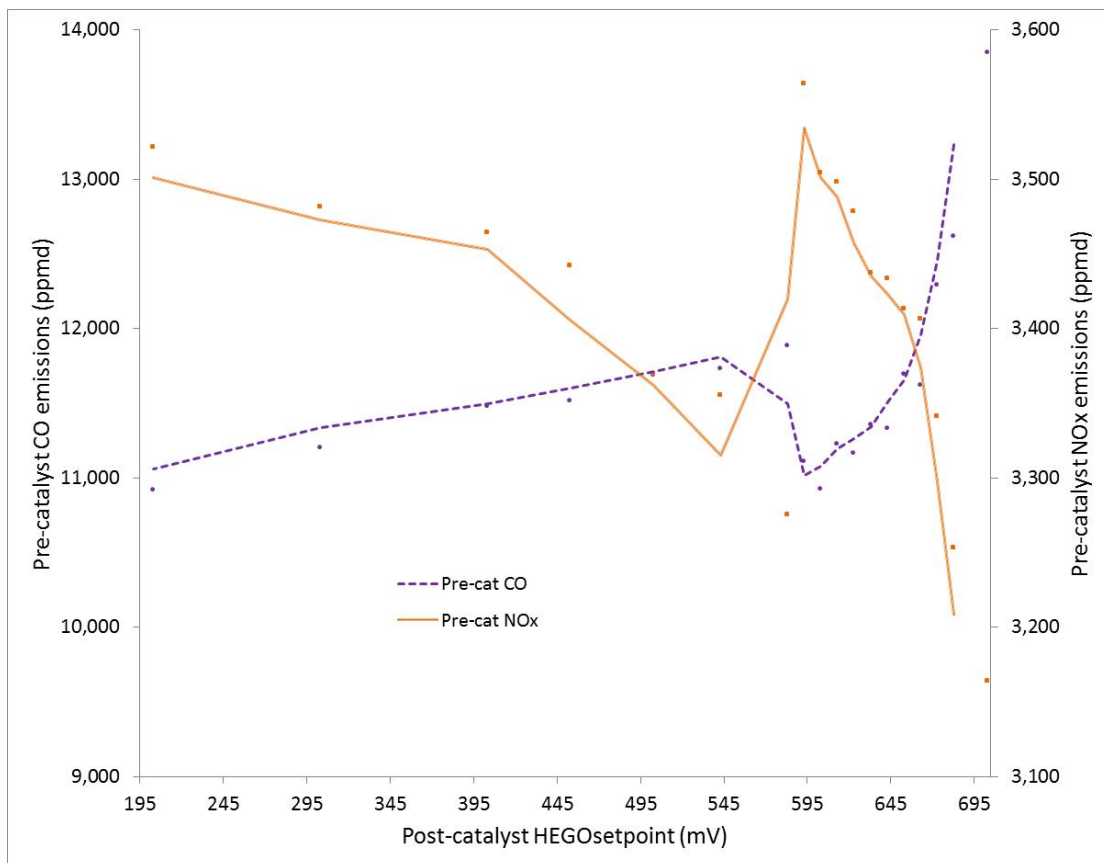


Figure 50: Simulated ϕ sweep vs. pre-catalyst emissions.

A possible explanation for this unexpected behavior is offered as follows:

Since the data was not recorded simultaneously (only one analyzer was used), an anomaly might have occurred during the pre-catalyst data segment that was not observed during the corresponding post-catalyst segment. An example of such an anomaly would be a temporary increase in oil leakage into the combustion chamber: since the O₂ sensors used to assess ϕ have varied responses to different fuels owing to the change in H/C and O/C ratios, and given that oil is a very different fuel than natural gas, during excessive oil leakage, the engine-out emissions will change but the O₂ sensor response will not reflect the appropriate ϕ value.

The emissions trend after retuning at HS/HL operation is seen in Figure 51. The post-catalyst CO:NOx ratio was readjusted to an acceptable value of 2.5, having respective CO and NOx contributions of 0.38 g/bhp-hr and 0.13 g/bhp-hr.

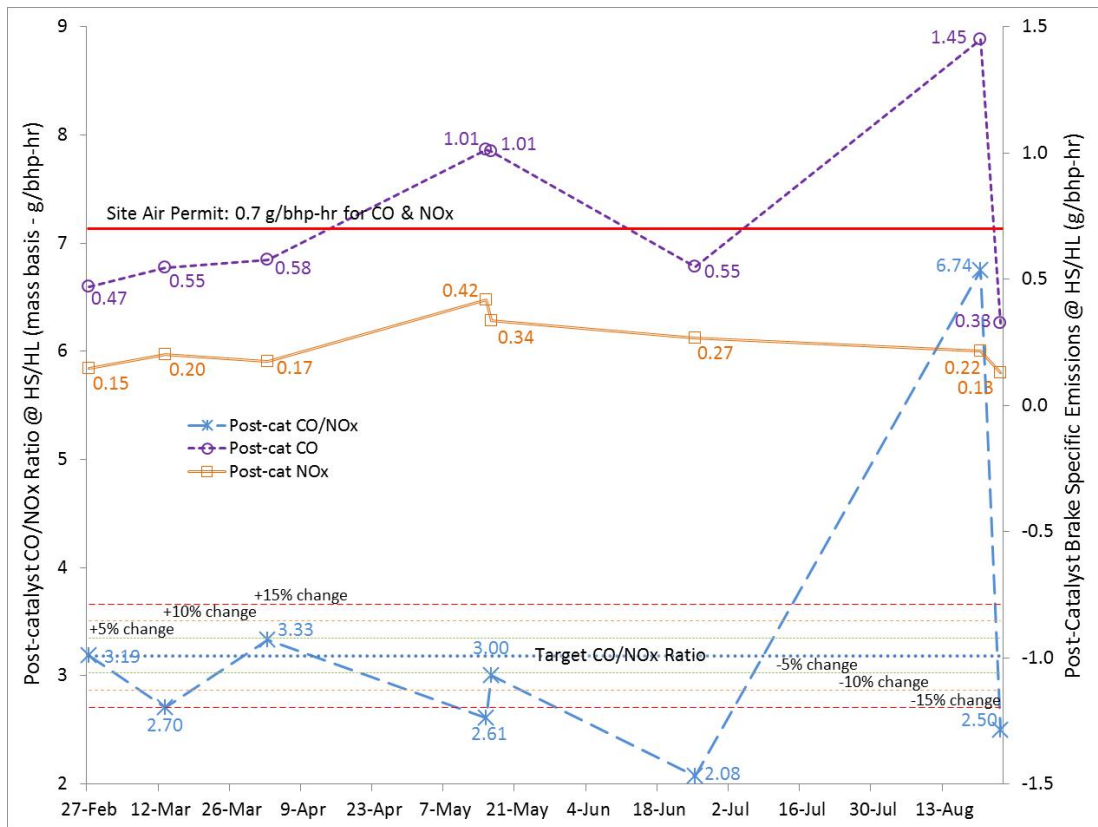


Figure 51: (New tuning) Trends of post-catalyst emissions and CO:NOx at HS/HL operation.

The emissions trend after retuning at MS/ML operation is shown in Figure 52. The post-catalyst CO:NOx ratio was readjusted to a value of 3.33, having respective CO and NOx contributions of 0.40 g/bhp-hr and 0.12 g/bhp-hr. While this is not an optimal CO:NOx ratio, it should be noted that time constraints prevented a ϕ sweep from being conducted to determine optimal controller settings at this operating condition. However, since emissions were within air permit limits for the site, performance was ascribed as satisfactory.

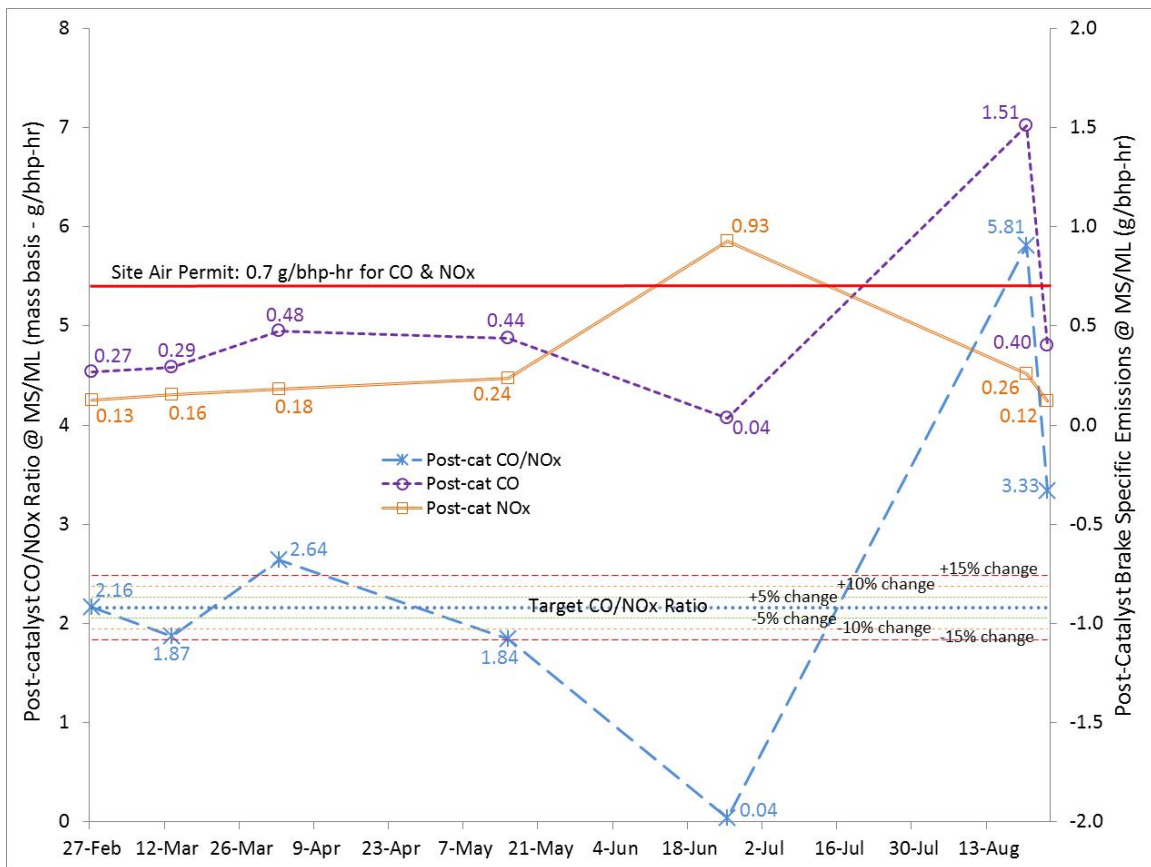


Figure 52: (New tuning) Trends of post-catalyst emissions and CO:NOx at MS/ML operation.

At the LS/LL condition, a cross-over occurred between CO and NOx emissions, indicating an AFR migration toward stoichiometry. This can also be deduced from the CO:NOx, in Figure 53, which plummeted to a value of 0.01, indicating an excess of NOx in the post-

catalyst exhaust gas stream. Despite the overage in NOx emissions (1.32 g/bhp-hr), E3RB settings were not optimized because it was concluded that the engine would likely never be used at this load point over the course of regular operations. A few attempts at minor adjustments in setpoints and PID biases showed the controller to be very sensitive at this load point; in one instance a change in post-catalyst HEGO setpoint of 1 mV created a cross-over scenario in which CO was over the limit and NOx, under.

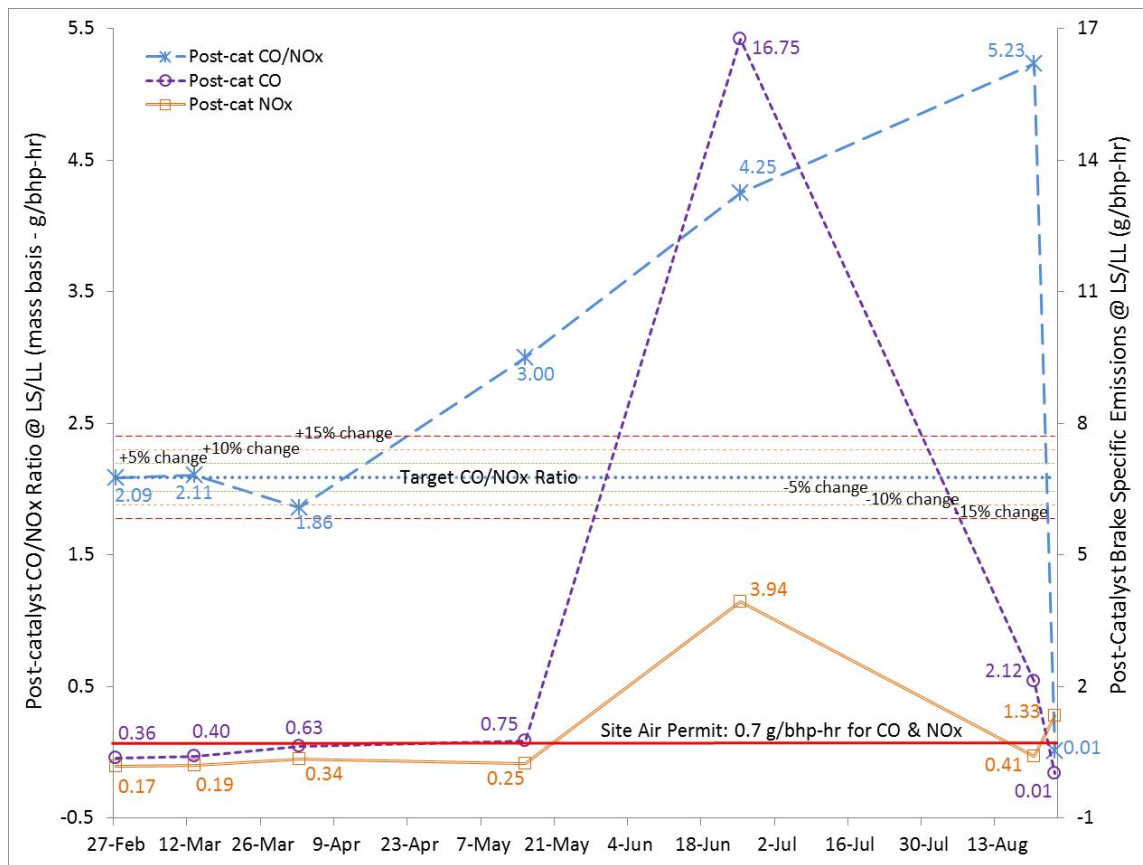


Figure 53: (New tuning) Trends of post-catalyst emissions and CO:NOx at LS/LL operation.

3.6 Fuel Gas Composition

In order to investigate the effect of variation in fuel gas composition on engine performance and related emissions output, a portable gas chromatograph was deployed at the site

from May 15 to May 16, during which time fuel gas composition was monitored for a period of 16 hours; Figure 54 shows the fuel gas composition recorded over a 12-hour subset of this same period. Methane composition in the fuel is seen to be stable, varying between 82 – 85 mole %, while CO₂ and Propane vary between 3.5 – 4% and 2.5 – 3 mole%, respectively. Ethane was not identified in the chromatogram owing to a peak-shift. The post-catalyst NO_x emissions for the same time period, recorded via SCADA as 15-minute averages, can be seen to fluctuate from 15 – 85 ppm. NO_x data for hours 1.5 – 5.5 were recorded as negative values and are not plotted in the figure.

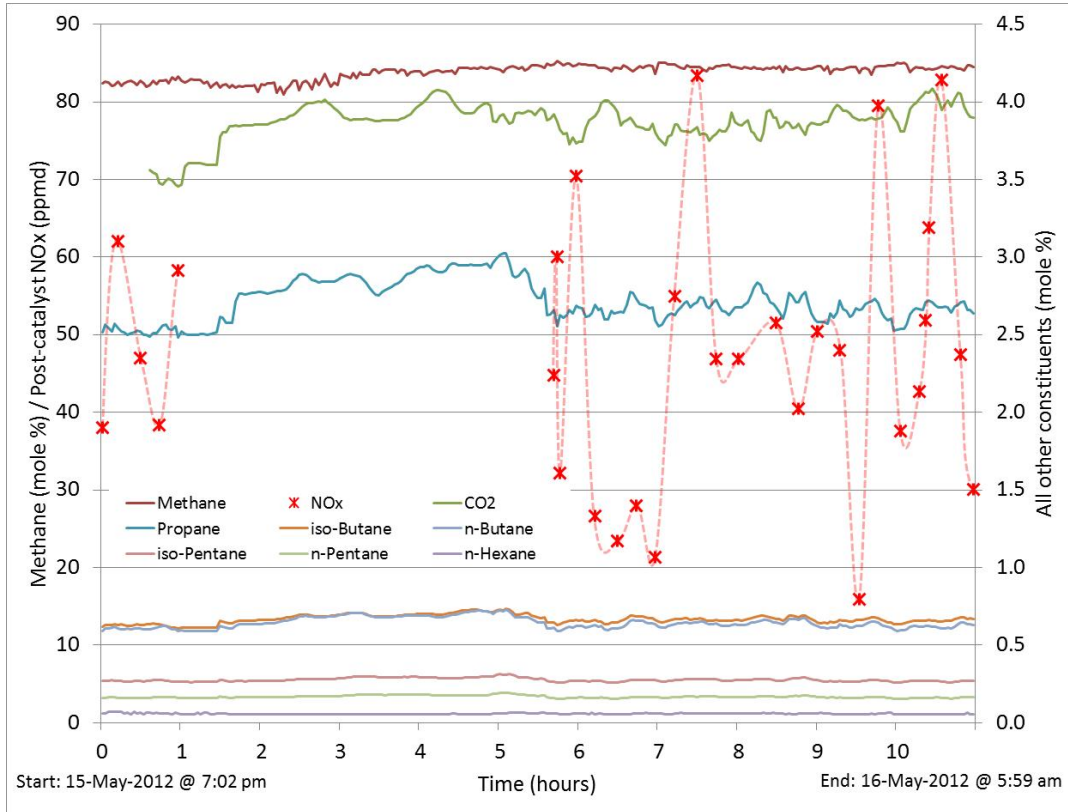


Figure 54: 12-hour trend of fuel gas composition and NO_x emissions.

Based on the trends in Figure 54, the following conclusions can be made:

- (i) Fuel gas composition at this site was stable during the monitoring period.

- (ii) Variations in NO_x emissions that occurred during this period are unrelated to fuel gas composition.

3.7 Diurnal Cycle

A 24-hour evaluation of E3RB operation was conducted from June 26th to 27th, encompassing one full diurnal cycle. During this time, engine emissions were monitored at speed/load settings determined by field operators; average engine speed was 1140 RPM and average load (as represented by the total inducted charge into the engine) was 2150 scfm. From an earlier section, it can be recalled that the ‘Total Inducted Charge’ is a parameter used by the E3RB controller (referred as Q_{mix}) to ascertain the operational load point of an engine. From Figure 55, NO_x emissions are seen to vary between 0.22 – 0.34 g/bhp-hr over the period of interest, while CO emissions range between 0.54 – 0.79 g/bhp-hr. From the CO:NO_x trend, it can be seen that the E3RB controls AFR within a narrow band of operation from Hour 2 – 12, beyond which there is a gradual richening of AFR until hour 17. At hour 18, there is a noticeable drop in CO:NO_x, indicating AFR migration to leaner conditions, followed by a gradual migration back to a richer region, comparable to operation during hours 3 – 7. In summary, although CO slightly exceeded the limit, there was sufficient compliance margin for NO_x that would allow the controller to be leaned out.

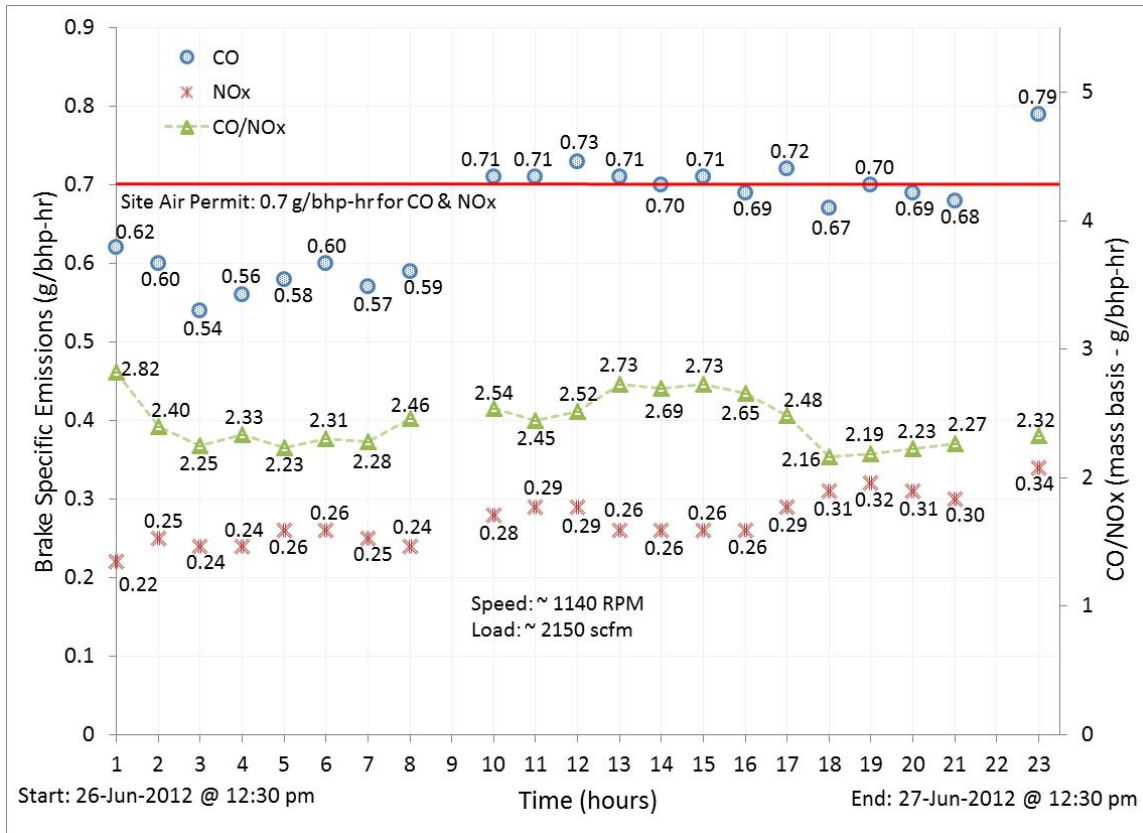


Figure 55: 24-hour evaluation of E3RB performance.

3.8 Remote Monitoring

During intervals between site visits, emissions were remotely monitored using NOx sensor output to SCADA. The accuracy of the post-catalyst NOx sensor was ± 30 ppm while that of the pre-catalyst sensor was $\pm 3\%$ of the measured reading. An analysis of the operating conditions (engine speed and load) showed that the engine was operating at or near the HS/HL point for over 95% of the time, during the period from April 4 to August 20. From the daily-average post-catalyst NOx trend in Figure 56, it can be seen that NOx emissions at HS/HL exceeded site air permit limits on April 24 (168 ppm), May 27 (173 ppm), May 28 (184 ppm), May 29 (184 ppm), and August 16 (204 ppm). It should be noted that given the low accuracy of

the post-catalyst sensor, only the recorded daily average of 204 ppm (on August 16) is of particular concern, with regards to exceeding the site air permit. It is not clear as to the reason for this emissions behavior on August 16. Between E3RB commissioning on February 20 and April 4, the post-catalyst NO_x sensor was not functioning properly therefore, the data for this period has been omitted from the NO_x trend.

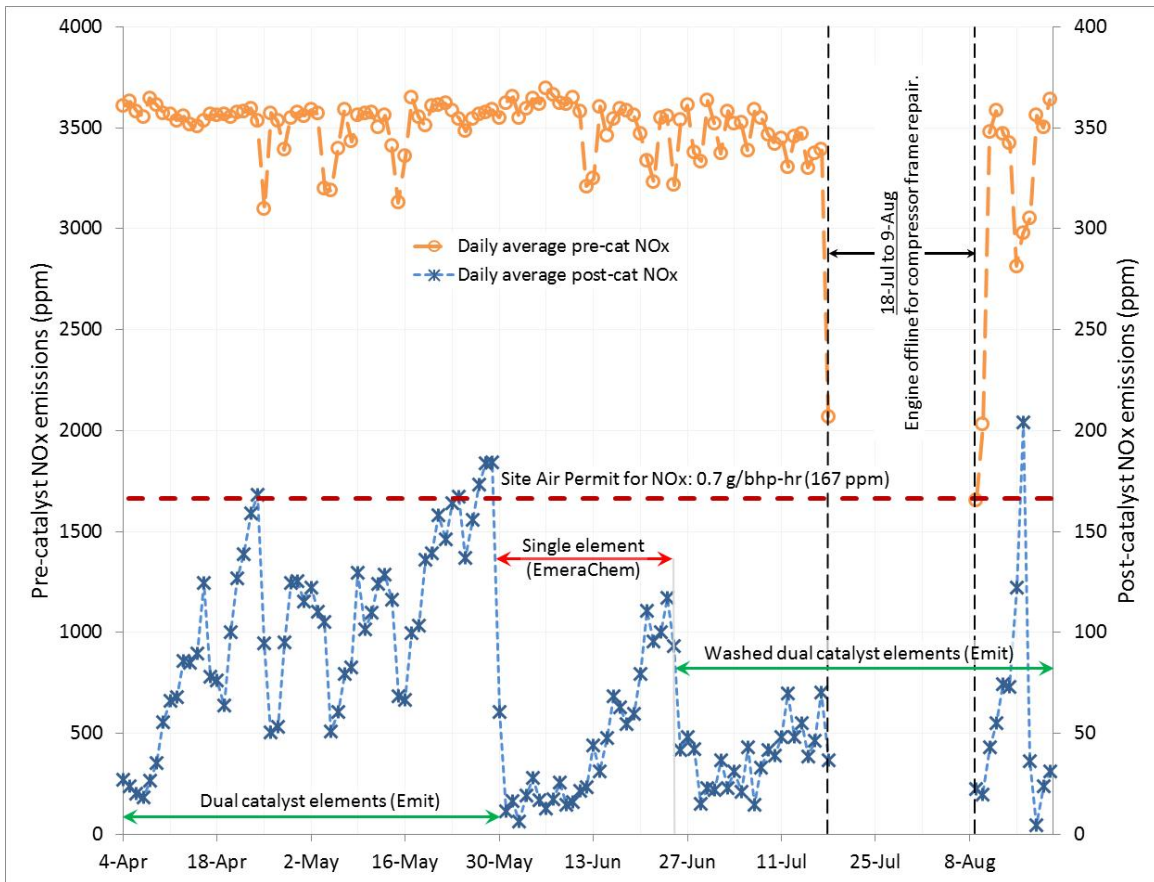


Figure 56: Daily average NO_x trends obtained from SCADA.

3.9 Transient Performance

3.9.1 Load Steps

The E3RB's transient response was monitored during load steps between each operating condition, as previously outlined in Table 4. An example of this transient response monitoring is provided in Figure 57, during a load change from HS/HL to MS/ML. The E3RB's dithering strategy can be observed in the trends for right and left bank HEGO actual. It can be seen that engine speed and load stabilize within the first 3 minutes and that E3RB HEGO signals (setpoints and actual) stabilize shortly thereafter (ie. within the following 2 – 3 minutes). This can be considered a good response to changes in engine operating condition. As can be expected, there is a slight decrease in both manifold air pressure (MAP) and temperature (MAT) in each bank, when transitioning to a lower speed/load point. However, this is hard to distinguish owing to the coarse scale used on the secondary y-axis. Similar trends for E3RB transient responses for each load changes during every site visit can be viewed in Appendix D.

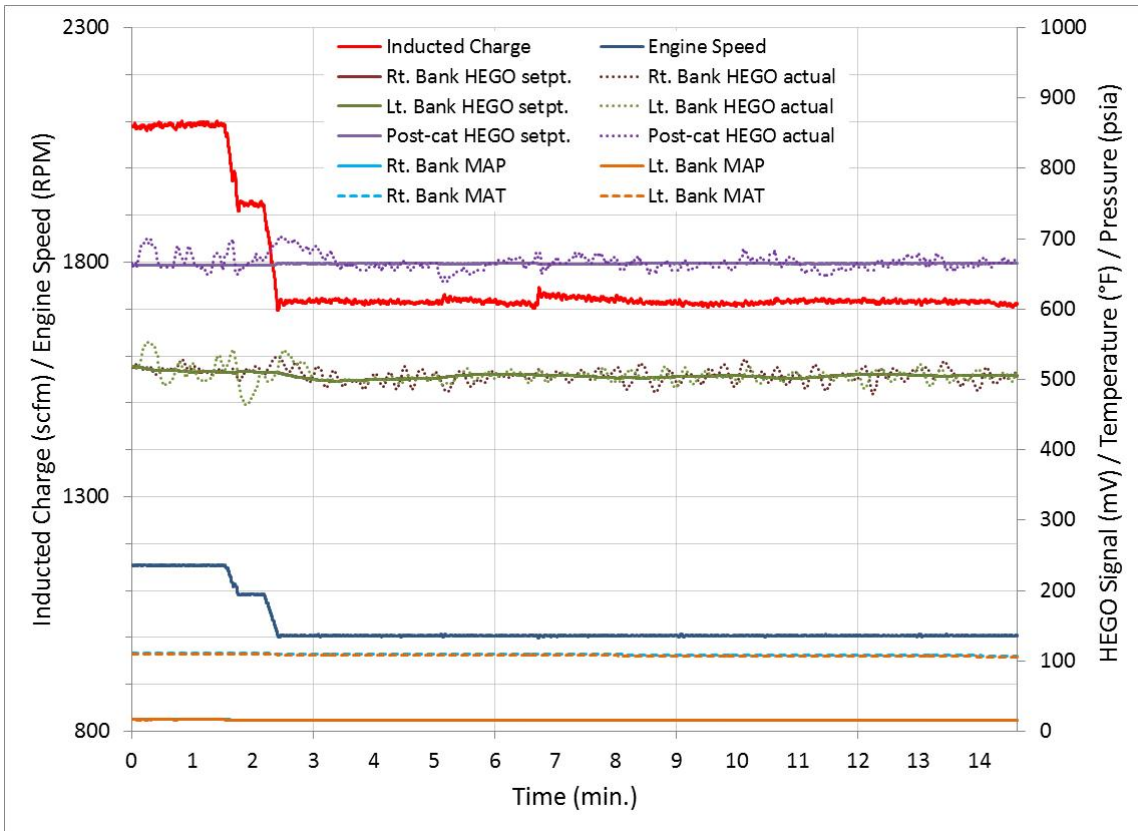


Figure 57: Transient response of E3RB parameters during load step from HS/HL to MS/ML.

3.9.2 Shutdown

E3RB response during an engine shutdown event on March 12 is shown in Figure 58. Of particular interest is the control behavior once the load drops below the threshold of 1000 scfm; from this time forward until shutdown, the actual HEGO signals diverge significantly from their respective setpoints, indicating a transition from closed-loop to open-loop setpoint tables.

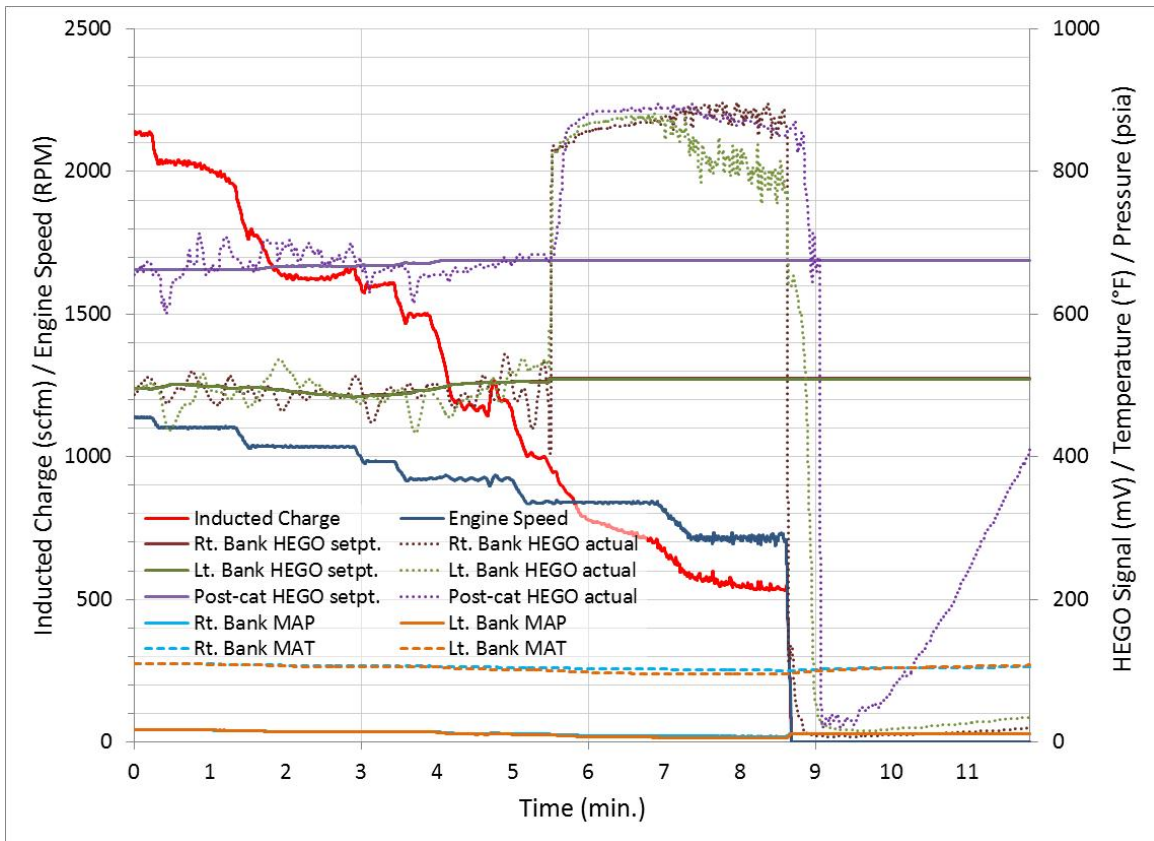


Figure 58: Transient response of E3RB parameters during engine shutdown on March 12.

3.9.3 Startup

Similarly, E3RB response was also recorded during an engine startup event on March 12. From Figure 59, it can be seen that the engine attains stable speed and load settings from minute 6, the pre-catalyst HEGO signals stabilize by minute 9, and the actual post-catalyst HEGO signal stabilizes by around minute 21. From an emissions perspective, the duration of the latter signal's instability roughly correlates with the period that NO_x emissions exceed the air permit (Figure 60). On the other hand, CO emissions are very reasonable until minute 20, after which time, it begins to exhibit spikes that exceed the air quality limit (Figure 61). The crossover in CO and

NOx emissions that occur during this time period is indicative of AFR migration from stoichiometry to rich operation.

It should be noted that while concentrations of NOx and CO, in certain instances, do exceed the limit, it does not represent an out-of-compliance condition since regulatory bodies allow a period of between 30 and 60 minutes following startup during which engine emissions are exempt from the air quality permit requirements issued for a given site.

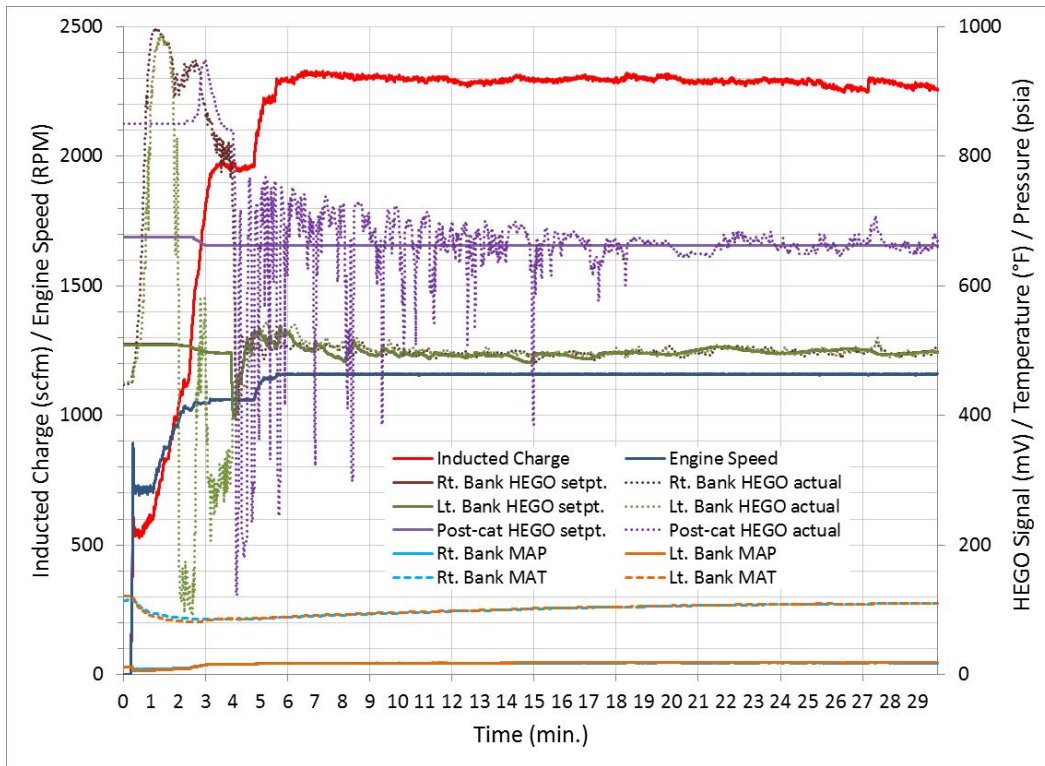


Figure 59: Transient response of E3RB parameters during engine startup on March 12.

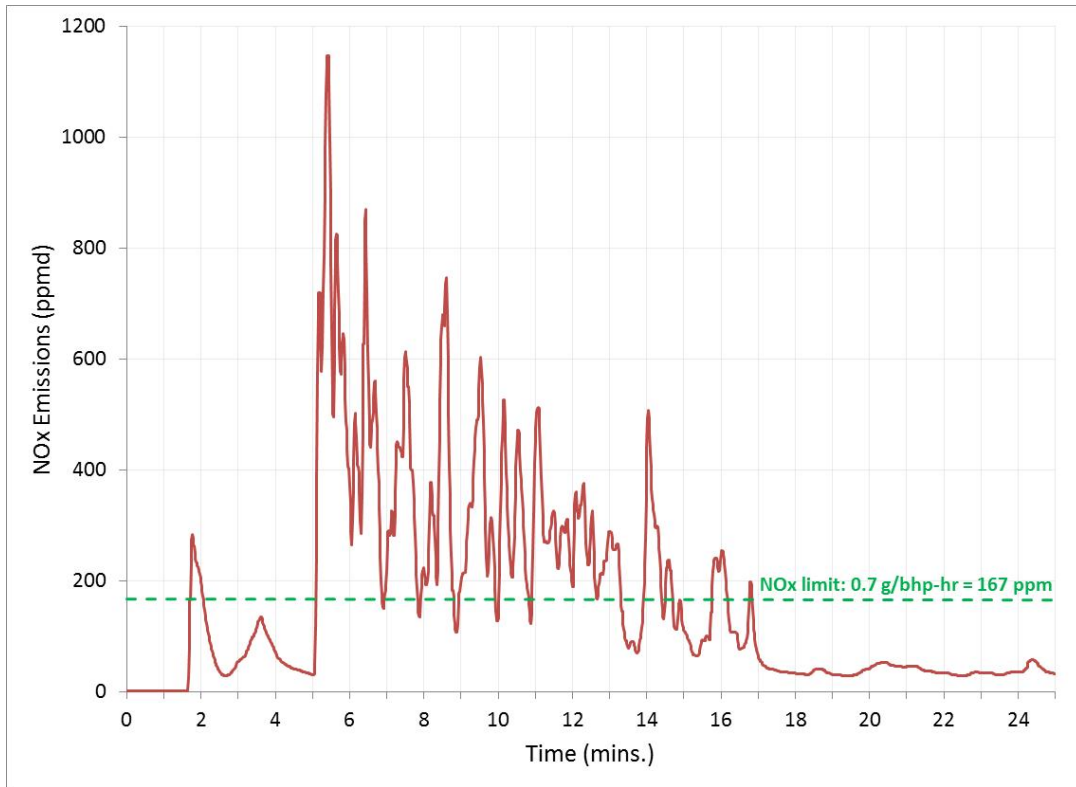


Figure 60: NOx emissions during engine startup on March 12.

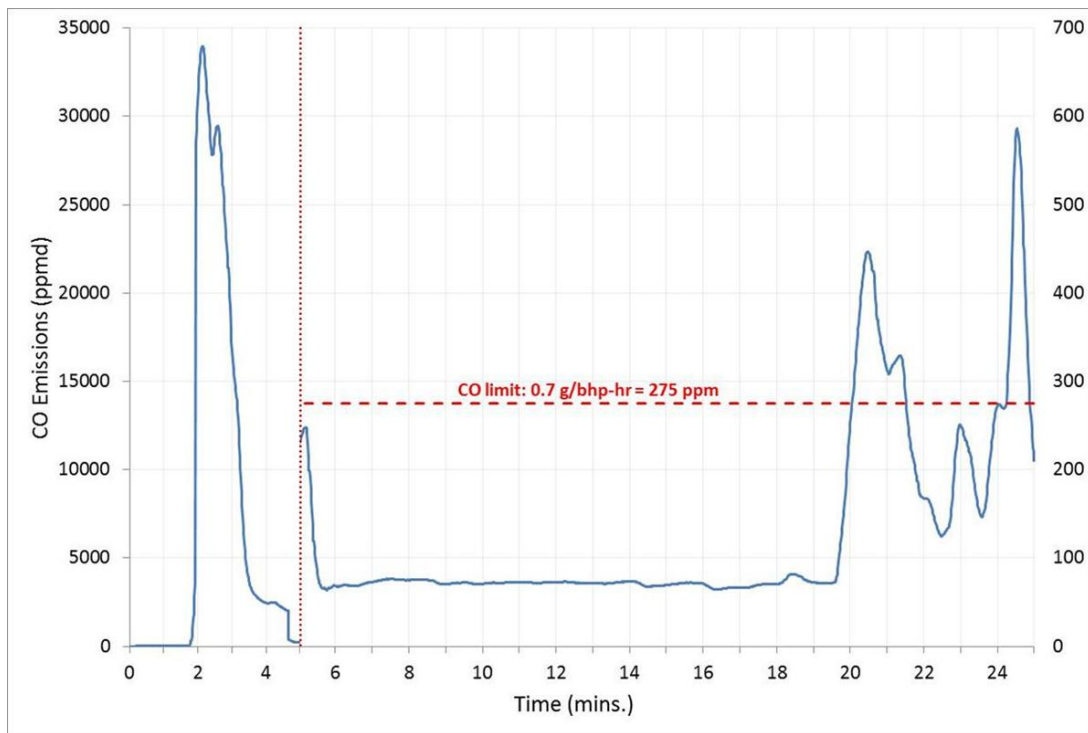


Figure 61: CO emissions during engine startup on March 12.

4. Conclusions and Recommendations

Performance of the E3RB AFR controller was evaluated for 6 months, starting February 20 and ending August 20. During this time, emissions monitoring site visits were conducted to assess controller performance. Based on the results presented in the previous section, the following conclusions and recommendations are made:

1. For the initial three month period (February 17 to May 15), the controller showed excellent AFR control of engine outlet emissions despite high lubrication oil consumption which could have caused degradation of the HEGO sensors. This demonstrated the robust capabilities of the E3RB in its ability to handle extraneous variables relating to engine health and assuring sustained sensor health.
2. For at least a 2-½ month period, as-found tests demonstrated compliance with emission limits, after the ash had been blown out of the catalyst. However, emissions taken May 15, June 25, and August 20 showed erratic behavior. Attempts to correct the problems included replacement of sparkplugs, replacement of HEGO sensors, and installation of a washed dual-element catalyst. Ash from high oil consumption had compromised the ability to verify E3RB performance.
3. Upon completion of the 6 month evaluation test, the engine was easily brought back into compliance by retuning the E3RB controller (changing the post-catalyst HEGO set point). Some of the problems encountered after May 15 may have been corrected by adjusting the controller.
4. As evidenced during the first three months of operation and subsequent diurnal tests, the E3RB's performance as a multi-point AFR control system was consistent, demonstrating

appropriate AFR adjustments to variation in engine operation, over a wide range of ambient conditions.

5. Due to the high levels of lubrication oil consumption, transient testing results were inconclusive.
6. The evaluation demonstrated proper operation of several alarms including misfire, system rich/lean, sensor failure, post-catalyst high temperature, pre-catalyst high temperature, and pre-catalyst low temperature.

5. References

1. DeFoort, M., Olsen, D., Willson, B., 2004. "The Effect of Air-Fuel Ratio Control Strategies on Nitrogen Compound Formation in Three-Way Catalysts," International Journal of Engine Research, Vol. 5, No. 1, pp 91-122.
2. Amadu, S., Olsen, D., 2008. "Operating Characteristics of an NSCR Catalyst on an 80 kW Cummins-Onan Genset," GMRC Gas Machinery Conference 2008.
3. Nuss-Warren, S., Toema, M., Chapman, K., McCarthy, J., McGrath, T., 2008. "Characterization of NSCR Performance on Four Stroke Natural Gas-Fueled Rich Burn Engines," GMRC Gas Machinery Conference 2008.
4. Tice, J., Nowak, C., Wachowiak, R., Allen, C., 2012. "Development and Field Test of an Advanced Air Fuel Ratio Controller in Pipeline Service," GMRC Gas Machinery Conference 2012.
5. Mizutani, A., Okawa, T., Matsuzaki, H., Kubota, H., Hosogai, S., 1998. "Oxygen Sensor for CNG Application as ULEV or Tighter Emission Vehicle," SAE Technical Paper 980264.
6. Personal communication between R. Joseph and Woodward application engineer.
7. DCL International Inc. (<http://www.dcl-inc.com/threewaycatalyst>)
8. Woodward E3RB Application Manual, Document # 26473; Revision/Version: N.A.
9. Personal communication between R. Joseph, field operators, and emissions monitoring personnel.
10. Acres, C. J. K., Thomas, J. M., Zamarev, K. I., 1991. "Perspectives in Catalysis," Blackwell Science Ltd.

11. Gandhi, H. S., Shelef, M., 1987. "The role of research in the development of new generation automotive catalysts," Catalysis and Automotive Pollution Control, p.200. Elsevier Science Ltd.
12. Stein, H. J., 1996. "Diesel oxidation catalysts for commercial vehicle engines: strategies on their application for controlling particulate emissions," Applied Catalysis B: Environmental, Vol. 10, pp 69-82.
13. Faiz, A., Weaver, C. S., Walsh, M. P., 1996. "Air Pollution from Motor Vehicles: Standards and Technologies for Controlling Emissions," World Bank Publications.
14. Zhang, C. B., He, H., Yu, Y. B., Zhang, R. D., 2004. "Research of selective catalytic reaction of NO with propene over catalyst Cu/Al₂O₃ in excess oxygen," Higher Education Press, Vol. 25, pp 136-139.
15. Griffin, J. D., Kolda, T. G., Lewis, R. M., 2006. Sandia National Laboratories Report # SAND 2006-4621.
16. BASF Corp. (<http://www.catalysts.basf.com/p02/USWeb-Internet/catalysts/en/content/microsites/catalysts/prods-inds/mobile-emissions/Int>)
17. Heywood, J. B., 1988. "Internal Combustion Engine Fundamentals," McGraw-Hill Publishers.
18. Pulkrabek, W., 2004. "Engineering Fundamentals of the Internal Combustion Engine," 2nd ed., Pearson Prentice Hall Publications.
19. Gattoni, J., 2012. "Advanced Control Techniques and Sensors for Gas Engines with NSCR," M.S. Thesis, Colorado State University, Fort Collins, Colorado.
20. Williams, S., Hu, L. (R.), Nakazono, T., Ohtsubo, H., Uchida, M., 2009. "Oxidation Catalysts for Natural Gas Engine Operating under HCCI or SI Conditions," SAE

International Journal of Fuels and Lubricants, Vol. 1, No. 1, pp 326-337. SAE Document 2008-01-0807.

21. Lampert, J., Kazi, M., Farrauto, R., 1997. "Palladium catalyst performance for methane emissions abatement from lean burn natural gas vehicles," Applied Catalysis B: Environmental, Vol. 14, pp 211-223.
22. McCormick, R., Newlin, A., Mowery, D., Graboski, M., Ohno, T., 1996. "Rapid Deactivation of Lean-Burn Natural Gas Engine Exhaust Oxidation Catalysts," SAE Technical Paper 961976.
23. Winkler, A., Ferri, D., Aguirre, M., 2009. "The influence of chemical and thermal aging on the catalytic activity of a monolithic diesel oxidation catalyst," Applied Catalysis B: Environmental, Vol. 93, pp 177-184.
24. Office of the Chief Economist, International Energy Agency (IEA), 2011. "Are we entering a golden age of gas?," Special Report – World Energy Outlook 2011.
http://www.worldenergyoutlook.org/media/weowebiste/2011/WEO2011_GoldenAgeofGasReport.pdf
25. Energy Information Administration (U.S. Department of Energy), 2011. "Review of Emerging Resources: U.S. Shale Gas and Shale Oil Plays".
<http://www.eia.gov/analysis/studies/usshalegas/pdf/usshaleplays.pdf>
26. Bonanza Creek Energy, Inc. (<http://www.bonanzacrk.com/about-bonanza/technology-innovation/>)
27. Personal communication between R. Joseph and Dr. D. B. Olsen.

Appendix A: Engine Specifications

Specifications

Cylinders: V12
Piston Displacement: 7040 cu. in. (115 L)
Bore & Stroke: 9.375" x 8.5" (238 x 216 mm)
Compression Ratio: 8:1
Jacket Water System Capacity: 100 gal. (379 L)
Lube Oil Capacity: 190 gal. (719 L)
Starting System: 125 - 150 psi air/gas 24V electric
Dry Weight: 21,000 lb. (9,525 kg)

Standard Equipment

AIR CLEANER – Two, 3" dry type filter with hinged rain shield and service indicator.

AIR FUEL RATIO CONTROL (AFR) – Integrated ESM® - AFR catalyst rich-burn control, main fuel gas regulator actuators, exhaust O2 sensor(s), and post turbocharger exhaust thermocouple. Factory mounted and tested. AFR maintains emissions through load and speed changes. The ESM AFR meets Canadian Standards Association Class 1, Division 2, Group A, B, C & D (Canada & US) hazardous location requirements. Note: For dual fuel applications, ESM AFR system will control the primary fuel source only.

BARRING DEVICE – Manual.

BATTERY BOX – Ship loose battery box designed to accommodate two series 31 12 VDC batteries. Includes power disconnect switch and 20 foot (6.1 m) cable for connection to ESM Power Distribution Box.

BEARINGS – Heavy duty, replaceable, precision type.

BREATHER – Self regulating, closed system.

CONNECTING RODS – Drop forged steel, rifle drilled.

CONTROL SYSTEM – Waukesha Engine System Manager (ESM) integrates spark timing control, speed governing, detonation detection, start-stop control, diagnostic tools, fault logging and engine safeties. Engine Control Unit (ECU) is central brain of the control system and main customer interface. Interface with ESM is through 25 foot (7.6 m) harness to local panel, through MODBUS RTU slave connection RS-485 multidrop hardware, and through the Electronic Service Program (ESP). Customer connections are only required to the local panel, fuel valve, and 24V DC power supply. Compatible with Woodward load sharing module. ESM meets Canadian Standards Association Class 1, Division 2, Group A, B, C & D (Canada & US) hazardous location requirements.

CRANKCASE – Integral crankcase and cylinder frame. Main bearing caps drilled and tapped for temperature sensors. Does not include sensors.

CRANKSHAFT – Forged steel, seven main bearings, counterweighted and dynamically balanced.

CYLINDERS – Removable wet bairnitic cast iron type cylinder liners, chrome plated on outer diameter.

CYLINDER HEADS – Twelve interchangeable. Four valves per cylinder, with water cooled exhaust valve seats. Roller valve lifters and hydraulic push rods. Flange mounted ignition coils.

ELECTRONIC SERVICE PROGRAM (ESP) – Microsoft® Windows-based program provided on CD-ROM for programming and interface to ESM. Includes E-Help for troubleshooting any ESM faults. Serial harness is provided for connection of a customer supplied laptop to the ECU RS-232 port.

ENGINE MONITORING DEVICES – Factory mounted and wired sensors for lube oil pressure and temperature; intake manifold temperature and pressure; overspeed; and jacket water temperature; all accessible through ESM®. ESM continually monitors combustion performance through accelerometers to provide detonation protection. Dual magnetic pick-ups are used for accurate engine speed monitoring. ESM provides predictive spark plug diagnostics as well as advanced diagnostics of engine and all ESM sensors and logs any faults into non-volatile flash memory. Sensors meet Canadian Standards Association Class 1, Division 2, Group A, B, C, & D (Canada & US) hazardous location requirements.



Average may not be an accurate representation of this model.

ENGINE ROTATION – Counterclockwise when facing flywheel.

EXHAUST OUTLET – Single vertical at rear. Flexible stainless steel connection with 8" (203 mm) pipe flange.

FLYWHEEL – Approx. WRF = 155000 lb-in²; with ring gear (208 teeth), machined to accept two drive adapters: 31.88" (810 mm) pilot bore, 30.25" (768 mm) bolt circle, (12) 0.75" - 10 tapped holes; or 28.88" (734 mm) pilot bore, 27.25" (692 mm) bolt circle, (12) 0.625" - 11 tapped holes and (12) 0.75" - 10 tapped holes.

FLYWHEEL HOUSING – No. 00 SAE.

FUEL SYSTEM – Single 3" ANSI flange fuel inlet connection. Two natural gas, 4" (102 mm) updraft carburetors and two mounted Fisher 99, 2" (51 mm) gas regulators, 30-60 psi (207-414 kPa) fuel inlet pressure required. 10 foot (3 m) harness provided for ESM control of customer supplied fuel shutoff valve.

GOVERNOR – Electric throttle actuator controlled by ESM with throttle position feedback. Governor tuning is performed using ESP. ESM includes option of a load-coming feature to improve engine response to step loads.

IGNITION SYSTEM – Ignition Power Module (IPM) controlled by ESM, with spark timing optimized for any speed-load condition. Dual voltage energy levels automatically controlled by ESM to maximize spark plug life. Shielded ignition components meet Canadian Standard Association Class 1, Division 2, Group A, B, C & D (Canada & US) hazardous location requirements.

INTERCOOLER – Air-to-water.

LEVELING BOLTS

LIFTING EYES – Requires 9.5 ton Working Load Limit (W.L.L.) anchor shackles.

LUBRICATION – Full pressure, gear type pump. Engine mounted full flow lube oil micro-fiberglass filters with mounted differential pressure gauge. MICROSPIN® bypass filter, engine mounted. Air/gas motor driven prelube pump, requires final piping.

MANIFOLDS – Exhaust, (2) water cooled.

OIL COOLER – Shell and tube type, with thermostatic temperature controller and pressure regulating valve. Factory mounted.

OIL PAN – Deep sump type. 190 gallon (719 L) capacity, including filter and cooler.

PAINT – Oilfield orange primer.

PISTONS – Aluminum with floating pin. Oil cooled. 8:1 compression ratio.

SHIPPING SKID – For domestic truck or rail.

TURBOCHARGERS – (2) with water-cooled bearing housing and adjustable wastegates.

VIBRATION DAMPER – Viscous type.

WATER CIRCULATING SYSTEM, AUXILIARY CIRCUIT – Belt driven water circulating high capacity pump for intercooler and lube oil cooler. See S6543-36 performance curve for use with standard 10" diameter crankshaft pulley.

WATER CIRCULATING SYSTEM, ENGINE JACKET – Belt driven water circulating pump. Cluster type thermostatic temperature regulating valve, full flow bypass type with 165° - 170° F (74° - 77° C) start to open thermostats. Flange connections and mating flanges for (2) 4" (102 mm) inlets and (1) 5" (127 mm) outlet.

POWER RATINGS: L7044GSI VHP Series Four Gas Engines

Model	C.R.	Bore & Stroke in. (mm)	Displ. cu. in. (litres)	Brake Horsepower (kWb Output) 130°F (54°C) I.C. Water Temperature							
				1200 RPM		1000 RPM		900 RPM		800 RPM	
				C	I	C	I	C	I	C	I
L7044GSI	8:1	9.375" x 8.5" (238 x 216)	7040 (115)	1680	1680	1400	1400	1260	1260	1120	1120
				(1253)	(1253)	(1044)	(1044)	(940)	(940)	(835)	(835)

		1200 rpm	1000 rpm
Emissions	Power bhp (kWb)	1680 (1253)	1400 (1044)
	BSFC (LHV) Btu/bhp-hr (kJ/kWh)	7744 (10955)	7559 (10693)
	Fuel Consumption Btu/hr x 1000 (kW)	13010 (3813)	10583 (3101)
	NOx g/bhp-hr (mg/nm ³ @ 5% O ₂)	13.30 (4922)	12.90 (4782)
	CO g/bhp-hr (mg/nm ³ @ 5% O ₂)	11.20 (4140)	9.40 (3477)
	THC g/bhp-hr (mg/nm ³ @ 5% O ₂)	2.40 (873)	2.30 (844)
Heat Balance	NMHC g/bhp-hr (mg/nm ³ @ 5% O ₂)	0.35 (131)	0.34 (127)
	Heat to Jacket Water Btu/hr x 1000 (kW)	3849 (1128)	3227 (946)
	Heat to Lube Oil Btu/hr x 1000 (kW)	567 (166)	462 (135)
	Heat to Intercooler Btu/hr x 1000 (kW)	179 (53)	122 (36)
	Heat to Radiation Btu/hr x 1000 (kW)	724 (212)	642 (188)
Intake/Exhaust System	Total Exhaust Heat Btu/hr x 1000 (kW)	3900 (1143)	2962 (868)
	Induction Air Flow scfm (Nm ³ /hr)	2424 (3651)	1972 (2970)
	Exhaust Flow lb/hr (kg/hr)	11273 (5113)	9171 (4160)
Exhaust Temperature °F (°C)		1179 (637)	1112 (600)

Typical heat data is shown, however no guarantee is expressed or implied. Consult your Dresser Waukesha Application Engineering Department for system application assistance.

All natural gas engine ratings are based on a fuel of 900 Btu/ft³ (35.3 MJ/nm³) SLHV, with a 91 WKH®. For conditions or fuels other than standard, consult the Dresser Waukesha Application Engineering Department.

Data based on standard conditions of 77°F (25°C) ambient temperature, 29.53 inches Hg (100kPa) barometric pressure, 30% relative humidity (0.3 inches HG / 1 kPa water vapor pressure).

Fuel consumption based on ISO3046/1-1995 with a tolerance of +5% for commercial quality natural gas having a 900 BTU/ft³ (35.3 MJ/nm³) SLHV.

Heat data based on fuel consumption +2%.

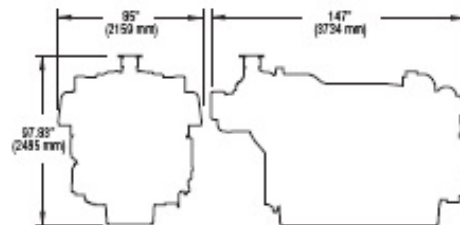
Heat rejection based on cooling exhaust temperature to 77°F (25°C).

Rating Standard: All models - Ratings are based on ISO 3046/1-1986 with mechanical efficiency of 90% and Tcrα (clause 10.1) as specified above limited to ± 10° F (5° C). Ratings are also valid for SAE J1349, BS5514, DIN6271 and AP17B-11C standard atmospheric conditions.

C = ISO Standard Power/Continuous Power Rating: The highest load and speed which can be applied 24 hours per day, seven days per week, 365 days per year except for normal maintenance. It is permissible to operate the engine at up to 10% overload, or a maximum load indicated by the intermittent rating, whichever is lower, for two hours in every 24 hour period.

I = Intermittent Service Rating: The highest load and speed that can be applied in variable speed mechanical system application only. Operation at this rating is limited to a maximum of 3500 hours per year.

Consult your local Waukesha representative for system application assistance. The manufacturer reserves the right to change or modify without notice, the design or equipment specifications as herein set forth without incurring any obligation either with respect to equipment previously sold or in the process of construction except where otherwise specifically guaranteed by the manufacturer.



Appendix B: Emissions Analyzer Calibration Log

Table 7: Calibration gas concentrations used during field test

Calibration gas concentration (ppm)		Lower Limit (- 5%)	Upper Limit (+ 5%)
NOx	202	192	212
CO – low	401	381	421
CO – high	6891	6547	7236

Table 8: Calibration log for portable emissions analyzer

Date	Sensor temperature (°F)		Post-test calibration check			Result (Pass/Fail)
	Initial	Final	NOx (ppm)	CO – low (ppm)	CO – high (ppm)	
February 27	69.5	70.1	203	395	---	Pass
March 13	79.7	80.4	202	391	6855	Pass
April 2	71.4	73.0	203	386	6885	Pass
May 15	80.9	84.0	200	384	6885	Pass
June 25	100.7	110.0	206	391	6740	Pass
June 26	109.5	86.5	Pass	Fail	---	---
June 27	90.3	94.0	203	404	---	Pass
August 20	91.2	99.5	199	397	6680	Pass

Appendix C: Alarm/Fault Checks

Misfire

This alarm (designated as AL370) was demonstrated on August 23, 2012, by disconnecting the ignition cable between the primary coil and the candle. The resulting fault was recorded in the fault log as well as realtime via Woodward's ToolKit trend (Figure 62).

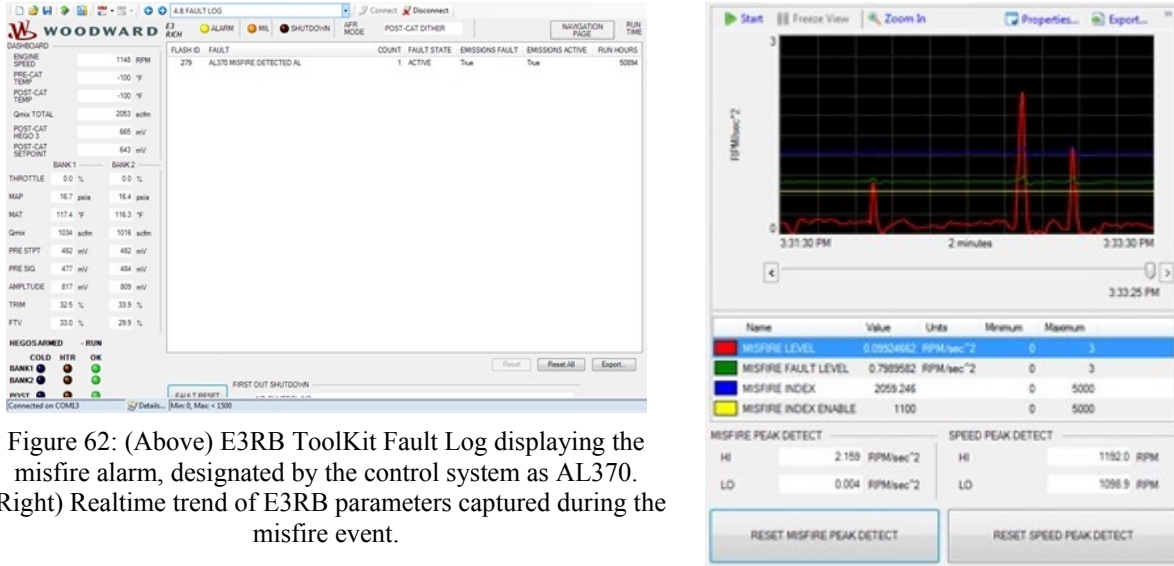


Figure 62: (Above) E3RB ToolKit Fault Log displaying the misfire alarm, designated by the control system as AL370. (Right) Realtime trend of E3RB parameters captured during the misfire event.

System Lean/Rich

These alarms (designated as AL10 for System Rich and AL15 for System Lean) were demonstrated on November 13, 2011, by manually adjusting the fuel trim valve so as to prevent the E3RB from obtaining the necessary fuel-air mixture. The faults were monitored in real-time using Woodward ToolKit trends (Figure 63).

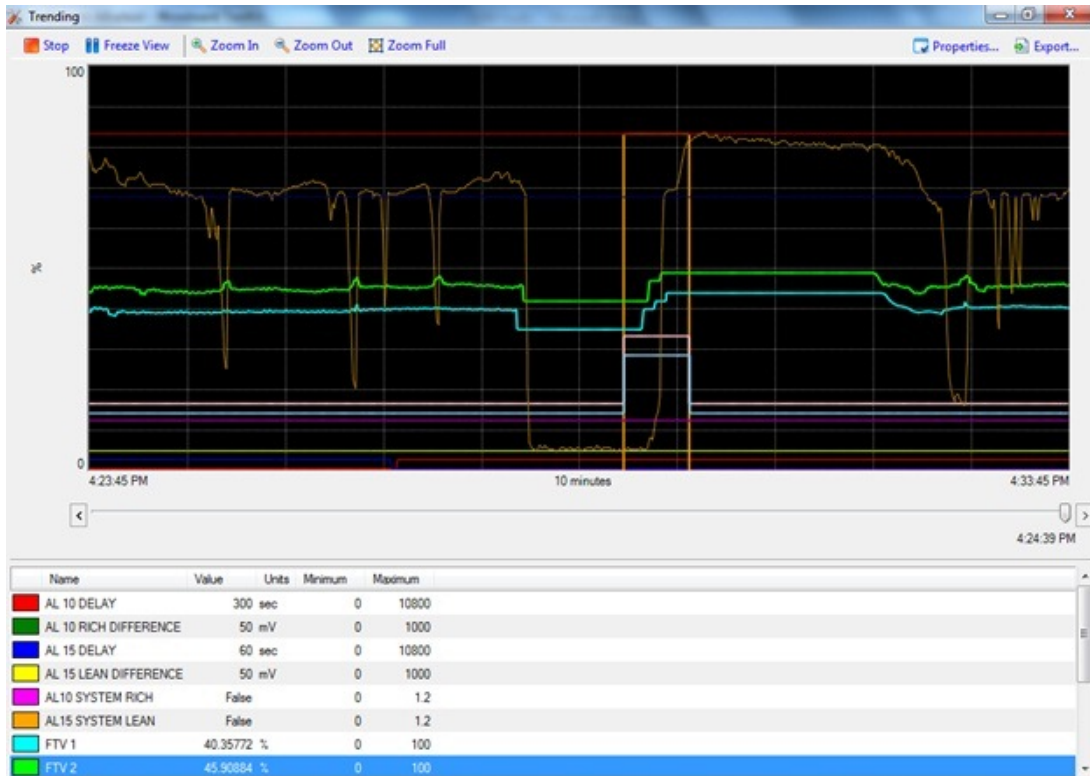


Figure 63: E3RB ToolKit trends displaying alarms for System Lean (orange trend - above) and System Rich (magenta trend - below) conditions.



Post-catalyst HEGO sensor

Alarms for post-catalyst HEGO sensor failure (designated as AL576 for HEGO 3 Heater Open Circuit and AL590 for HEGO 3 Sensor Failed) were demonstrated on November 13, 2011, by disconnecting the post-catalyst HEGO sensor from the E3RB system. The faults were monitored in real-time using a Woodward ToolKit trend (Figure 64).

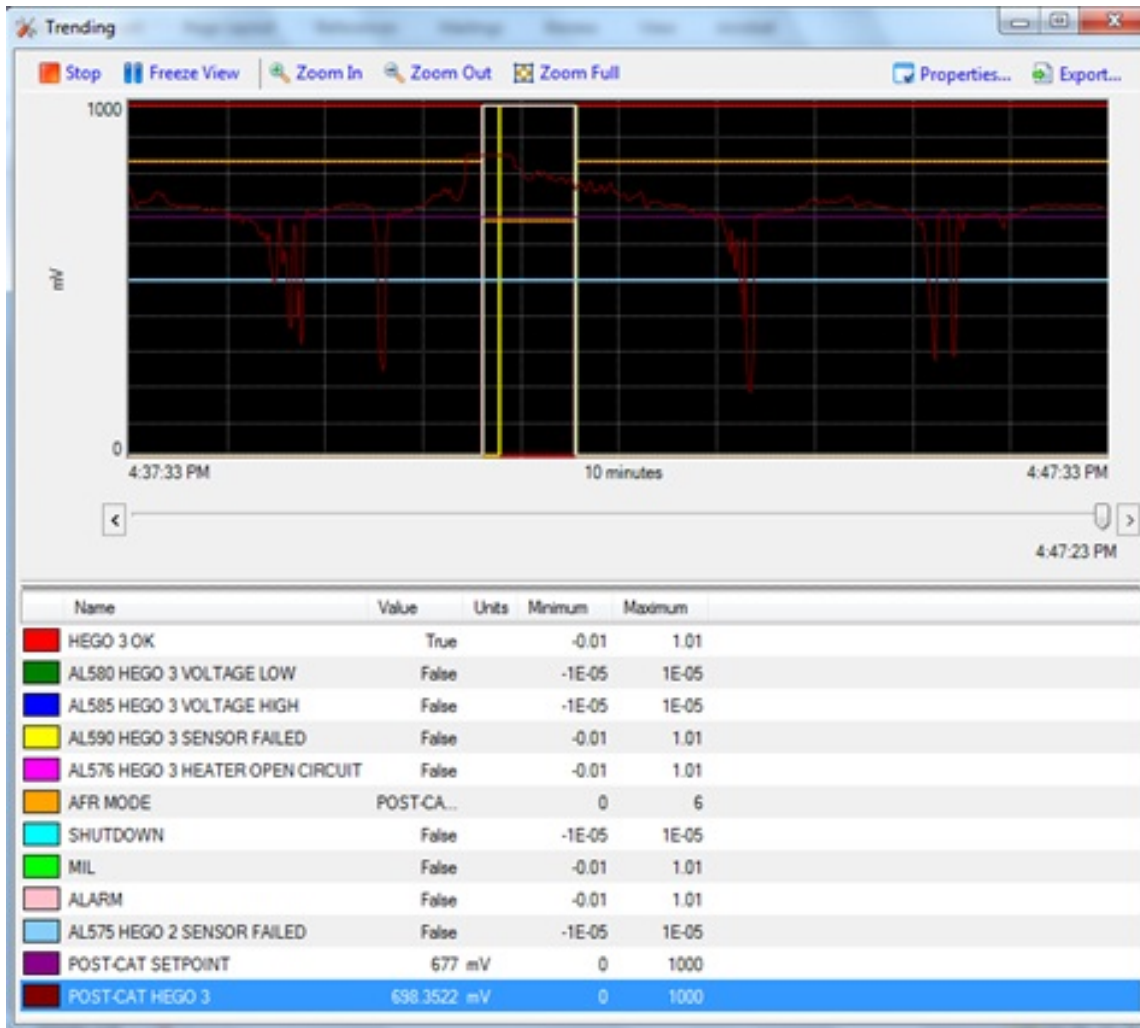


Figure 64: E3RB ToolKit trend displaying an alarm during simulated failure of the post-catalyst HEGO sensor (identified as HEGO 3).

Post-catalyst High Temperature

The post-catalyst high temperature alarm (designated as AL453) was demonstrated on February 18, 2012, by simulating an appropriate voltage signal to AN19 on the controller. The faults were monitored in real-time using a Woodward ToolKit trend (Figure 65). A simulation was required to showcase this feature on the E3RB as post-catalyst temperature thresholds at this site were monitored only by the PLC.

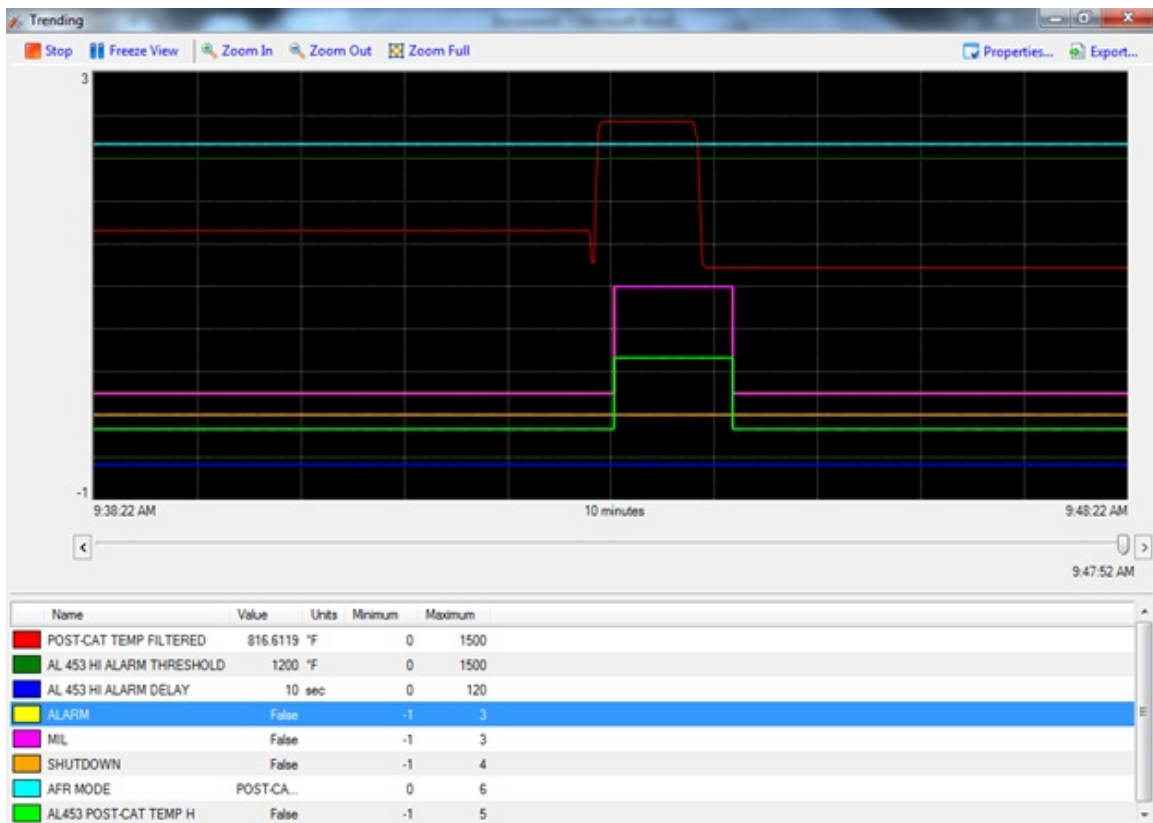


Figure 65: E3RB ToolKit trend displaying an alarm during a simulated exceedance of the high temperature limit recorded by the post-catalyst temperature sensor (not installed).

Pre-catalyst High/Low Temperature

The pre-catalyst high/low temperature alarms (designated as AL451 for High and AL470 for Low) were demonstrated on February 18, 2012, by simulating appropriate voltage signals to AN18 on the controller. The faults were monitored in real-time using Woodward ToolKit trends (Figure 66 and Figure 67). A simulation was required to showcase this feature on the E3RB as catalyst temperature thresholds were monitored only by the PLC at this site.

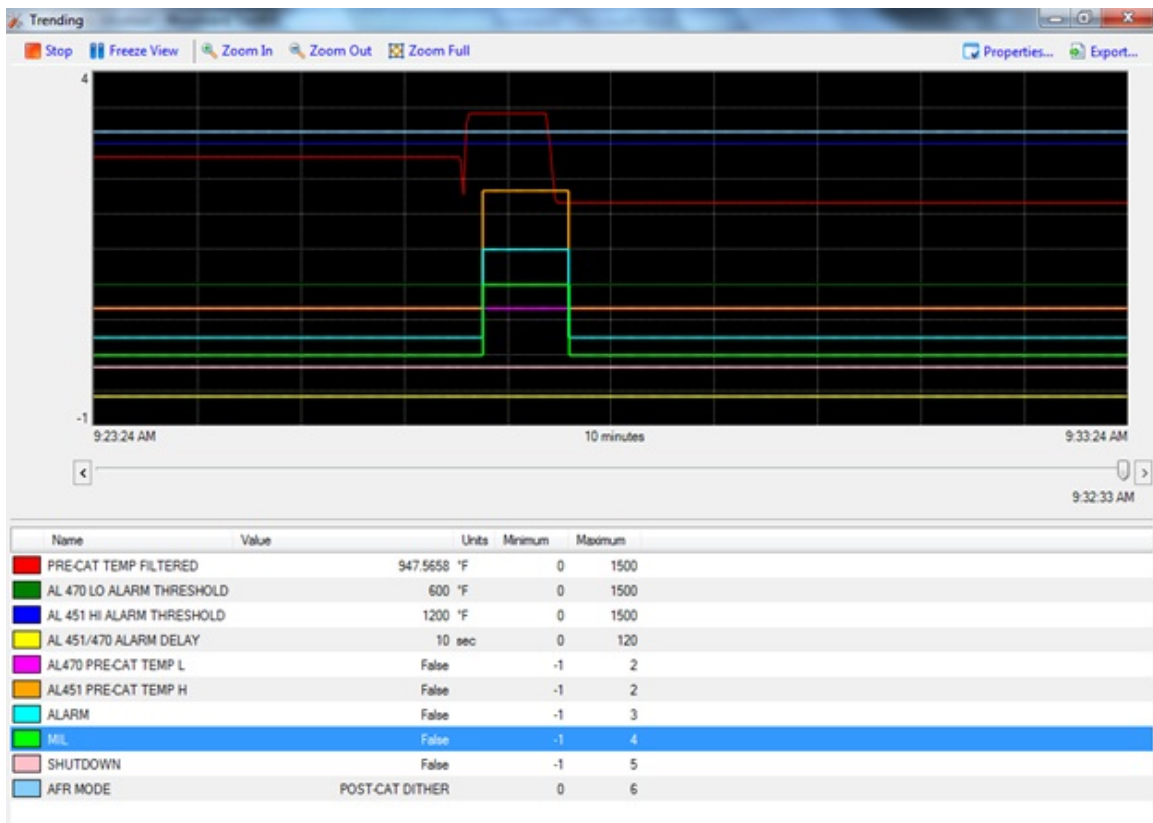


Figure 66: E3RB ToolKit trend displaying an alarm during a simulated exceedance of the high temperature limit recorded by the pre-catalyst temperature sensor (not installed).

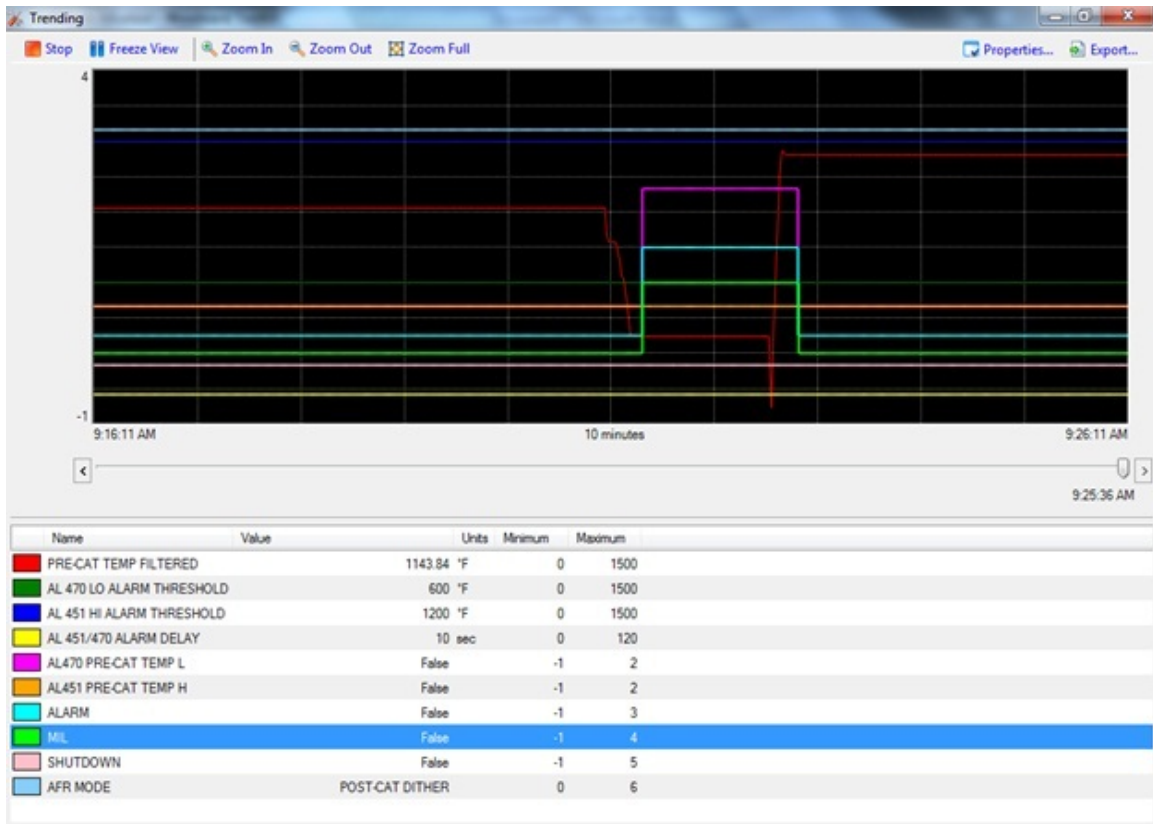


Figure 67: E3RB ToolKit trend displaying an alarm during a simulated exceedance of the low temperature limit recorded by the pre-catalyst temperature sensor (not installed).

Pre-catalyst HEGO sensors

Alarms for pre-catalyst HEGO sensor failures (designated as AL560 for Bank 1 [Right] and AL575 for Bank 2 [Left]) were demonstrated on February 19, 2012, by disconnecting the pre-catalyst HEGO sensors from the E3RB system and the resulting faults monitored in real-time using Woodward ToolKit trends (Figure 68).

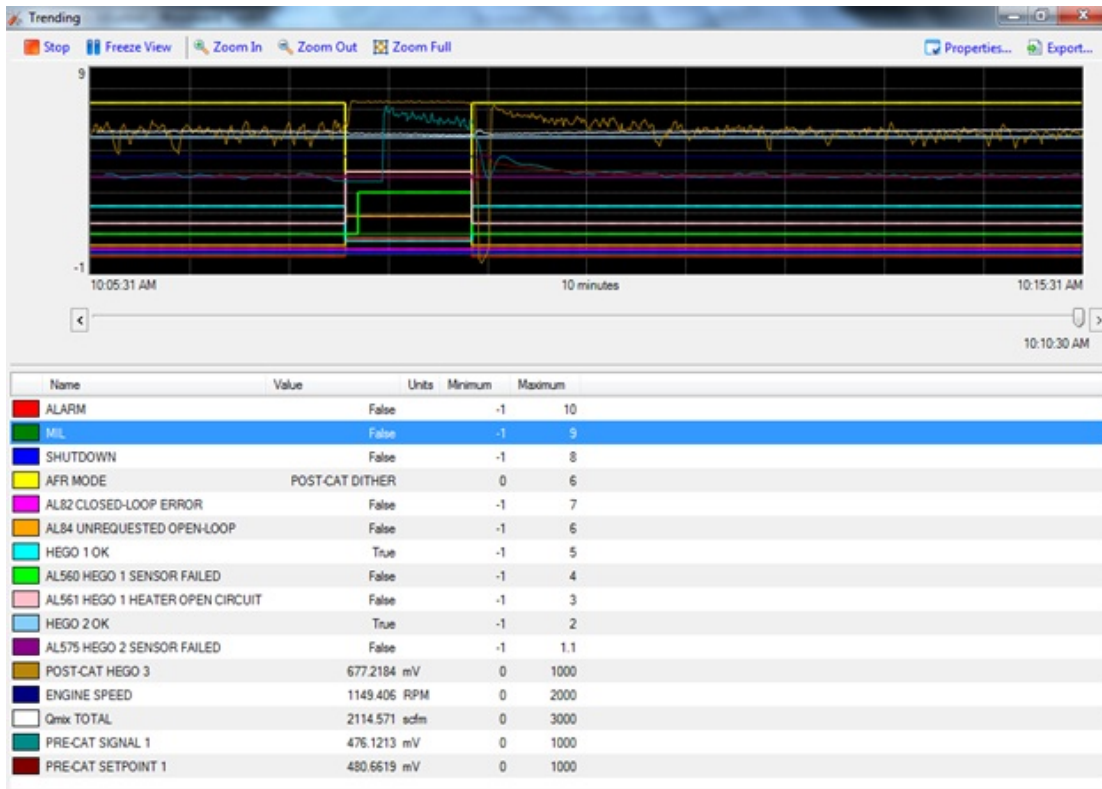
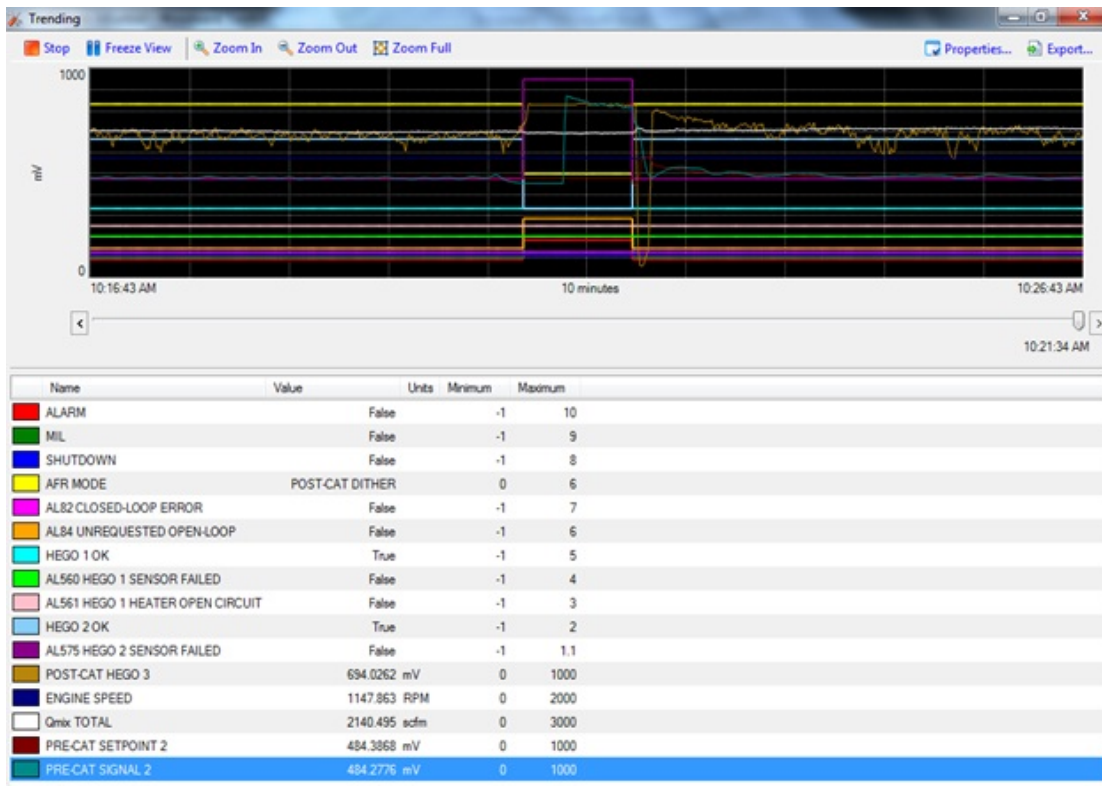


Figure 68: E3RB ToolKit trend displaying alarm incidents during simulated failure of the pre-catalyst HEGO sensors; AL560/HEGO 1 – Right bank (above) and AL575/HEGO 2 – Left bank (below).



Appendix D: Transient Response

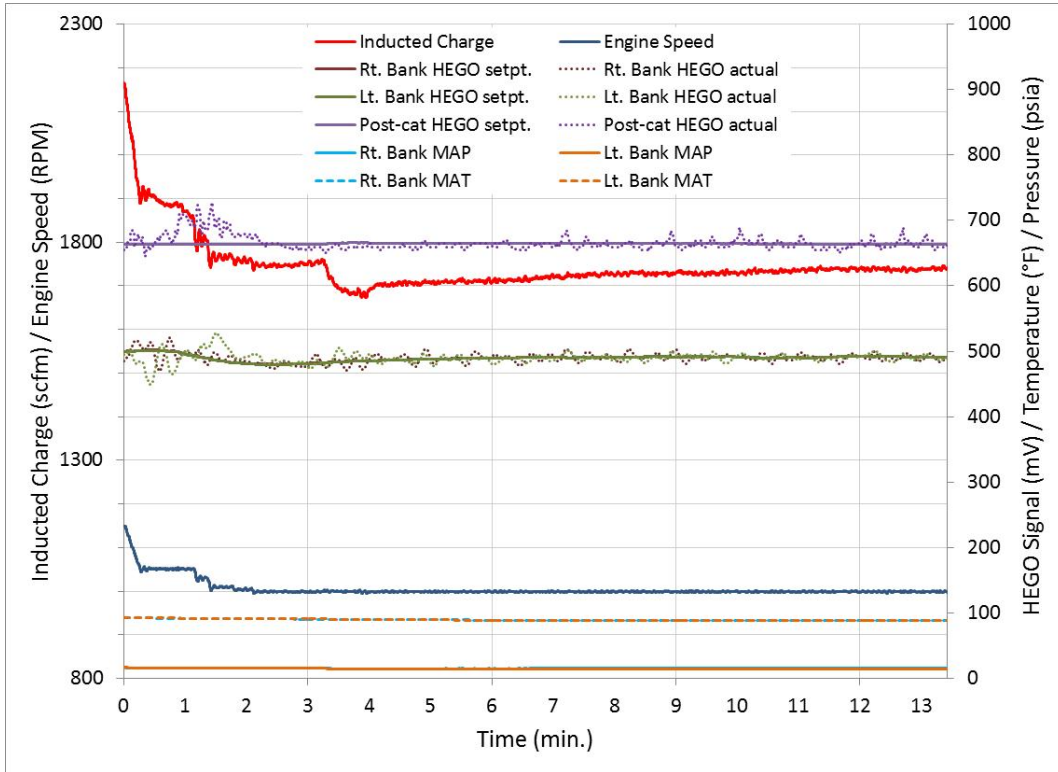


Figure 69: Transition from HS/HL to MS/ML on 27-Feb

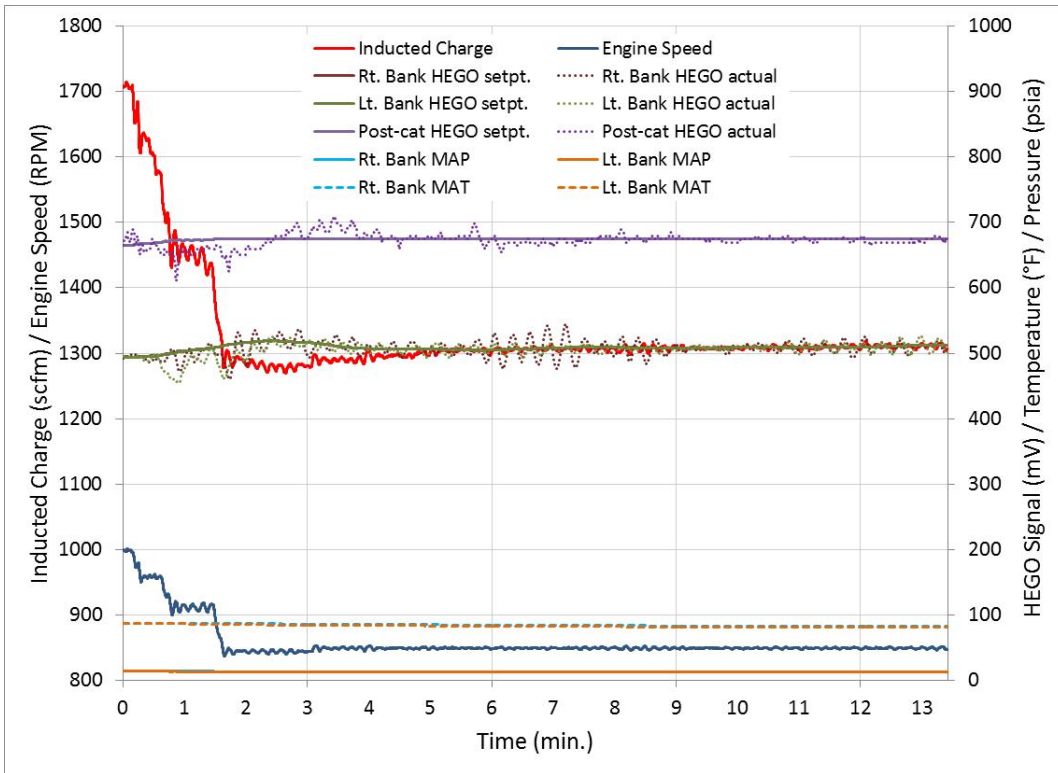


Figure 70: Transition from MS/ML to LS/LL on 27-Feb

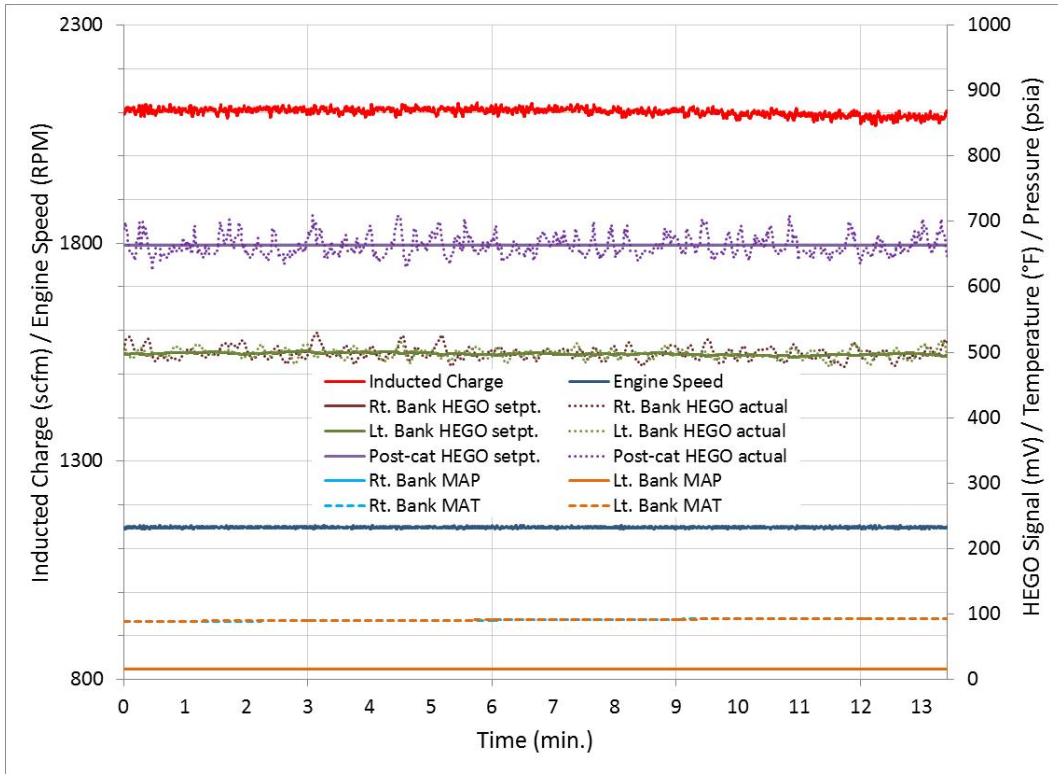


Figure 71: Transition from LS/LL to HS/HL on 27-Feb

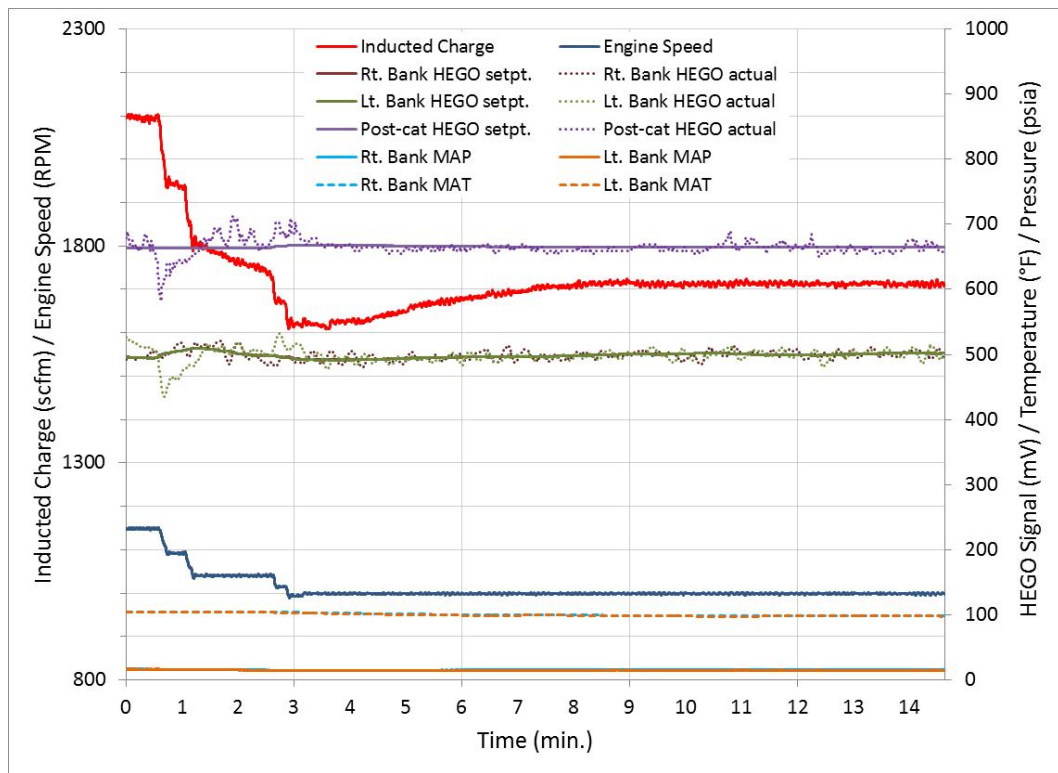


Figure 72: Transition from HS/HL to MS/ML on 13-Mar

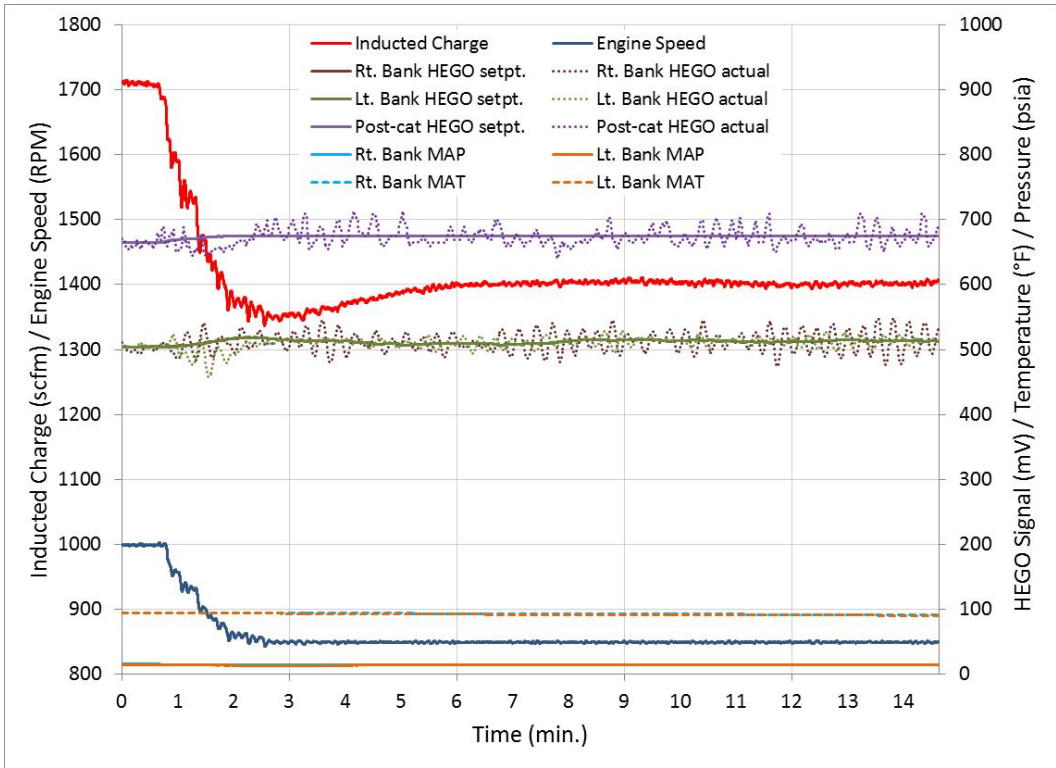


Figure 73: Transition from MS/ML to LS/LL on 13-Mar

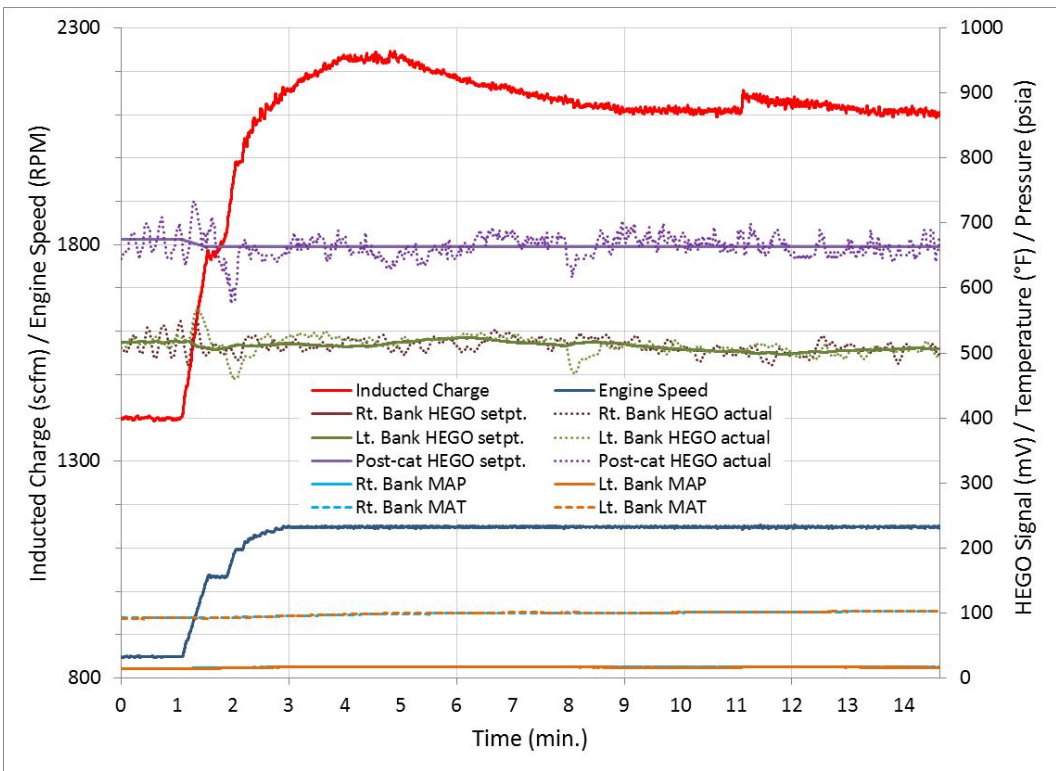


Figure 74: Transition from LS/LL to HS/HL on 13-Mar

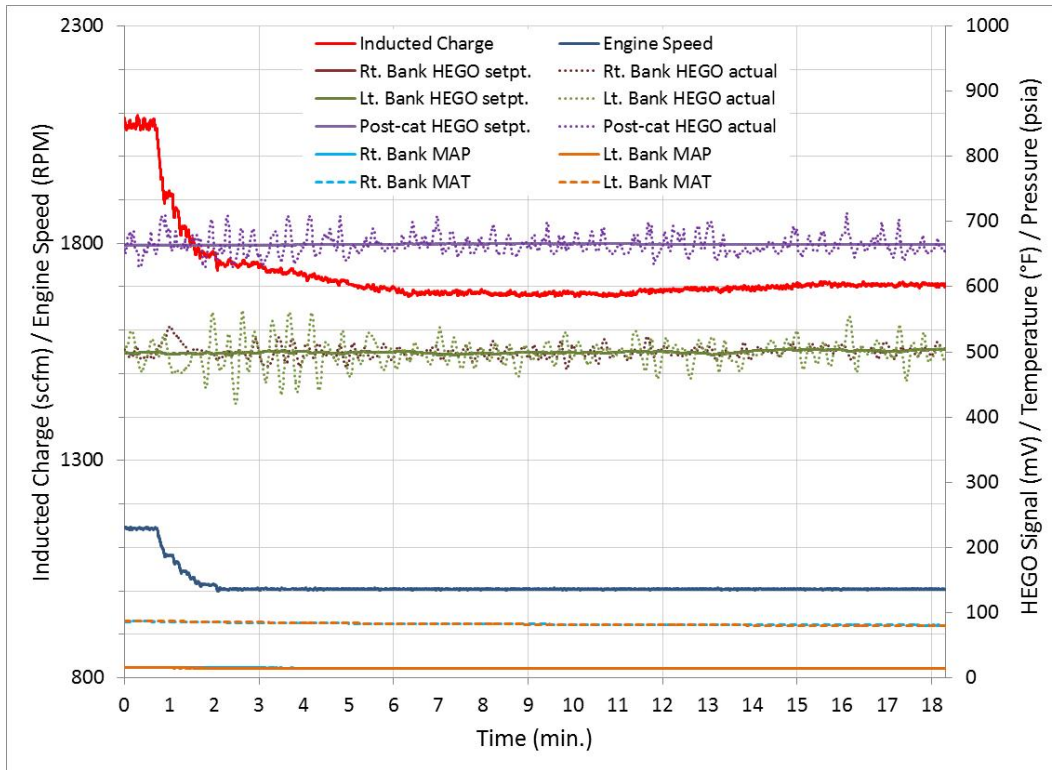


Figure 75: Transition from HS/HL to MS/ML on 02-Apr

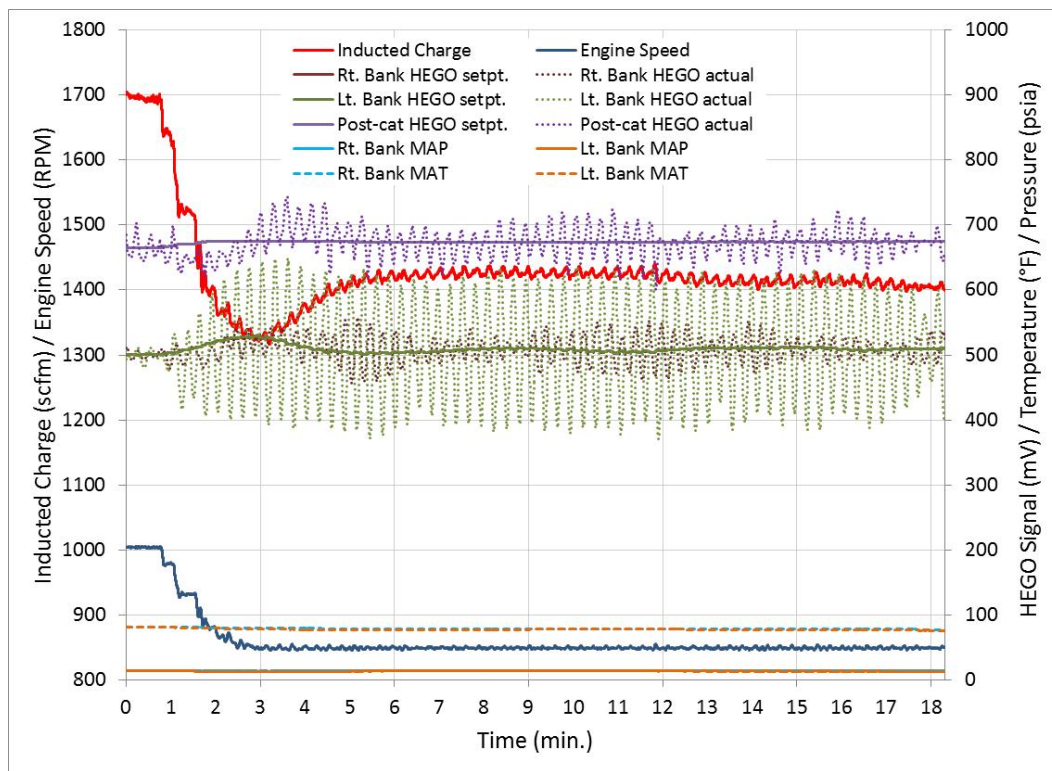


Figure 76: Transition from MS/ML to LS/LL on 02-Apr

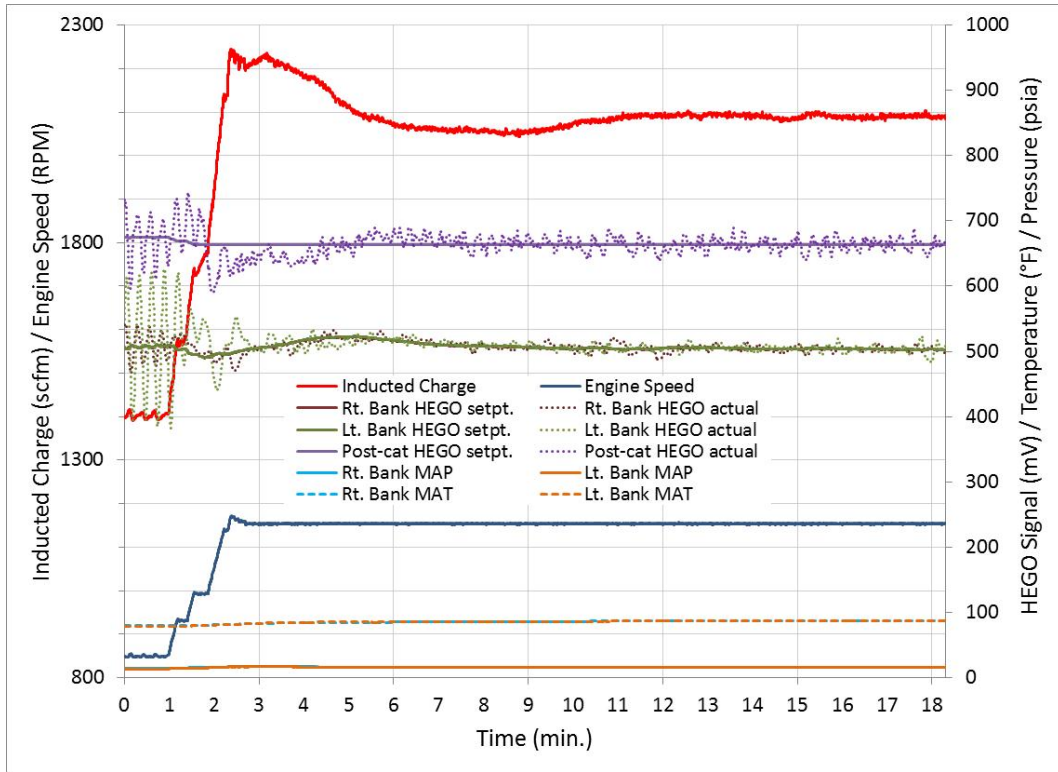


Figure 77: Transition from LS/LL to HS/HL on 02-Apr

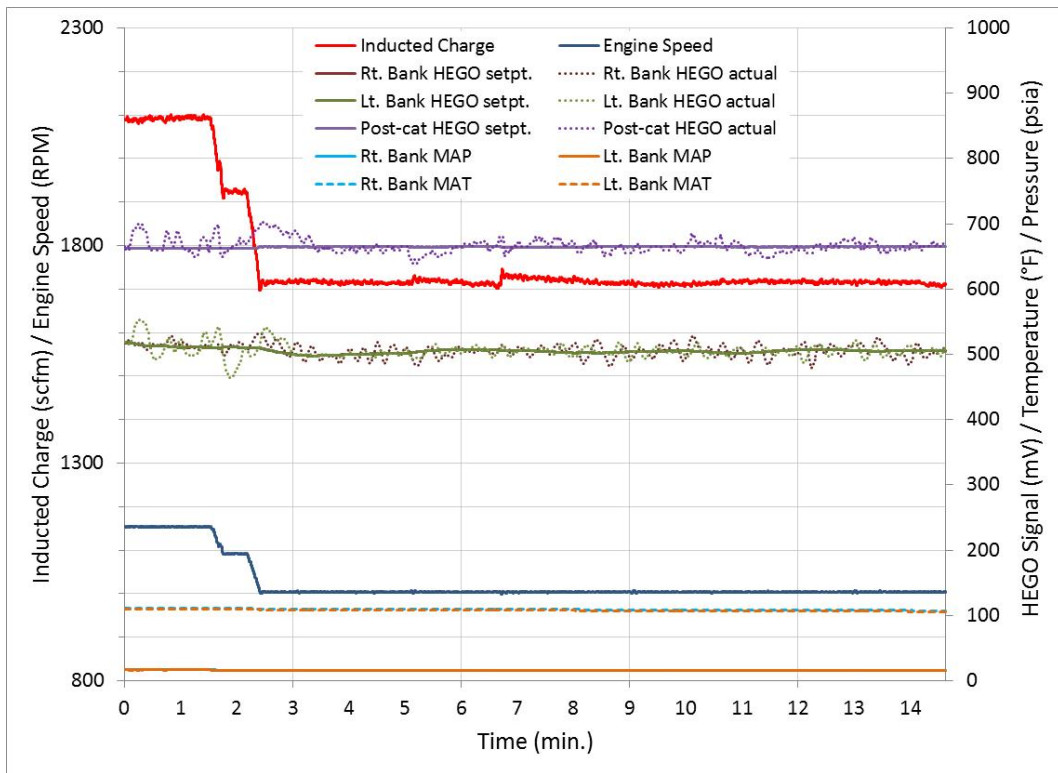


Figure 78: Transition from HS/HL to MS/ML on 15-May

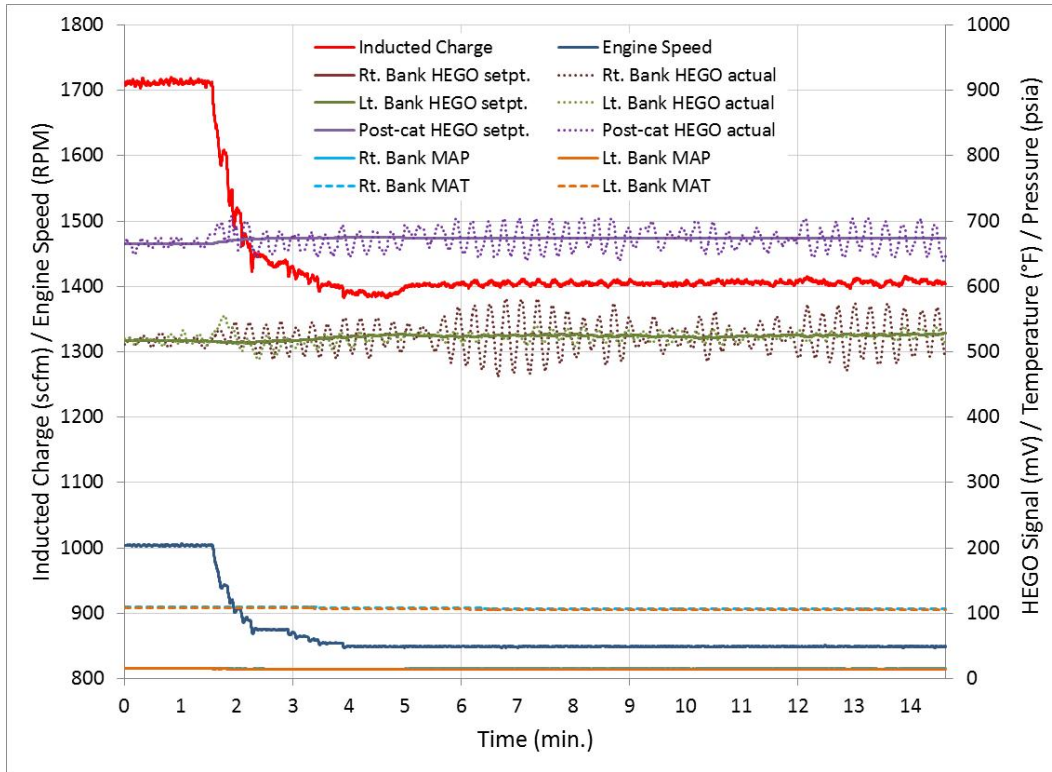


Figure 79: Transition from MS/ML to LS/LL on 15-May

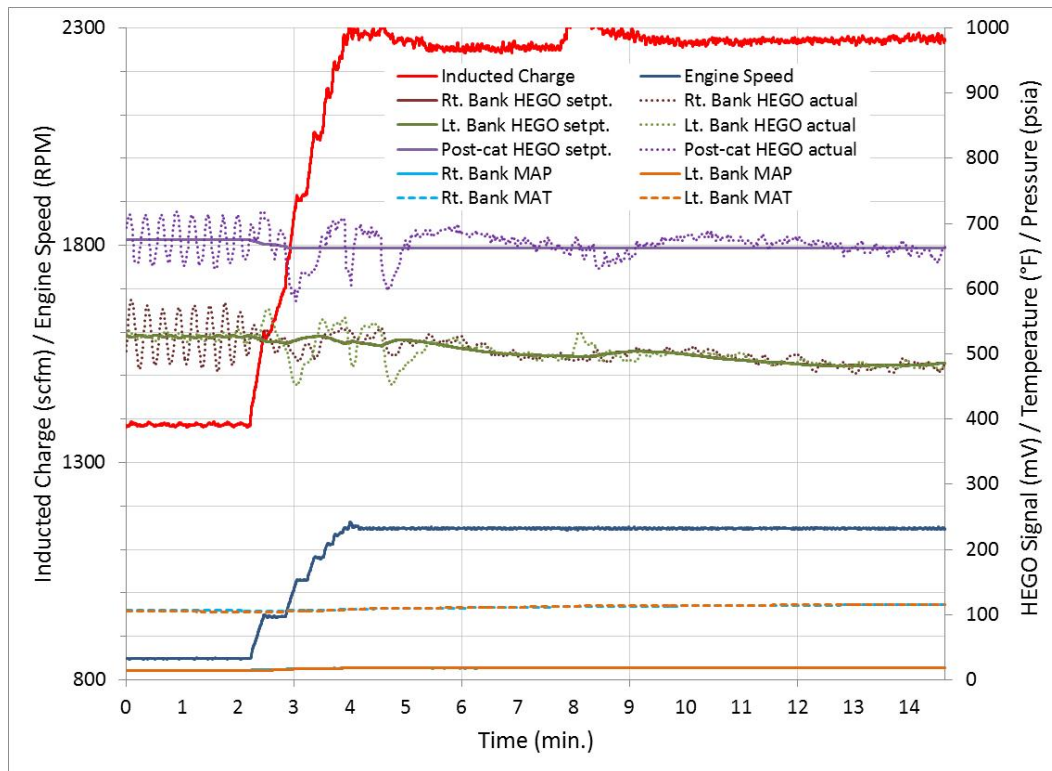


Figure 80: Transition from LS/LL to HS/HL on 15-May

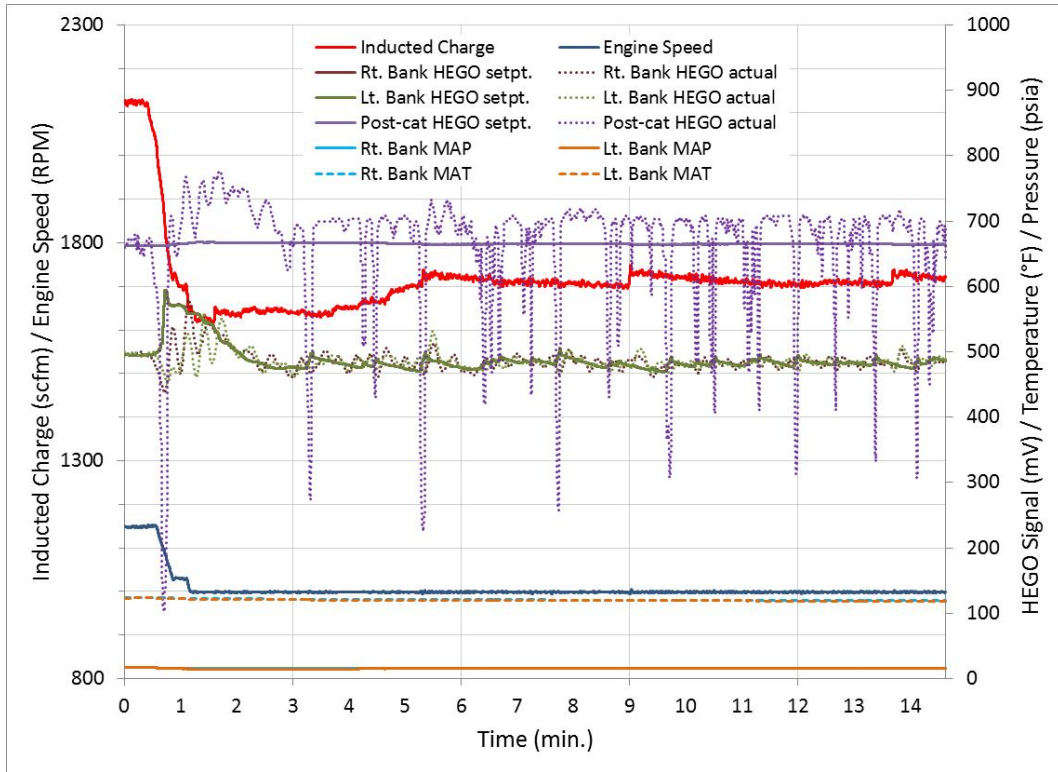


Figure 81: Transition from HS/HL to MS/ML on 25-Jun

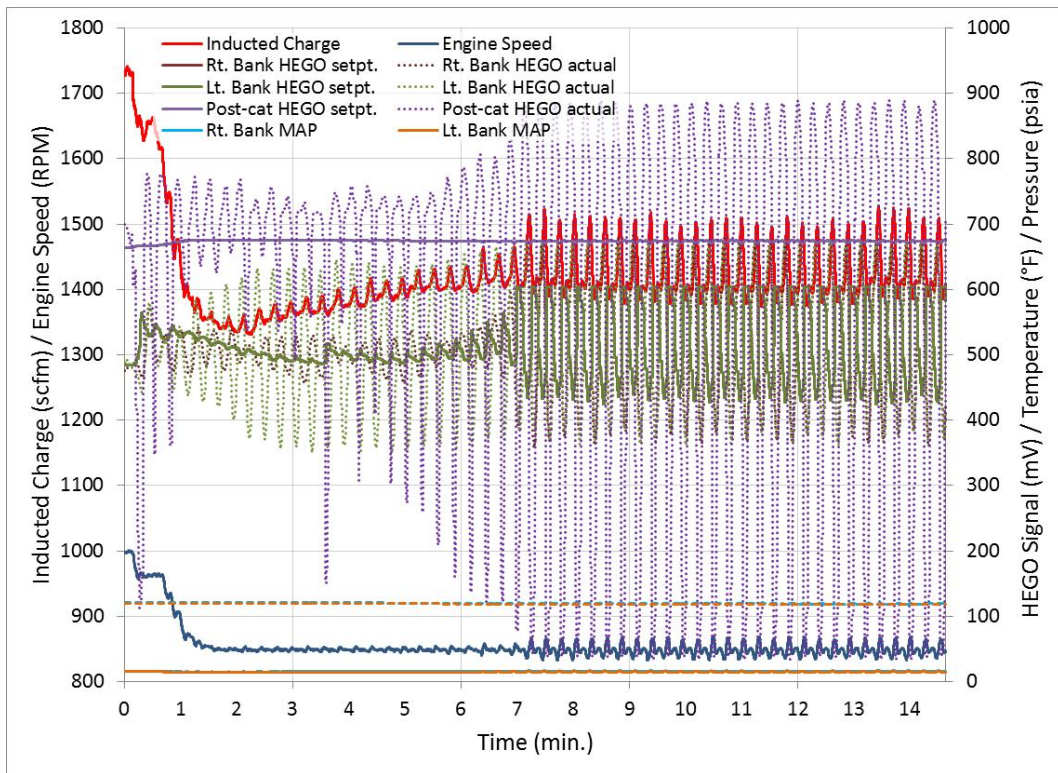


Figure 82: Transition from MS/ML to LS/LL on 25-Jun

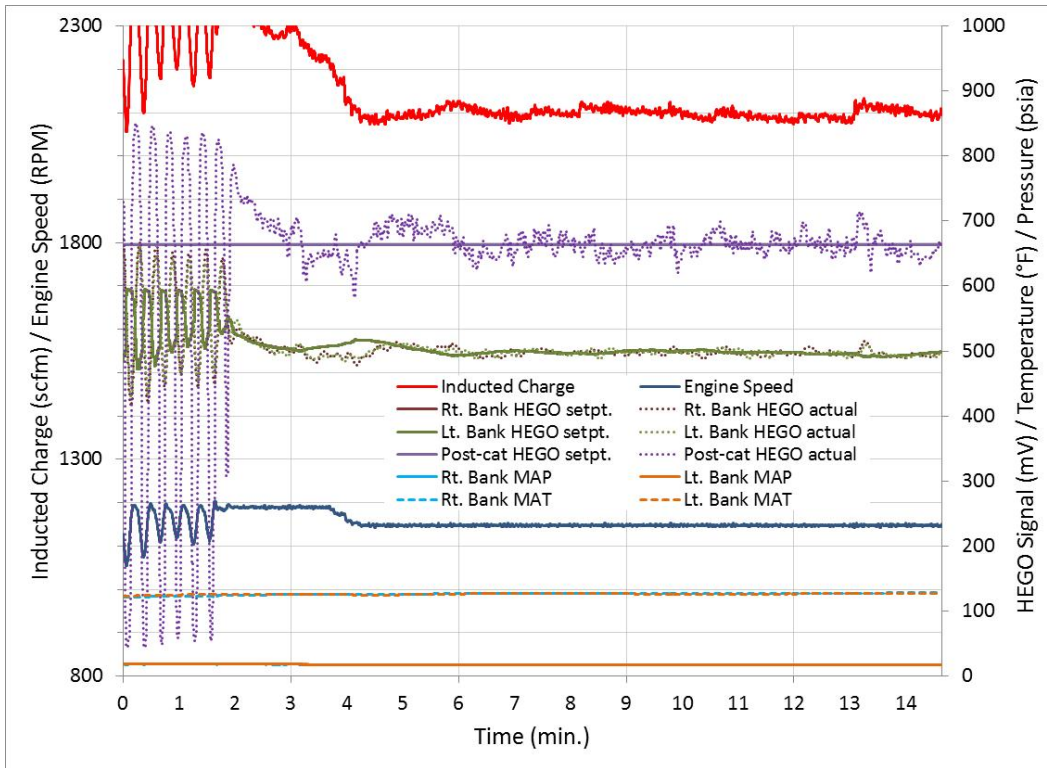


Figure 83: Transition from LS/LL to HS/HL on 25-Jun

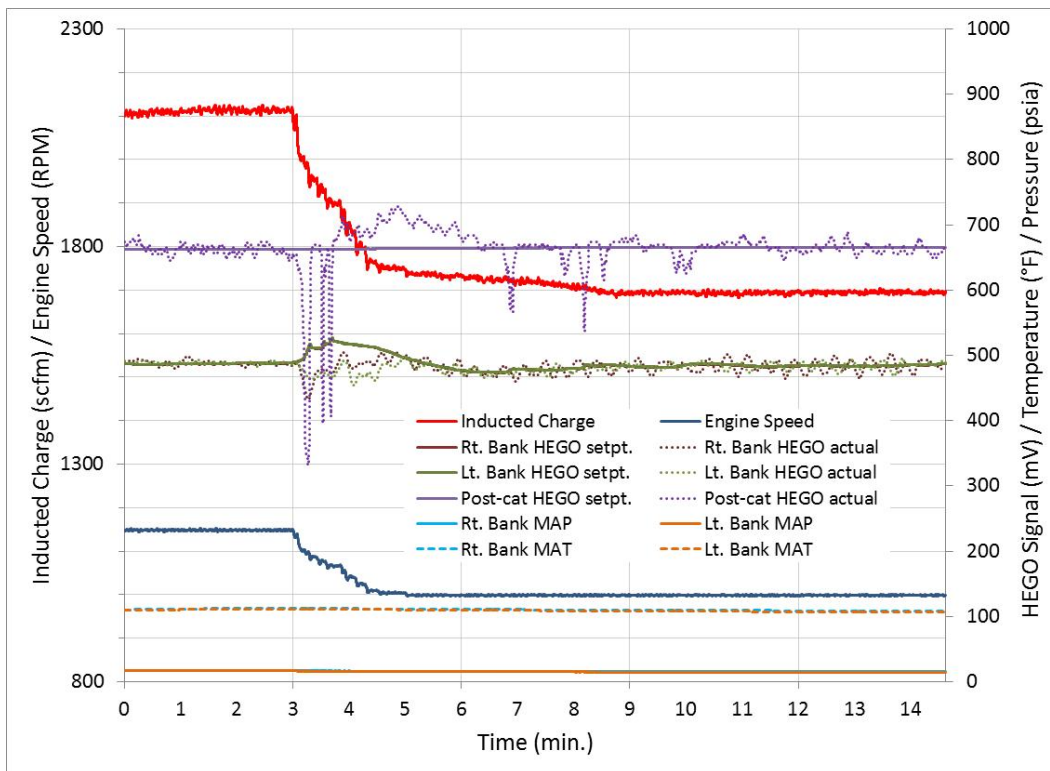


Figure 84: Transition from HS/HL to MS/ML on 20-Aug

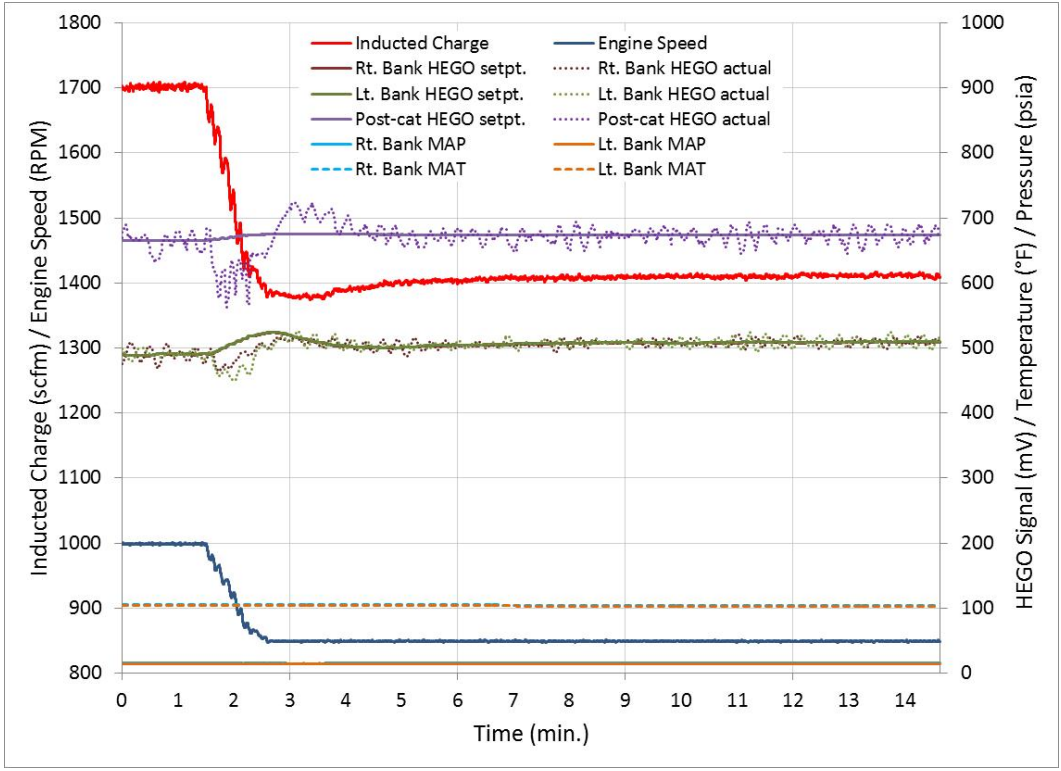


Figure 85: Transition from MS/ML to LS/LL on 20-Aug

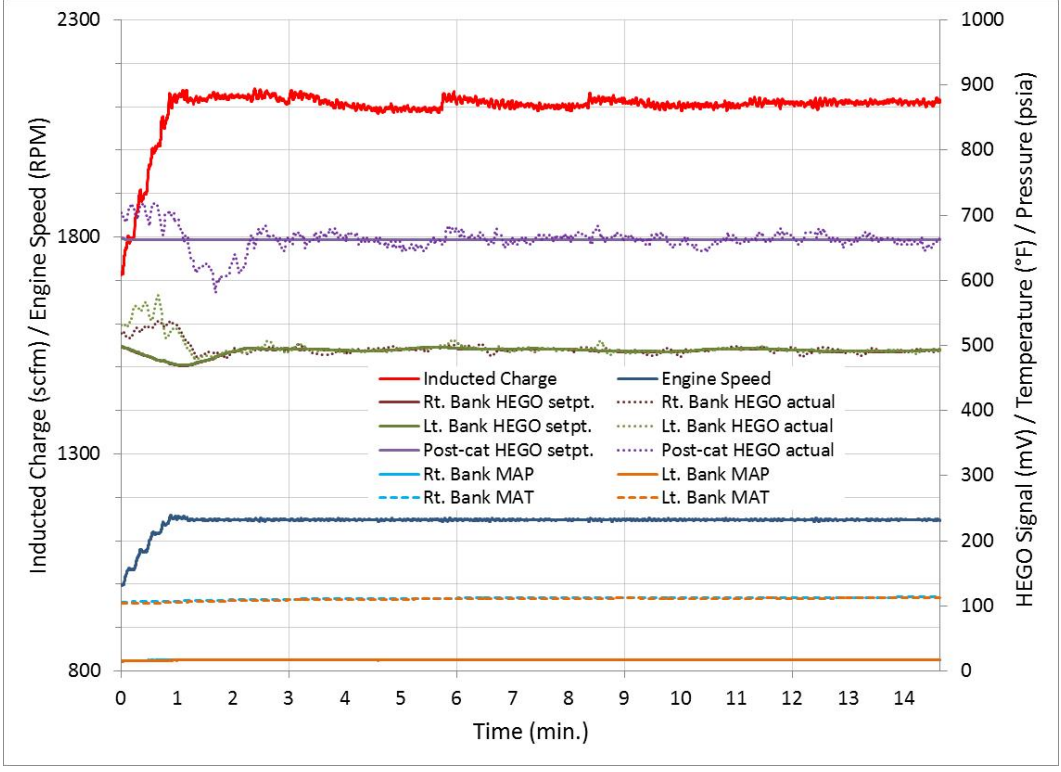


Figure 86: Transition from LS/LL to HS/HL on 20-Aug

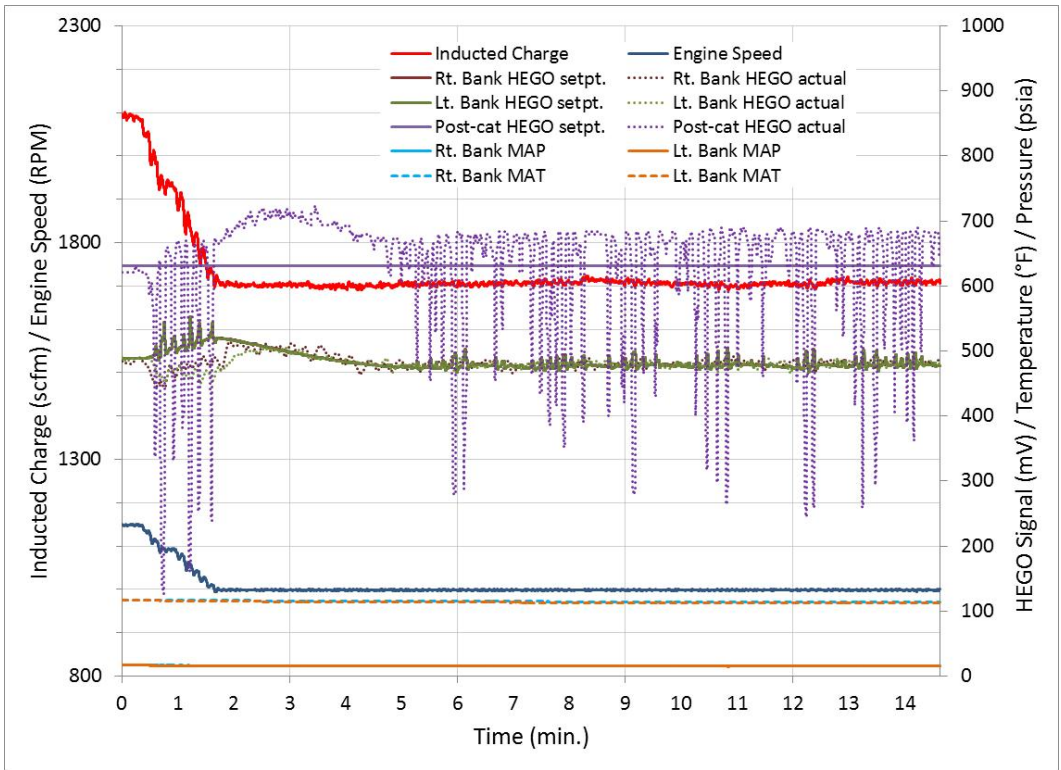


Figure 87: Transition from HS/HL to MS/ML on 24-Aug (after retuning)

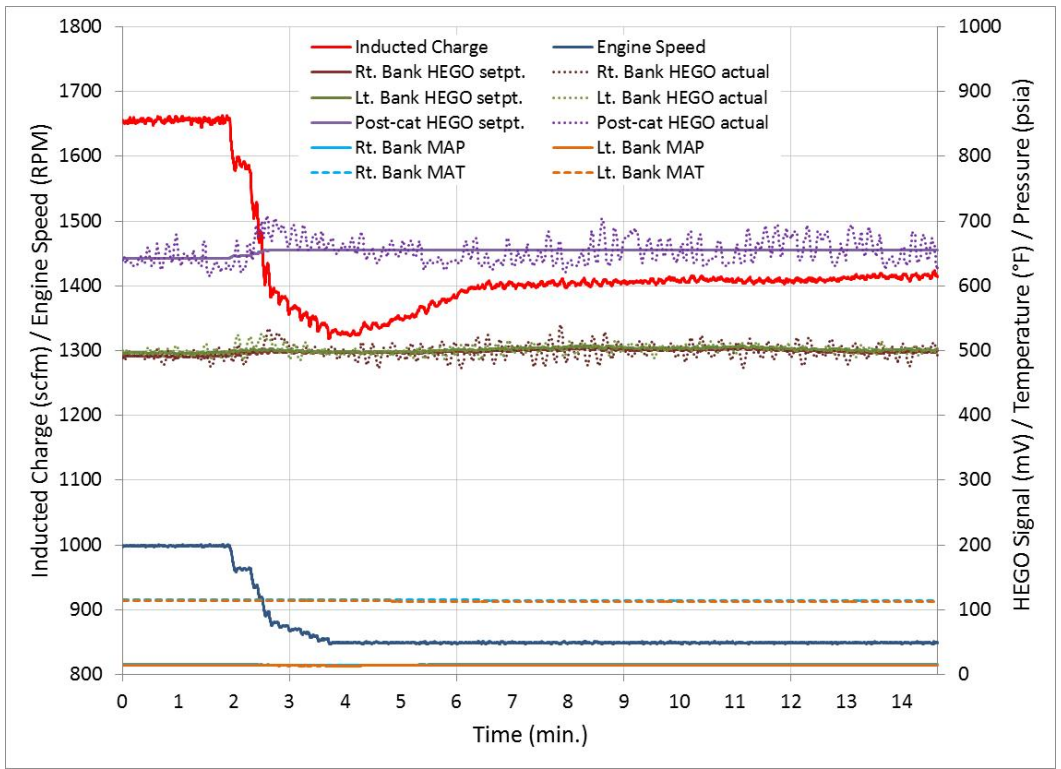


Figure 88: Transition from MS/ML to LS/LL on 24-Aug (after retuning)

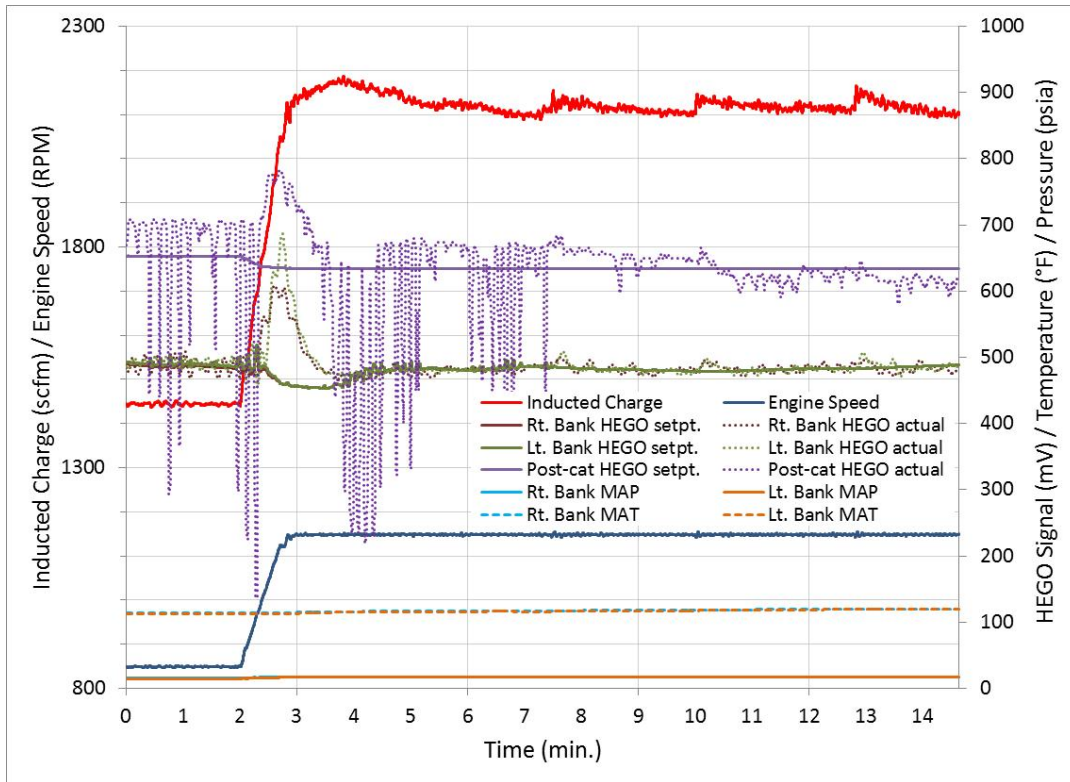


Figure 89: Transition from LS/LL to HS/HL on 24-Aug (after retuning)

Appendix E: Field Data

Table 9: Field data log from February 27 (Site visit # 1)

Run	1/1	1/2	2/1	2/2	3/1	3/2	4A/1	4A/2	4B
Date	27-Feb-12								
Time	9:59	10:39	11:25	12:01	12:45	13:23	14:08	14:50	16:20
Qmix Setpoint	2100	2100	1700	1700	1300	1300	2100	2100	2100
Speed Setpoint	1150	1150	1000	1000	850	850	1150	1150	1150
Test Duration [min]	15	15	15	15	15	15	15	15	15
Speed/Load Characterization	HS/HL	HS/HL	MS/ML	MS/ML	LS/LL	LS/LL	HS/HL	HS/HL	HS/HL
Engine									
Engine Runtime [hr]	47595	47596	47597	47597	47598	47599	47599	47600	47602
Volumetric Flow [SCFM]	2050	2100	1765	1705	1306	1300	2095	2120	2095
Ambient Temperature [°F]	70.1	69.0	70.1	70.3	69.9	70.5	70.3	71.0	70.7
Suction Pressure [psig]	120	125	130	122	108	107	125	127	125
Discharge Pressure [psig]	924	929	917	914	900	895	915	909	904
Discharge Temperature [°F]	115	120	115	113	101	103	123	124	122
Right Bank MAP [psig]	5	5	4	4	2	3	5	5	5
Left Bank MAP [psig]	5	5	4	4	1	1	4	5	4
Jacket Water Temperature [°F]	177	178	178	177	176	176	178	179	178
Jacket Water Pressure [psig]	22	21	19	18	16	16	21	21	22
Oil temperature [°F]	194	194	193	193	193	193	194	193	193
Oil pressure [psig]	54	54	49	50	43	43	54	53	53
Average MAT [°F]									
Fuel Flow [SCFD]	62	65	46	43	24	24	64	67	64
ESM Load [%]	86	86	81	81	70	70	83	84	83
Throttle Position [%]	44	45	38	34	27	27	44	46	46
Ignition Timing	24	24	26	26	26	26	22 ↔ 24	24	24
Right Fuel/Air Pressure [”H2O]		1.0	3.0	4.0	4.5	5.0	3.0	2.0	
Left Fuel/Air Pressure [”H2O]		2.0	3.3	4.0	4.5	4.0	2.5	2.0	
Fuel pressure [psig]	142	142	146	146	147	147	142	142	142
Catalyst ΔP [”H2O]	6.0	6.2	4.7	4.4	2.8	3.0	6.0	6.1	6.0
POST CATALYST									
NO _x sensor [V] - NO _x 1	1.019	1.038	1.010	1.011	1.045	1.027	1.035	1.037	1.017
Outlet Temperature [°F]	1119	1120	1056	1046	956	953	1115	1116	1109
PRE CATALYST									
NO _x sensor [V] - NO _x 2	3.244	3.243	3.311	3.253	2.977	2.935	3.231	3.230	3.257
Inlet Temperature [°F]	1070	1072	1011	1005	937	935	1071	1075	1069
POST CATALYST Emissions									
Raw CO [ppm]	191	176	102	112	135	154	189	180	
Brake specific CO [g/bhp-hr]	0.49	0.45	0.26	0.28	0.33	0.38	0.48	0.46	
Raw NO _x [ppm]	34	34	29	31	39	43	37	36	
Brake specific NO _x [g/bhp-hr]	0.14	0.14	0.12	0.13	0.16	0.18	0.16	0.15	
PRE CATALYST Emissions									
Raw CO [ppm]									9431
Brake specific CO [g/bhp-hr]									22.73
Raw NO _x [ppm]									3692
Brake specific NO _x [g/bhp-hr]									14.61
CO ₂ [%] / O ₂ [%]									11.53/0.27

Table 10: Field data log from March 13 (Site visit # 2)

Run	14A/1	14A/2	14A/3	14B	15A/1	15A/2	16A/1	16A/2	17A/1	17A/2
Date	13-Mar-12	13-Mar-12	13-Mar-12	13-Mar-12	13-Mar-12	13-Mar-12	13-Mar-12	13-Mar-12	13-Mar-12	13-Mar-12
Time	10:44	11:25	12:13	12:36	13:33	14:00	14:04	15:03	15:51	16:14
Qmix Setpoint	2100	2100	2100	2100	1700	1700	1400	1400	2100	2100
Speed Setpoint	1150	1150	1150	1150	1000	1000	850	850	1150	1150
Test Duration [min]	15	15	15	15	15	15	15	15	15	15
Speed/Load Characterization	HS/HL	HS/HL	HS/HL	HS/HL	MS/ML	MS/ML	LS/LL	LS/LL	HS/HL	HS/HL
Engine										
Engine Runtime [hr]	47952	47953	47954	47954	47955	47955	47956	47956	47957	47958
Volumetric Flow [SCFM]	2065	2110	2090	2090	1710	1710	1403	1400	2103	2110
Ambient Temperature [°F]	79.3	78.2	77.1	78.4	76.6	77.5	78	78.2	78.8	75.7
Suction Pressure [psig]	120	124	124	123	121	120	123	123	126	122
Discharge Pressure [psig]	972	963	947	947	940	938	936	935	961	976
Discharge Temperature [°F]	124	121	112	117	98	97	90	93	108	106
Right Bank MAP [psig]	5	5	5	5	4	4	3	3	5	5
Left Bank MAP [psig]	5	5	5	5	3	3	3	3	5	5
Jacket Water Temperature [°F]	181	181	178	178	176	176	176	177	177	177
Jacket Water Pressure [psig]	21	22	21	21	19	18	16	16	22	21
Oil temperature [°F]	192	193	193	193	192	192	192	192	193	193
Oil pressure [psig]	54	54	53	54	51	51	43	43	53	53
Average MAT [°F]	107	106	102	103	96	96	90	92	102	102
Fuel Flow [SCFD]	62	66	65	65	44	43	28	28	66	65
ESM Load [%]	84	85	85	84	78	78	76	77	84	84
Throttle Position [%]	47	50	49	48	37	37	32	32	50	49
Ignition Timing	24	24	24	24	26	26	26	26	22↔24	23↔24
Right Fuel/Air Pressure [“H2O]										
Left Fuel/Air Pressure [“H2O]										
Fuel pressure [psig]	144	143	142	142	145	144	145	144	144	143
Catalyst ΔP [“H2O]	4.2	4.2	4.3	4.0	3.3	3.2	2.4	2.5	4.4	4.4
POST CATALYST										
NO _x sensor [V] - NO _x 1										
Outlet Temperature [°F]	1098	1096	1094	1088	1009	1008	929	929	1088	1086
PRE CATALYST										
NO _x sensor [V] - NO _x 2										
Inlet Temperature [°F]	1072	1072	1070	1063	993	993	936	934	1070	1066
POST CATALYST Emissions										
Raw CO [ppm]	234	199	212		115	117	152	170	230	191
Brake specific CO [g/bhp-hr]	0.60	0.51	0.54		0.29	0.29	0.38	0.42	0.59	0.49
Raw NO _x [ppm]	46	45	46		38	36	45	49	57	48
Brake specific NO _x [g/bhp-hr]	0.19	0.19	0.19		0.16	0.15	0.18	0.20	0.24	0.20
PRE CATALYST Emissions										
Raw CO [ppm]				9527						
Brake specific CO [g/bhp-hr]				22.97						
Raw NO _x [ppm]				3769						
Brake specific NO _x [g/bhp-hr]				14.93						
CO ₂ [%] / O ₂ [%]				11.51 / 0.3						

Table 11: Field data log from April 2 (Site visit # 3)

Run	19A/1	19A/2	20A/1	20A/2	21A/1	21A/2	21A/3	22A/1	22A/2	22B
Date	2-Apr-12									
Time	14:40	15:05	15:50	16:15	17:05	17:30	18:00	18:40	19:05	19:30
Qmix Setpoint	2100	2100	1700	1700	1400	1400	1400	2100	2100	2100
Speed Setpoint	1150	1150	1000	1000	850	850	850	1150	1150	1150
Test Duration [min]	15	15	15	15	15	15	15	15	15	15
Speed/Load Characterization	HS/HL	HS/HL	MS/ML	MS/ML	LS/LL	LS/LL	LS/LL	HS/HL	HS/HL	HS/HL
Engine										
Engine Runtime [hr]	48432	48432	48433	48433	48434	48435	48435	48436	48436	48437
Volumetric Flow [SCFM]	2105	2070	1696	1700	1397	1398	1400	2075	2100	2097
Ambient Temperature [°F]	69.4	69.8	70	70.8	70.5	70.5	70.1	71.4	71.6	71.7
Suction Pressure [psig]	121	116	111	111	115	115	115	118	118	117
Discharge Pressure [psig]	978	1004	989	982	976	983	976	993	1006	1004
Discharge Temperature [°F]	96	93	91	94	103	105	105	115	115	114
Right Bank MAP [psig]	5	4	3	3	3	3	3	5	5	4
Left Bank MAP [psig]	4	4	2	2	1	2	2	4	4	4
Jacket Water Temperature [°F]	176	176	176	176	177	177	177	176	176	176
Jacket Water Pressure [psig]	18	18	15	15	12	12	12	17	17	17
Oil temperature [°F]	195	195	195	194	194	194	194	195	195	195
Oil pressure [psig]	53	52	50	50	42	42	43	52	53	53
Average MAT [°F]	85	84	80	81	79	80	80	86	86	85
Fuel Flow [SCFD]	140	140	128	127	104	27	27	62	63	62
ESM Load [%]	83	82	75	75	71	71	71	83	83	82
Throttle Position [%]	46	45	34	34	30	31	30	44	44	43
Ignition Timing	25	25	26	26	26	26	26	25	25	25
Right Fuel/Air Pressure [“H2O]										
Left Fuel/Air Pressure [“H2O]										
Fuel pressure [psig]	141	140	140	142	142	145	144	145	145	145
Catalyst ΔP [“H2O]	4.0	4.0	3.0	3.0	2.2	2.2	2.3	4.0	4.0	4.0
POST CATALYST										
NO _x sensor [V] - NO _x 1										
Outlet Temperature [°F]	1085	1081	1010	1014	947	945	948	1091	1078	1077
PRE CATALYST										
NO _x sensor [V] - NO _x 2										
Inlet Temperature [°F]	1073	1071	1008	1009	953	954	954	1075	1076	1074
POST CATALYST Emissions										
Raw CO [ppm]	238	251	176	203	176	338	247	208	203	
Brake specific CO [g/bhp-hr]	0.61	0.64	0.44	0.51	0.44	0.83	0.61	0.53	0.52	
Raw NO _x [ppm]	41	46	41	45	69	74	107	38	41	
Brake specific NO _x [g/bhp-hr]	0.17	0.19	0.17	0.19	0.28	0.30	0.43	0.16	0.17	
PRE CATALYST Emissions										
Raw CO [ppm]										8227
Brake specific CO [g/bhp-hr]										19.95
Raw NO _x [ppm]										3599
Brake specific NO _x [g/bhp-hr]										14.34
CO ₂ [%] / O ₂ [%]										11.57 / 0.21

Table 12: Field data log from May 15 – Part 1/2 (Site visit # 4)

Run	24A/1	24A/2	25A/1	25A/2	25A/3	25A/4	26A/1	26A/2
Date	15-May-12							
Time	10:35	11:01	12:30	12:55	13:30	14:00	14:45	15:10
Qmix Setpoint	2100	2100	1700	1700	1700	1700	1400	1400
Speed Setpoint	1150	1150	1000	1000	1000	1000	850	850
Test Duration [min]	15	15	15	15	15	15	15	15
Speed/Load Characterization	HS/HL	HS/HL	MS/ML	MS/ML	MS/ML	MS/ML	LS/LL	LS/LL
Engine								
Engine Runtime [hr]	49443	49443	49445	49445	49446	49446	49447	49447
Volumetric Flow [SCFM]	2100		1710	1740	1725	1720	1409	1392
Ambient Temperature [°F]	89	90.1	91.7	91.5	93.3	94.4	95	94.2
Suction Pressure [psig]	99	99	98	98	98	98	102	100
Discharge Pressure [psig]	935	938	920	966	951	973	1004	1004
Discharge Temperature [°F]	109	108	108	111	108	111	109	111
Right Bank MAP [psig]	5	5	4	4	4	4	3	3
Left Bank MAP [psig]	5	5	3	3	3	3	3	3
Jacket Water Temperature [°F]	178	178	177	177	177	178	177	177
Jacket Water Pressure [psig]	22	21	18	18	18	17	15	15
Oil temperature [°F]	193	193	191	191	191	191	190	190
Oil pressure [psig]	52	52	49	49	49	49	42	42
Average MAT [°F]	109	110	107	109	109	109	107	107
Fuel Flow [SCFD]	64	----	41	41		42	29	29
ESM Load [%]	85	85	79	79	79	78	77	77
Throttle Position [%]	----	----	----	----	----	----	----	----
Ignition Timing	24	24	26	26	26	24↔26	26	26
Right Fuel/Air Pressure ["H2O]	-0.5↔3.5	2.0	0.5↔2.0	2.0↔3.5	2.0↔3.0	2.5↔4.0	4.0↔6.0	3.0↔6.0
Left Fuel/Air Pressure ["H2O]	2.0↔3.0	1.5	0.0↔1.0	2.0	3.0	3.0	3.5↔4.0	3.0↔3.5
Fuel pressure [psig]	149	150	152	152	153	153	148	144
Catalyst ΔP ["H2O]	4.0	4.0	3.0	3.0	3.0	3.0	2.2	2.2
POST CATALYST								
NO _x sensor [V] - NO _x 1	2.266		1.371	0.877	0.877	1.641	1.753	2.788
Outlet Temperature [°F]	1131	1131	1059	1062	1063	1063	992	990
PRE CATALYST								
NO _x sensor [V] - NO _x 2	3.567		3.541	3.558	3.601	3.519	3.176	3.404
Inlet Temperature [°F]	1084	1084	1015	1018	1020	1019	962	960
POST CATALYST Emissions								
Raw CO [ppm]	381	383	261	59	136	239	308	301
Brake specific CO [g/bhp-hr]	0.98	0.98	0.66	0.15	0.34	0.60	0.76	0.74
Raw NO _x [ppm]	95	106	69	34	67	58	61	62
Brake specific NO _x [g/bhp-hr]	0.40	0.45	0.29	0.14	0.28	0.24	0.25	0.25
PRE CATALYST Emissions								
Raw CO [ppm]								
Brake specific CO [g/bhp-hr]								
Raw NO _x [ppm]								
Brake specific NO _x [g/bhp-hr]								
CO ₂ [%] / O ₂ [%]								

Table 13: Field data log from May 15 and 16 – Part 2/2 (Site visit # 4)

Run	27A/1	27A/2	27B	28A/1	28A/2	28B
Date	15-May-12	15-May-12	15-May-12	16-May-12	16-May-12	16-May-12
Time	16:35	17:00	19:30	16:50	17:15	17:50
Qmix Setpoint	2100	2100	2100	2100	2100	2100
Speed Setpoint	1150	1150	1150	1150	1150	1150
Test Duration [min]	15	15	15	15	15	15
Speed/Load Characterization	HS/HL	HS/HL	HS/HL	HS/HL	HS/HL	HS/HL
Engine						
Engine Runtime [hr]	49449	Engine shutdown owing to excessive vibration. Run aborted.		49468	49469	49469
Volumetric Flow [SCFM]	2095			2095	2110	2140
Ambient Temperature [°F]	96.4			94.4	94.2	92.6
Suction Pressure [psig]	101			101	101	101
Discharge Pressure [psig]	965			1024	1081	1133
Discharge Temperature [°F]	113			112	113	114
Right Bank MAP [psig]	5			5	5	5
Left Bank MAP [psig]	6			5	5	5
Jacket Water Temperature [°F]	178			178	178	179
Jacket Water Pressure [psig]	21			21	21	20
Oil temperature [°F]	193			192	193	193
Oil pressure [psig]	53			53	52	51
Average MAT [°F]	115			114	115	115
Fuel Flow [SCFD]	70					
ESM Load [%]	86			84	85	86
Throttle Position [%]	----			----	----	----
Ignition Timing	22↔23			24	24	23
Right Fuel/Air Pressure ["H2O]	0.5↔3.0		0.5↔2.0	0.0↔2.0	0.5↔2.0	
Left Fuel/Air Pressure ["H2O]	1.0↔2.5		0.5↔1.5	1.5↔2.0	1.0↔2.0	
Fuel pressure [psig]	141		122	130	130	
Catalyst ΔP ["H2O]	4.2		4.2	4.3	4.3	
POST CATALYST						
NO _x sensor [V] - NO _x 1	2.77			2.898	2.267	2.817
Outlet Temperature [°F]	1138			1126	1134	1137
PRE CATALYST						
NO _x sensor [V] - NO _x 2	3.553			3.702	3.771	3.761
Inlet Temperature [°F]	1094			1077	1085	1089
POST CATALYST Emissions						
Raw CO [ppm]	421			365	422	
Brake specific CO [g/bhp-hr]	1.08			0.93	1.08	
Raw NO _x [ppm]	94			73	86	
Brake specific NO _x [g/bhp-hr]	0.40			0.31	0.36	
PRE CATALYST Emissions						
Raw CO [ppm]			9979			9876
Brake specific CO [g/bhp-hr]			23.99			23.77
Raw NO _x [ppm]			3382			3544
Brake specific NO _x [g/bhp-hr]			13.36			14.01
CO ₂ [%] / O ₂ [%]			11.5 / 0.3			11.5/0.3

Table 14: Field data log from June 25 (Site visit # 5)

Run	30A/1	30A/2	31A/1	31A/2	32A/1	32A/2	33A/1	33A/2	33B
Date	25-Jun-12								
Time	12:35	13:00	13:45	14:15	15:00	15:20	16:05	16:30	17:00
Qmix Setpoint	2100	2100	1700	1700	1400	1400	2100	2100	2100
Speed Setpoint	1150	1150	1000	1000	850	850	1150	1150	1150
Test Duration [min]	15	15	15	15	15	15	15	15	15
Speed/Load Characterization	HS/HL	HS/HL	MS/ML	MS/ML	LS/LL	LS/LL	HS/HL	HS/HL	HS/HL
Engine									
Engine Runtime [hr]	50410	50410	50411	50411	50412	50413	50413	50414	50414
Volumetric Flow [SCFM]	2089	2110	1700	1700	1400	1450	2100	2100	2075
Ambient Temperature [°F]	108	108	109	110	111	111	111	111	106
Suction Pressure [psig]	91	91	90	90	96	94	92	92	92
Discharge Pressure [psig]	876	896	893	912	849	861	909	922	859
Discharge Temperature [°F]	116	118	116	118	119	116	121	120	119
Right Bank MAP [psig]	5	5	4	4	4	4	5	5	5
Left Bank MAP [psig]	5	5	4	4	3	3	6	6	6
Jacket Water Temperature [°F]	180	180	179	179	180	179	183	181	181
Jacket Water Pressure [psig]	22	22	18	19	16	16	22	22	22
Oil temperature [°F]	193	193	190	190	190	190	194	193	193
Oil pressure [psig]	52	51	47	47	41	41	50	50	51
Average MAT [°F]	124	124	121	122	121	120	131	129	127
Fuel Flow [SCFD]	75	74	48	49	30	35	73	72	71
ESM Load [%]	84	85	79	80	78	77	86	86	84
Throttle Position [%]	57	59	45	46	41	41	64	65	58
Ignition Timing	20↔24	21↔24	26	22↔26	26	26	21↔23	21↔23	21↔24
Right Fuel/Air Pressure [”H2O]	0.0↔3.5	0.0↔3.0	3.0↔5.5	3.0↔4.5	4.5↔7.0	4.0↔6.5	0.5↔3.0	0.0↔2.0	
Left Fuel/Air Pressure [”H2O]	3.0↔4.0	3.5↔5.0	4.0↔5.5	4.0↔5.5	5.0↔5.5	4.5↔6.0	4.0↔5.0	3.0↔4.0	
Fuel pressure [psig]	140	141	142	142	147	146	145	146	143
Catalyst ΔP [”H2O]	4.0	4.2	3.0	3.0	2.2	2.1	4.2	4.2	4.2
POST CATALYST									
NO _x sensor [V] - NO _x 1	2.08	1.206	1.396	5.078	5.079	5.078	0.956	1.446	1.245
Outlet Temperature [°F]	1173	1172	1095	1095	1010	1007	1179	1181	1165
PRE CATALYST									
NO _x sensor [V] - NO _x 2	3.178	3.189	3.406	3.394	4.464	4.284	3.501	3.104	3.54
Inlet Temperature [°F]	1092	1087	1017	1022	942	941	1093	1098	1081
POST CATALYST Emissions									
Raw CO [ppm]	221	186	16	12	7257	6971	216	233	
Brake specific CO [g/bhp-hr]	0.57	0.48	0.04	0.03	17.06	16.43	0.55	0.60	
Raw NO _x [ppm]	68	63	229	220	1013	1025	57	62	
Brake specific NO _x [g/bhp-hr]	0.29	0.27	0.95	0.91	3.91	3.97	0.24	0.26	
PRE CATALYST Emissions									
Raw CO [ppm]									12469
Brake specific CO [g/bhp-hr]									29.39
Raw NO _x [ppm]									3232
Brake specific NO _x [g/bhp-hr]									12.51
CO ₂ [%] / O ₂ [%]					11.6/0.2	11.6/0.2			11.5/0.3

Table 15: Field data log from 24-hour test on June 26 – Part 1/4 (Site visit # 5)

Run	35A	36A	37A	38A	39A	40A
Date	26-Jun-12	26-Jun-12	26-Jun-12	26-Jun-12	26-Jun-12	26-Jun-12
Time	14:05	15:05	16:05	17:05	18:05	19:05
Qmix Setpoint	As found					
Speed Setpoint	1140	1140	1140	1140	1140	1140
Test Duration [min]	15	15	15	15	15	15
Speed/Load Characterization	As found					
Engine						
Engine Runtime [hr]	50435	50436	50437	50438	50439	50440
Volumetric Flow [SCFM]	2120	2140	2110	2118	2120	2117
Ambient Temperature [°F]	103	104	103	108	106	105
Suction Pressure [psig]	97	94	97	97	97	97
Discharge Pressure [psig]	925	924	916	905	924	917
Discharge Temperature [°F]	118	119	119	120	118	117
Right Bank MAP [psig]	6	5	5	5	5	5
Left Bank MAP [psig]	6	5	5	5	5	5
Jacket Water Temperature [°F]	182	182	182	181	182	180
Jacket Water Pressure [psig]	21	22	22	22	22	22
Oil temperature [°F]	193	194	194	194	193	193
Oil pressure [psig]	50	50	50	50	50	51
Average MAT [°F]	128	129	128	128	127	124
Fuel Flow [SCFD]	77	77	76	75	75	75
ESM Load [%]	86	86	85	85	85	86
Throttle Position [%]	68	69	67	67	65	65
Ignition Timing	23	23	24	24	23	23
Right Fuel/Air Pressure [“H2O]	Hour 0	Hour 1	Hour 2	Hour 3	Hour 4	Hour 5
Left Fuel/Air Pressure [“H2O]	--	--	--	--	--	--
Fuel pressure [psig]	138	138	140	138	139	138
Catalyst ΔP [“H2O]	4.2	4.2	4.2	4.2	4.2	4.2
POST CATALYST						
NO _x sensor [V] - NO _x 1	2.01	1.053	0.882	1.094	1.463	2.155
Outlet Temperature [°F]	1161	1157	1152	1156	1156	1156
PRE CATALYST						
NO _x sensor [V] - NO _x 2	3.702	3.619	3.682	3.691	3.701	3.7
Inlet Temperature [°F]	1080	1077	1074	1076	1077	1077
POST CATALYST Emissions						
Raw CO [ppm]	243	233	211	217	227	236
Brake specific CO [g/bhp-hr]	0.62	0.60	0.54	0.56	0.58	0.60
Raw NO _x [ppm]	52	60	56	58	61	61
Brake specific NO _x [g/bhp-hr]	0.22	0.25	0.24	0.24	0.26	0.26

Table 16: Field data log from 24-hour test on June 26 and 27 – Part 2/4 (Site visit # 5)

Run	41A	42A	43A	44A	45A	46A
Date	26-Jun-12	26-Jun-12	26-Jun-12	27-Jun-12	27-Jun-12	27-Jun-12
Time	20:05	21:05	23:05	0:05	1:05	2:05
Qmix Setpoint	As found					
Speed Setpoint	1140	1140	1140	1140	1140	1140
Test Duration [min]	15	15	15	15	15	15
Speed/Load Characterization	As found					
Engine						
Engine Runtime [hr]	50441	50442	50444	50445	50446	50447
Volumetric Flow [SCFM]	2135	2140	2150	2180	2200	2214
Ambient Temperature [°F]	102	98	93	91	86	88
Suction Pressure [psig]	97	97	97	97	97	97
Discharge Pressure [psig]	930	936	950	1010	1046	1055
Discharge Temperature [°F]	114	111	108	109	110	110
Right Bank MAP [psig]	5	5	5	6	6	6
Left Bank MAP [psig]	5	5	5	5	6	6
Jacket Water Temperature [°F]	178	178	177	178	178	178
Jacket Water Pressure [psig]	22	21	22	22	21	21
Oil temperature [°F]	192	192	192	192	192	192
Oil pressure [psig]	50	51	51	51	50	51
Average MAT [°F]	121	115	110	110	109	108
Fuel Flow [SCFD]	76	77	77	78	79	81
ESM Load [%]	86	86	86	87	88	88
Throttle Position [%]	67	62	62	67	66	71
Ignition Timing	24	24	24	23	23	23
Right Fuel/Air Pressure ["H2O]	Hour 6	Hour 7	Hour 9	Hour 10	Hour 11	Hour 12
Left Fuel/Air Pressure ["H2O]	--	--	--	--	--	--
Fuel pressure [psig]	138	138	136	138	138	135
Catalyst ΔP ["H2O]	4.2	4.2	4.2	4.3	4.3	4.4
POST CATALYST						
NO _x sensor [V] - NO _x 1	2.145	1.113	2.095	2.222	1.593	1.59
Outlet Temperature [°F]	1154	1153	1156	1158	1159	1165
PRE CATALYST						
NO _x sensor [V] - NO _x 2	3.611	3.645	3.632	3.629	3.667	3.566
Inlet Temperature [°F]	1075	1076	1078	1083	1084	1084
POST CATALYST Emissions						
Raw CO [ppm]	221	229	277	276	286	276
Brake specific CO [g/bhp-hr]	0.57	0.59	0.71	0.71	0.73	0.71
Raw NO _x [ppm]	59	56	66	68	69	63
Brake specific NO _x [g/bhp-hr]	0.25	0.24	0.28	0.29	0.29	0.26

Table 17: Field data log from 24-hour test on June 27 – Part 3/4 (Site visit # 5)

Run	47A	48A	49A	50A	51A	52A
Date	27-Jun-12	27-Jun-12	27-Jun-12	27-Jun-12	27-Jun-12	27-Jun-12
Time	3:05	4:05	5:05	6:05	7:05	8:05
Qmix Setpoint	As found					
Speed Setpoint	1140	1140	1140	1140	1140	1140
Test Duration [min]	15	15	15	15	15	15
Speed/Load Characterization	As found					
Engine						
Engine Runtime [hr]	50448	50449	50450	50451	50452	50453
Volumetric Flow [SCFM]	2200	2220	2206	2160	2160	2150
Ambient Temperature [°F]	85	89	89	90	90	88
Suction Pressure [psig]	97	97	97	97	97	97
Discharge Pressure [psig]	1023	1056	1031	924	933	936
Discharge Temperature [°F]	108	111	112	105	107	107
Right Bank MAP [psig]	6	6	6	5	5	5
Left Bank MAP [psig]	6	6	6	6	6	6
Jacket Water Temperature [°F]	177	178	178	177	177	177
Jacket Water Pressure [psig]	21	22	22	22	21	21
Oil temperature [°F]	191	192	192	191	191	191
Oil pressure [psig]	51	51	51	52	51	51
Average MAT [°F]	105	108	107	104	106	106
Fuel Flow [SCFD]	81	80	80	74	77	77
ESM Load [%]	89	88	88	87	87	87
Throttle Position [%]	65	68	63	56	56	56
Ignition Timing	23	23	23	23	23	23
Right Fuel/Air Pressure ["H2O]	Hour 13	Hour 14	Hour 15	Hour 16	Hour 17	Hour 18
Left Fuel/Air Pressure ["H2O]	--	--	--	--	--	--
Fuel pressure [psig]	134	135	134	136	134	134
Catalyst ΔP ["H2O]	4.4	4.4	4.4	4.2	4.2	4.2
POST CATALYST						
NO _x sensor [V] - NO _x 1	1.9	1.723	2.24	2.14	1.49	2.535
Outlet Temperature [°F]	1166	1172	1172	1158	1146	1148
PRE CATALYST						
NO _x sensor [V] - NO _x 2	3.577	3.613	3.631	3.632	3.661	3.581
Inlet Temperature [°F]	1085	1087	1086	1077	1077	1077
POST CATALYST Emissions						
Raw CO [ppm]	272	279	268	281	263	274
Brake specific CO [g/bhp-hr]	0.70	0.71	0.69	0.72	0.67	0.70
Raw NO _x [ppm]	61	63	63	69	74	76
Brake specific NO _x [g/bhp-hr]	0.26	0.26	0.26	0.29	0.31	0.32

Table 18: Field data log from 24-hour test on June 27 – Part 4/4 (Site visit # 5)

Run	53A	54A	55A
Date	27-Jun-12	27-Jun-12	27-Jun-12
Time	9:05	10:05	12:05
Qmix Setpoint	As found	As found	As found
Speed Setpoint	1140	1140	1140
Test Duration [min]	15	15	15
Speed/Load Characterization	As found	As found	As found
Engine			
Engine Runtime [hr]	50454	50455	50457
Volumetric Flow [SCFM]	2160	2150	2150
Ambient Temperature [°F]	91	94	98
Suction Pressure [psig]	97	98	98
Discharge Pressure [psig]	941	941	940
Discharge Temperature [°F]	112	113	114
Right Bank MAP [psig]	5	5	5
Left Bank MAP [psig]	6	6	6
Jacket Water Temperature [°F]	178	178	179
Jacket Water Pressure [psig]	21	22	21
Oil temperature [°F]	191	191	192
Oil pressure [psig]	52	51	50
Average MAT [°F]	109	112	119
Fuel Flow [SCFD]	77	79	79
ESM Load [%]	87	87	88
Throttle Position [%]	59	61	66
Ignition Timing	23	23	20↔23
Right Fuel/Air Pressure [“H2O]	Hour 19	Hour 20	Hour 22
Left Fuel/Air Pressure [“H2O]	--	--	--
Fuel pressure [psig]	134	134	138
Catalyst ΔP [“H2O]	4.2	4.2	4.2
POST CATALYST			
NO _x sensor [V] - NO _x 1	2.303	2.833	2.505
Outlet Temperature [°F]	1149	1151	1155
PRE CATALYST			
NO _x sensor [V] - NO _x 2	3.597	3.638	3.545
Inlet Temperature [°F]	1076	1081	1088
POST CATALYST Emissions			
Raw CO [ppm]	268	265	310
Brake specific CO [g/bhp-hr]	0.69	0.68	0.79
Raw NO _x [ppm]	74	72	80
Brake specific NO _x [g/bhp-hr]	0.31	0.30	0.34

Table 19: Field data log from August 20 (Site visit # 6)

Run	57A/1	57A/2	58A/1	58A/2	59A/1	59A/2	60A/1	60A/2	60B
Date	20-Aug-12								
Time	11:05	11:30	12:15	12:40	13:55	14:20	15:05	15:35	16:00
Qmix Setpoint	2100	2100	1700	1700	1400	1400	2100	2100	2100
Speed Setpoint	1150	1150	1000	1000	850	850	1150	1150	1150
Test Duration [min]	15	15	15	15	15	15	15	15	15
Speed/Load Characterization	HS/HL	HS/HL	MS/ML	MS/ML	LS/LL	LS/LL	HS/HL	HS/HL	HS/HL
Engine									
Engine Runtime [hr]	46873	46874	46874	46875	46876	46876	46877	46878	46878
Volumetric Flow [SCFM]	2105	2110	1690	1695	1405	1395	2100	2090	2100
Ambient Temperature [°F]	95	95	95	94	95	96	96	98	97
Suction Pressure [psig]	93	93	89	89	93	93	90	91	91
Discharge Pressure [psig]	920	915	918	928	928	934	943	934	916
Discharge Temperature [°F]	103	101	98	98	99	101	105	106	105
Right Bank MAP [psig]	5	5	5	5	4	4	5	5	5
Left Bank MAP [psig]	5	5	4	4	3	3	5	5	5
Jacket Water Temperature [°F]	179	178	178	177	179	179	179	180	179
Jacket Water Pressure [psig]	18	18	15	14	12	12	18	18	18
Oil temperature [°F]	193	193	190	191	191	191	193	193	193
Oil pressure [psig]	51	51	49	47	41	42	51	51	51
Average MAT [°F]	112	111	106	105	105	107	115	117	116
Fuel Flow [SCFD]	77	76	49	50	33	33	76	75	74
ESM Load [%]	85	85	82	81	78	78	84	84	83
Throttle Position [%]	--	--	--	--	--	--	--	--	--
Ignition Timing	24	24	26	26	26	26	22↔24	23↔24	24
Right Fuel/Air Pressure [”H2O]	--	--	--	--	--	--	--	--	--
Left Fuel/Air Pressure [”H2O]	--	--	--	--	--	--	--	--	--
Fuel pressure [psig]	130	130	133	134	136	135	134	134	134
Catalyst ΔP [”H2O]	4.9	4.7	3.4	3.4	2.6	2.6	4.8	4.8	4.8
POST CATALYST									
NO _x sensor [V] - NO _x 1	1.531	2.301	1.49	2.357	2.627	3.34	1.37	1.881	2.212
Outlet Temperature [°F]	1136	1134	1056	1053	985	984	1140	1140	1134
PRE CATALYST									
NO _x sensor [V] - NO _x 2	3.599	3.651	3.469	3.602	3.183	3.402	3.516	3.454	3.067
Inlet Temperature [°F]	1075	1073	1003	1002	955	954	1077	1079	1072
POST CATALYST Emissions									
Raw CO [ppm]	546	556	589	612	877	848	580	594	
Brake specific CO [g/bhp-hr]	1.40	1.40	1.48	1.54	2.16	2.08	1.48	1.52	
Raw NO _x [ppm]	50	52	61	65	100	102	51	54	
Brake specific NO _x [g/bhp-hr]	0.21	0.21	0.25	0.27	0.40	0.41	0.21	0.23	
PRE CATALYST Emissions									
Raw CO [ppm]									12407
Brake specific CO [g/bhp-hr]									29.49
Raw NO _x [ppm]									3090
Brake specific NO _x [g/bhp-hr]									12.06
CO ₂ [%] / O ₂ [%]									11.5/0.4

Table 20: Field data log from August 24 – after retuning (Site visit # 6)

Run	84A	85A	86A	87A	88A	89A	89B
Date	24-Aug-12						
Time	10:15	12:05	13:52	14:25	15:15	15:45	16:05
Qmix Setpoint	2100	2100	1700	1400	1400	2100	2100
Speed Setpoint	1150	1150	1000	850	850	1150	1150
Test Duration [min]	15	15	15	15	15	15	15
Speed/Load Characterization	HS/HL	HS/HL	MS/ML	LS/LL	LS/LL	HS/HL	HS/HL
Engine							
Engine Runtime [hr]	46968	46970	46972	46972	46973	46973	46974
Volumetric Flow [SCFM]	2090	2090	1675	1425	1450	2090	2110
Ambient Temperature [°F]	99	99	99	98	99	99	99
Suction Pressure [psig]	89	91	86	93	93	87	88
Discharge Pressure [psig]	914	890	937	986	1042	1055	1057
Discharge Temperature [°F]	103	107	108	107	109	113	112
Right Bank MAP [psig]	5	6	4	4	4	5	5
Left Bank MAP [psig]	5	5	3	2	3	5	5
Jacket Water Temperature [°F]	178	179	179	180	180	180	180
Jacket Water Pressure [psig]	18	18	14	12	12	18	18
Oil temperature [°F]	192	193	191	190	190	193	194
Oil pressure [psig]	52	51	49	41	42	50	50
Average MAT [°F]	113	118	117	115	115	121	121
Fuel Flow [SCFD]	78	76	49	35	36	77	78
ESM Load [%]	86	85	77	76	78	84	84
Throttle Position [%]	--	--	--	--	--	--	--
Ignition Timing	22	23	26	26	26	21↔24	22↔24
Right Fuel/Air Pressure [“H2O]	633	631	640	654	653	634	
Left Fuel/Air Pressure [“H2O]	--	--	--	--	--	--	--
Fuel pressure [psig]	129	133	141	134	135	132	132
Catalyst ΔP [“H2O]	4.7	4.7	3.4	2.6	2.7	4.8	4.8
POST CATALYST							
NO _x sensor [V] - NO _x 1							
Outlet Temperature [°F]	1139	1134	1055	994	997	1131	1133
PRE CATALYST							
NO _x sensor [V] - NO _x 2							
Inlet Temperature [°F]	1078	1076	1007	956	957	1074	1077
POST CATALYST Emissions							
Raw CO [ppm]	10	92	160	338	6	161	
Brake specific CO [g/bhp-hr]	0.03	0.24	0.40	0.83	0.01	0.41	
Raw NO _x [ppm]	173	25	30	55	327	36	
Brake specific NO _x [g/bhp-hr]	0.73	0.11	0.12	0.22	1.33	0.15	
PRE CATALYST Emissions							
Raw CO [ppm]							10543
Brake specific CO [g/bhp-hr]							25.24
Raw NO _x [ppm]							3668
Brake specific NO _x [g/bhp-hr]							14.42
CO ₂ [%] / O ₂ [%]							11.5/0.4

Appendix F: Installation Details

TORQUE TENSION RELATIONSHIP FOR SAE J429 GRADE BOLTS

NOMINAL THREAD SIZE	SAE J429 GRADE 2		SAE J429 GRADE 5		SAE J429 GRADE 8	
	CLAMP LOAD (LBS)	TIGHTENING TORQUE (K=15)	CLAMP LOAD (LBS)	TIGHTENING TORQUE (K=20)	CLAMP LOAD (LBS)	TIGHTENING TORQUE (K=20)
1/4-20	1,300	49 in-lbs	2,000	75 in-lbs	2,850	107 in-lbs
5/16-18	2,150	101	3,350	157	4,700	220
3/8-16	3,200	15 ft-lbs	4,950	23 ft-lbs	6,950	32.5 ft-lbs
7/16-14	4,400	24	6,800	37	9,600	53
1/2-13	5,850	36.5	9,050	57	12,800	80
9/16-12	7,500	53	11,600	82	16,400	115
5/8-11	9,300	73	14,500	113	20,300	159
3/4-10	13,800	129	21,300	200	30,100	282
7/8-9	11,425	125	29,435	321	41,550	454
1-8	15,000	187.5	39,600	482.5	54,540	680

UNIFIED FINE THREAD SERIES						
1/4-28	1,500	55 in-lbs	75 in-lbs	85 in-lbs	115 in-lbs	3,250
5/16-24	2,400	112	150	173	230	6,200
3/8-24	3,600	17 ft-lbs	22.5 ft-lbs	5,600	26 ft-lbs	7,900
7/16-20	4,900	27	36	7,550	42	10,700
1/2-20	6,600	41	55	10,200	64	14,400
9/16-18	8,400	59	79	13,000	92	18,300
5/8-18	10,600	83	110	16,300	128	23,000
3/4-16	15,400	144	193	23,800	223	33,600
7/8-14	12,610	138	184	32,480	355	45,855
1-12	16,410	205	273	42,270	528	704

CAUTION: ALL TORQUE VALUES LISTED IN THESE CHARTS ARE APPROXIMATE ONLY, AND THEIR USE BY ANYONE IS EXPLICITLY VOLUNTARY. INSURANCE OR LIABILITY CLAIMS ARISING FROM THE USE OF THESE CHARTS WITHOUT THE NECESSARY KNOWLEDGE AND EXPERIENCE OF THE USER, OR WITHOUT ACCURATELY DETERMINING THE CORRECT TORQUE VALUE TO BE USED, WILL BE THE SOLE RESPONSIBILITY OF THE USER. THE USER SHALL BE RESPONSIBLE FOR THE ACCURACY OF THE TORQUE VALUES LISTED IN THESE CHARTS. THE USER SHALL BE RESPONSIBLE FOR THE ACCURACY OF THE TORQUE VALUES LISTED IN THESE CHARTS. THE USER SHALL BE RESPONSIBLE FOR THE ACCURACY OF THE TORQUE VALUES LISTED IN THESE CHARTS.

CLAMP LOAD ESTIMATED AS TEN PER CENT OF TENSILE STRENGTH FOR ALL GRADES. ALL OTHER TORQUE VALUES ARE FOR FINE THREAD. TORQUE VALUES FOR 1/4 AND 5/16 INCH SERIES ARE IN INCH POUNDS. ALL OTHER TORQUE VALUES ARE FOOT POUNDS. TORQUE VALUES WILL BE CALCULATED FROM FORMULA T=K*F*DI FOR ALL UNIFIED COARSE AND FINE THREAD SERIES.

UNDOCKED DRAWINGS ARE FOR REFERENCE ONLY

PRELIMINARY FOR CONSTRUCTION
 AS BUILT

APP BY: _____ DATE: _____
 APP BY: *KRF* DATE: *10/12*

APP BY: _____ DATE: _____

THE DRAWING IS THE PROPERTY OF DRESSER RAND. IT IS TO BE USED ONLY FOR THE PROJECT AND LOCATION SPECIFICALLY IDENTIFIED ON THE DRAWING. IT IS NOT TO BE REPRODUCED, COPIED, OR TRANSMITTED IN ANY FORM OR BY ANY MEANS, ELECTRONIC OR MECHANICAL, INCLUDING PHOTOCOPYING, RECORDING, OR BY ANY INFORMATION STORAGE AND RETRIEVAL SYSTEM, WITHOUT THE WRITTEN PERMISSION OF DRESSER RAND.

LEGEND

SYMBOL	DESCRIPTION
1	UNDOCKED TORQUE
2	UNDOCKED TORQUE
3	UNDOCKED TORQUE
4	UNDOCKED TORQUE
5	UNDOCKED TORQUE
6	UNDOCKED TORQUE
7	UNDOCKED TORQUE
8	UNDOCKED TORQUE

DRESSER RAND
 ENGINEERING
 4870 Baskin Ave. Suite 501
 Fort Collins, CO 80525 USA

TORQUE TENSION RELATIONSHIP
 SHEET 1 OF 1

8 7 6 5 4 3 2 1

D C B A

A B C D

8 7 6 5 4 3 2 1

D C B A

UNDESIGNED DIMENSIONS ARE FOR REFERENCE ONLY

DESIGNED FOR CUSTOMER REVIEW APP BY: _____ DATE: _____
 AS BUILT APP BY: *KH* DATE: *11/12*

ISSUED FOR CONSTRUCTION APP BY: _____ DATE: _____

THE DRAWING COMPANY, CONTRACTOR, AND TRADE SUPPLIER ASSUMES ALL LIABILITY IN CONNECTION WITH THE DESIGN, CONSTRUCTION, AND INSTALLATION OF THE PROJECT. THE DRAWING COMPANY SHALL NOT BE RESPONSIBLE FOR ANY DAMAGE TO PERSONS OR PROPERTY, INCLUDING THE PROJECT, ARISING FROM THE DESIGN, CONSTRUCTION, OR INSTALLATION OF THE PROJECT. THE DRAWING COMPANY SHALL NOT BE RESPONSIBLE FOR ANY DAMAGE TO PERSONS OR PROPERTY, INCLUDING THE PROJECT, ARISING FROM THE DESIGN, CONSTRUCTION, OR INSTALLATION OF THE PROJECT.

LEGEND	
.....	EXISTING
.....	PROPOSED
.....	EQUIPMENT
.....	NEW
.....	PROPOSED EQUIPMENT

NO.	DATE	DESCRIPTION	BY	CHKD.
1		ISSUED FOR CONSTRUCTION		

NO.	DATE	DESCRIPTION	BY	CHKD.
1		ISSUED FOR CONSTRUCTION		

DRESSER-RAND

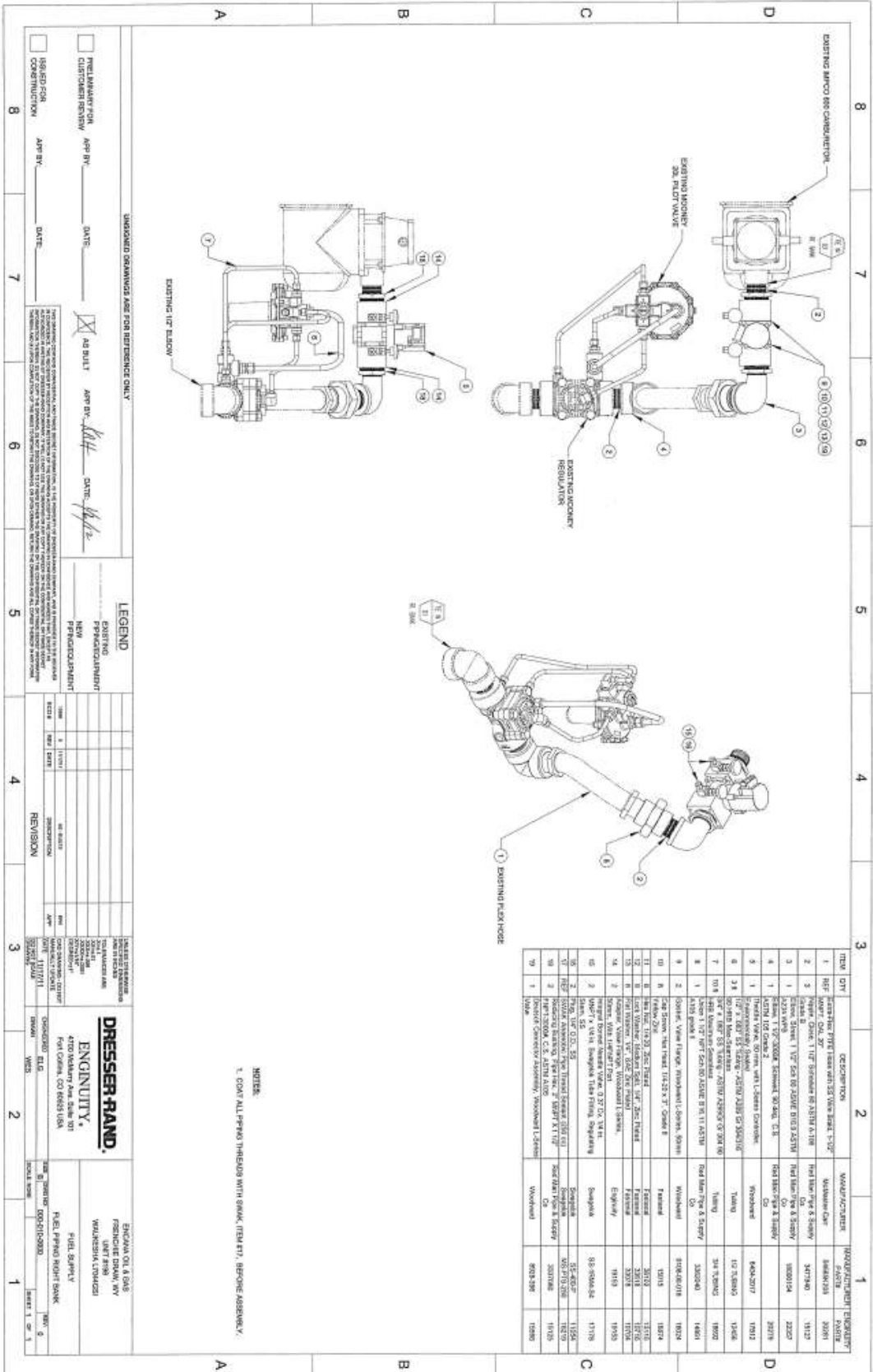
ENGINEERING
 4700 McKinley Ave. Suite 101
 Fair Oakes, CO 80828 USA

EXTENSION OR S.O.D.
 PREPARED BY: _____
 WASHINGTON, D.C.

DESIGN/CHKD:
 PAUL GARDNER

DATE: 11/12
 TOTAL SHEETS: 090910-2000
 SHEET 1 OF 1

NOTES
 1. REMOVE EXISTING MOTOR REGULATION, DO NOT DISCARD. SEE DRAWING 000910-2000 FOR DETAILS.
 2. REMOVE EXISTING 575 VOLT WINDING. SEE DRAWING 000910-2000 FOR DETAILS.



ITEM	QTY	DESCRIPTION	MANUFACTURER	INDUSTRY/COMPANY EQUIVALENT
1	REF	EXISTING FLEX HOSE WITH 1/2" NPT END	WALSH	11524
2	1	REGULATOR	WALSH	11524
3	1	EXISTING MOUNTING RESULATOR	WALSH	11524
4	1	EXISTING MOUNTING 20.0 PLECT VALVE	WALSH	11524
5	1	EXISTING FLEX HOSE WITH 1/2" NPT END	WALSH	11524
6	1	EXISTING FLEX HOSE WITH 1/2" NPT END	WALSH	11524
7	1	EXISTING FLEX HOSE WITH 1/2" NPT END	WALSH	11524
8	1	EXISTING FLEX HOSE WITH 1/2" NPT END	WALSH	11524
9	1	EXISTING FLEX HOSE WITH 1/2" NPT END	WALSH	11524
10	1	EXISTING FLEX HOSE WITH 1/2" NPT END	WALSH	11524
11	1	EXISTING FLEX HOSE WITH 1/2" NPT END	WALSH	11524
12	1	EXISTING FLEX HOSE WITH 1/2" NPT END	WALSH	11524
13	1	EXISTING FLEX HOSE WITH 1/2" NPT END	WALSH	11524
14	1	EXISTING FLEX HOSE WITH 1/2" NPT END	WALSH	11524
15	1	EXISTING FLEX HOSE WITH 1/2" NPT END	WALSH	11524
16	1	EXISTING FLEX HOSE WITH 1/2" NPT END	WALSH	11524
17	1	EXISTING FLEX HOSE WITH 1/2" NPT END	WALSH	11524
18	1	EXISTING FLEX HOSE WITH 1/2" NPT END	WALSH	11524
19	1	EXISTING FLEX HOSE WITH 1/2" NPT END	WALSH	11524
20	1	EXISTING FLEX HOSE WITH 1/2" NPT END	WALSH	11524
21	1	EXISTING FLEX HOSE WITH 1/2" NPT END	WALSH	11524
22	1	EXISTING FLEX HOSE WITH 1/2" NPT END	WALSH	11524
23	1	EXISTING FLEX HOSE WITH 1/2" NPT END	WALSH	11524
24	1	EXISTING FLEX HOSE WITH 1/2" NPT END	WALSH	11524
25	1	EXISTING FLEX HOSE WITH 1/2" NPT END	WALSH	11524
26	1	EXISTING FLEX HOSE WITH 1/2" NPT END	WALSH	11524
27	1	EXISTING FLEX HOSE WITH 1/2" NPT END	WALSH	11524
28	1	EXISTING FLEX HOSE WITH 1/2" NPT END	WALSH	11524
29	1	EXISTING FLEX HOSE WITH 1/2" NPT END	WALSH	11524
30	1	EXISTING FLEX HOSE WITH 1/2" NPT END	WALSH	11524
31	1	EXISTING FLEX HOSE WITH 1/2" NPT END	WALSH	11524
32	1	EXISTING FLEX HOSE WITH 1/2" NPT END	WALSH	11524
33	1	EXISTING FLEX HOSE WITH 1/2" NPT END	WALSH	11524
34	1	EXISTING FLEX HOSE WITH 1/2" NPT END	WALSH	11524
35	1	EXISTING FLEX HOSE WITH 1/2" NPT END	WALSH	11524
36	1	EXISTING FLEX HOSE WITH 1/2" NPT END	WALSH	11524
37	1	EXISTING FLEX HOSE WITH 1/2" NPT END	WALSH	11524
38	1	EXISTING FLEX HOSE WITH 1/2" NPT END	WALSH	11524
39	1	EXISTING FLEX HOSE WITH 1/2" NPT END	WALSH	11524
40	1	EXISTING FLEX HOSE WITH 1/2" NPT END	WALSH	11524
41	1	EXISTING FLEX HOSE WITH 1/2" NPT END	WALSH	11524
42	1	EXISTING FLEX HOSE WITH 1/2" NPT END	WALSH	11524
43	1	EXISTING FLEX HOSE WITH 1/2" NPT END	WALSH	11524
44	1	EXISTING FLEX HOSE WITH 1/2" NPT END	WALSH	11524
45	1	EXISTING FLEX HOSE WITH 1/2" NPT END	WALSH	11524
46	1	EXISTING FLEX HOSE WITH 1/2" NPT END	WALSH	11524
47	1	EXISTING FLEX HOSE WITH 1/2" NPT END	WALSH	11524
48	1	EXISTING FLEX HOSE WITH 1/2" NPT END	WALSH	11524
49	1	EXISTING FLEX HOSE WITH 1/2" NPT END	WALSH	11524
50	1	EXISTING FLEX HOSE WITH 1/2" NPT END	WALSH	11524
51	1	EXISTING FLEX HOSE WITH 1/2" NPT END	WALSH	11524
52	1	EXISTING FLEX HOSE WITH 1/2" NPT END	WALSH	11524
53	1	EXISTING FLEX HOSE WITH 1/2" NPT END	WALSH	11524
54	1	EXISTING FLEX HOSE WITH 1/2" NPT END	WALSH	11524
55	1	EXISTING FLEX HOSE WITH 1/2" NPT END	WALSH	11524
56	1	EXISTING FLEX HOSE WITH 1/2" NPT END	WALSH	11524
57	1	EXISTING FLEX HOSE WITH 1/2" NPT END	WALSH	11524
58	1	EXISTING FLEX HOSE WITH 1/2" NPT END	WALSH	11524
59	1	EXISTING FLEX HOSE WITH 1/2" NPT END	WALSH	11524
60	1	EXISTING FLEX HOSE WITH 1/2" NPT END	WALSH	11524
61	1	EXISTING FLEX HOSE WITH 1/2" NPT END	WALSH	11524
62	1	EXISTING FLEX HOSE WITH 1/2" NPT END	WALSH	11524
63	1	EXISTING FLEX HOSE WITH 1/2" NPT END	WALSH	11524
64	1	EXISTING FLEX HOSE WITH 1/2" NPT END	WALSH	11524
65	1	EXISTING FLEX HOSE WITH 1/2" NPT END	WALSH	11524
66	1	EXISTING FLEX HOSE WITH 1/2" NPT END	WALSH	11524
67	1	EXISTING FLEX HOSE WITH 1/2" NPT END	WALSH	11524
68	1	EXISTING FLEX HOSE WITH 1/2" NPT END	WALSH	11524
69	1	EXISTING FLEX HOSE WITH 1/2" NPT END	WALSH	11524
70	1	EXISTING FLEX HOSE WITH 1/2" NPT END	WALSH	11524

NOTE:
1. COAT ALL PIPING THREADS WITH GUNK (ITEM #7), BEFORE ASSEMBLY.

UNLOAD DRAWINGS ARE FOR REFERENCE ONLY.

DESIGNED BY: _____ DATE: _____
 CHECKED BY: _____ DATE: _____
 APPR BY: *KLL* DATE: *1/1/11*

ISSUED FOR CONSTRUCTION

LEGEND

EXISTING	NEW
PPRAC/COMPLIMENT	PPRAC/COMPLIMENT

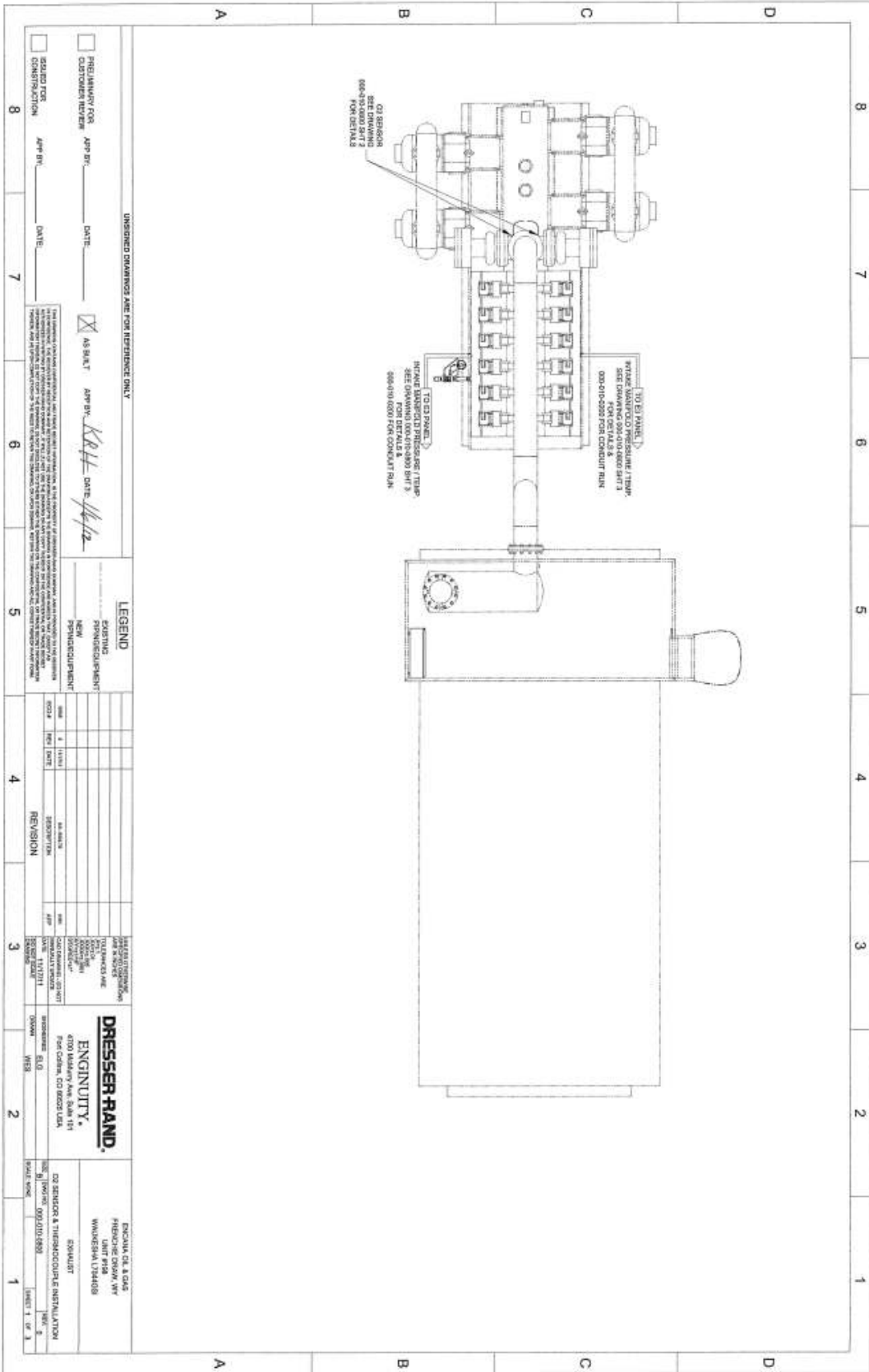
REVISION

NO.	DATE	DESCRIPTION	BY
1	1/1/11	ISSUED FOR CONSTRUCTION	KLL

DRESSER RAND
ENGINEERING
 4700 Valley Ave. Suite 101
 Fort Collins, CO 80525 USA

ENCINA OIL & GAS
 ENGINEERING GROUP
 WASHINGTON, DISTRICT OF COLUMBIA

FUEL SYSTEM
 FUEL PIPING RIGHT BANK



UNORDERED DRAWINGS ARE FOR REFERENCE ONLY

REGULATORY FOR APP BY: _____ DATE: _____

CUSTOMER REVIEW FOR APP BY: *KRH* DATE: *11/12*

AS BUILT

DESIGN FOR CONSTRUCTION APP BY: _____ DATE: _____

THESE DRAWINGS ARE THE PROPERTY OF DRESSER RAND. THEY ARE TO BE USED ONLY FOR THE PROJECT AND SITE SPECIFICALLY IDENTIFIED HEREIN. ANY REUSE OR MODIFICATION OF THESE DRAWINGS WITHOUT THE WRITTEN PERMISSION OF DRESSER RAND IS STRICTLY PROHIBITED. DRESSER RAND ASSUMES NO LIABILITY FOR ANY ERRORS OR OMISSIONS IN THESE DRAWINGS.

LEGEND

ASBESTOS
PRINCIPAL/DESIGNER
NEW
PRINCIPAL/CLIENT

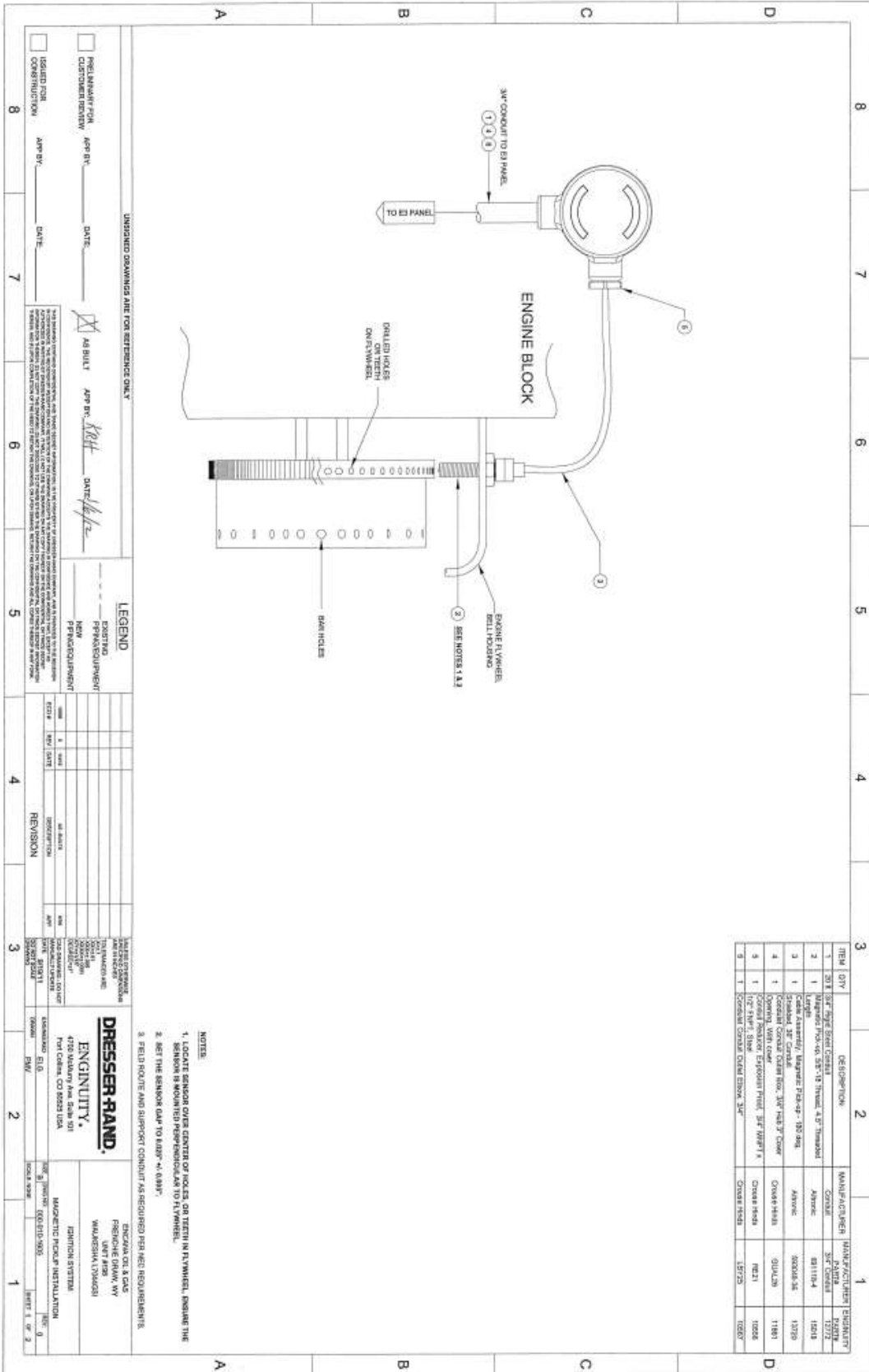
NO.	DATE	REVISION	BY
1	11/12	AS BUILT	APP

DATE OF THIS DRAWING: 11/12/11
 DRAWN BY: _____
 CHECKED BY: _____
 APPROVED BY: _____

DRESSER RAND
ENGINEERING
 4700 Midway Ave, Suite 154
 Fort Collins, CO 80525 USA
 PHONE: 970.221.1111
 FAX: 970.221.1112
 WWW.DRESSER-RAND.COM

ENCLINA OIL & GAS
 FIBERGLASS DRY AIR
 WANDERSMA L194488

DESIGNER & THERMOCUPLE INSTALLATION
 SHEET 1 OF 3



ITEM	QTY	DESCRIPTION	MANUFACTURER	MANUFACTURE PART#
1	1	3/4\"/>	CONRAD	1272
2	1	3/4\"/>	ANYONE	1248
3	1	Cable assembly, Magnetic Pick-up - 100 Ohm	ANYONE	1270
4	1	Constant Contact Valve Pos. 3/4\"/>	CONRAD	1181
5	1	Constant Contact Valve Pos. 3/4\"/>	CONRAD	1226
6	1	Constant Contact Valve Pos. 3/4\"/>	CONRAD	1227

- NOTES**
1. LOCATE SENSOR OVER CENTER OF HOLES, OR TEETH IN TYPICAL. ENSURE THE SENSOR IS MOUNTED PERPENDICULAR TO TYPICAL.
 2. SET THE SENSOR GAP TO .005\"/>
 3. FIELD ROUTE AND SUPPORT CONDUIT AS REQUIRED PER NET REQUIREMENTS.

DRESSER-RAND
ENGINEERING
 4700 Valley Ave. Suite 501
 Fort Collins, CO 80525 USA

ENCLOSURE & Dwg
 FRENCH ENGINE, NY
 WASHINGTON, D.C.

MAGNETIC PICKUP INSTALLATION

DATE: 11/22/81
 DRAWN BY: JWG
 CHECKED BY: JWG

UNISSUED DRAWINGS ARE FOR REFERENCE ONLY

ISSUED FOR: _____ APP BY: _____ DATE: _____

CUSTOMER REVIEW: _____ APP BY: _____ DATE: _____

AS BUILT: _____ APP BY: _____ DATE: _____

DESIGNED: _____
 PPM/EQUIPMENT: _____
 DRAWN: _____
 PPM/EQUIPMENT: _____

REVISION

NO.	DATE	DESCRIPTION	APP.	CHK.
1	11/22/81	AS BUILT	JWG	JWG

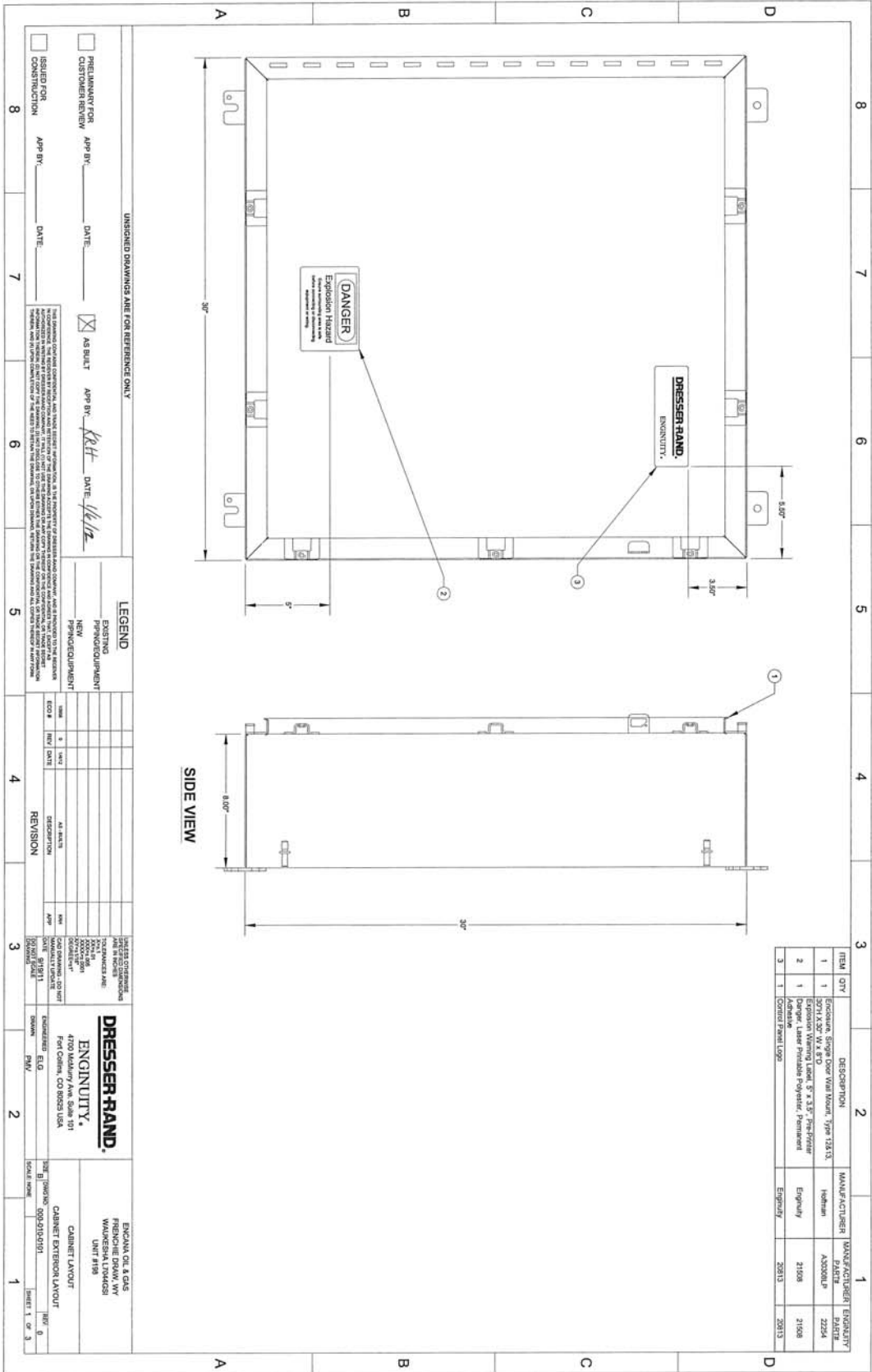
DATE: 11/22/81

APP BY: _____

DATE: _____

ISSUED FOR: _____

CONSTRUCTION: _____



UNDESIGNED DRAWINGS ARE FOR REFERENCE ONLY

ISSUED FOR CONSTRUCTION

APR BY: DATE: 1/4/12

AS BUILT

APR BY: KRT DATE: 1/4/12

LEGEND

EXISTING PIPE/EQUIPMENT

NEW PIPE/EQUIPMENT

DATE: 1/4/12

NO.	DATE	DESCRIPTION	BY	CHKD
1	1/4/12	AS BUILT	KRT	

ENGINEER: E.D. SWAN

DATE: 1/4/12

SCALE: 1/8" = 1'-0"

DRESSER RAND.

ENGINEERING

4700 Madbury Ave, Suite 101

Fort Collins, CO 80525 USA

ENGINEER: E.D. SWAN

DATE: 1/4/12

SCALE: 1/8" = 1'-0"

ENGINEER: E.D. SWAN

DATE: 1/4/12

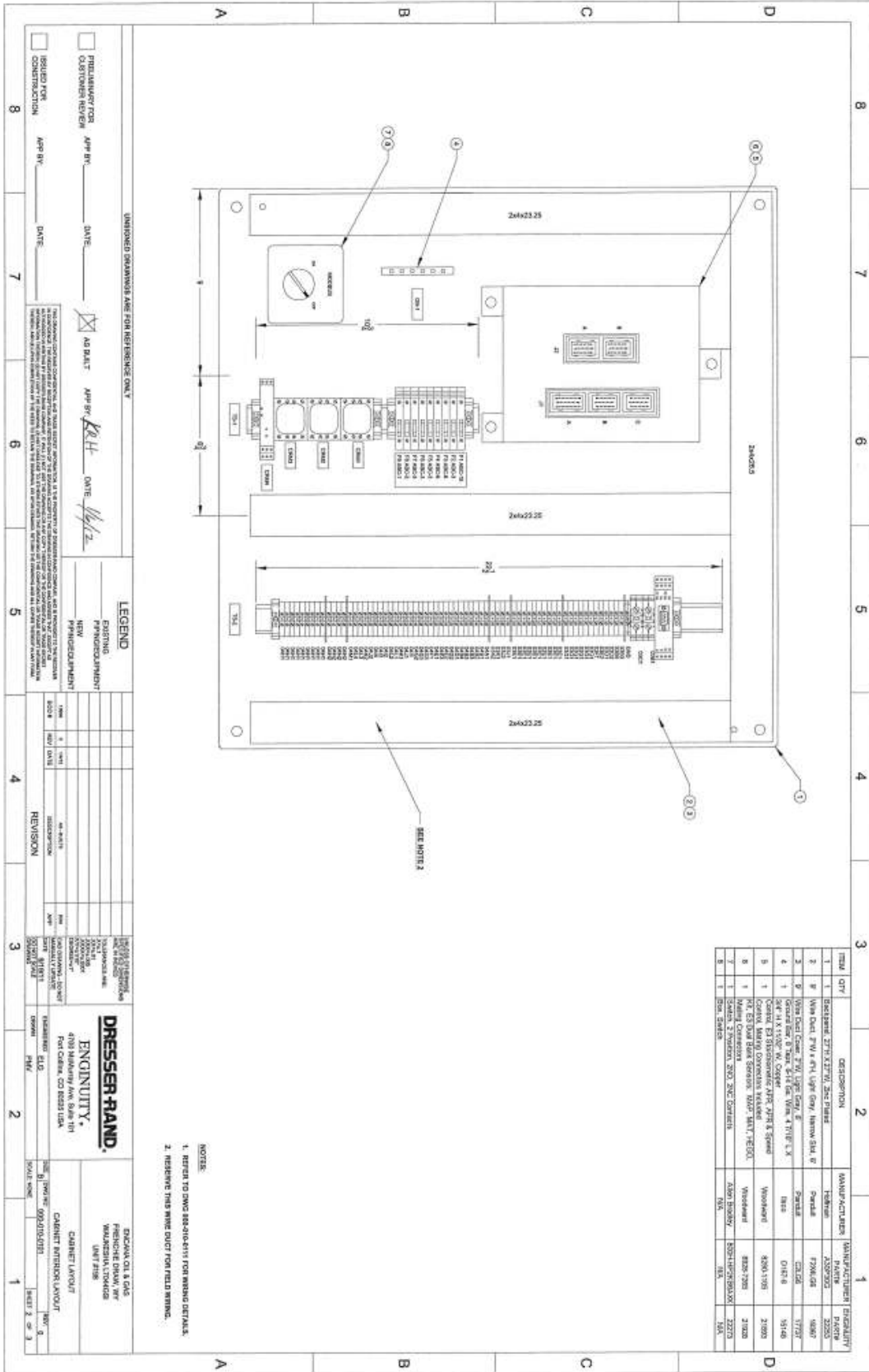
SCALE: 1/8" = 1'-0"

CABINET LAYOUT

ENGINEER: E.D. SWAN

DATE: 1/4/12

SCALE: 1/8" = 1'-0"



ITEM	QTY	DESCRIPTION	MANUFACTURER	FINISH	MANUFACTURER	FINISH
1	1	Backpanel 27 1/2" x 27 1/2" 2x2 Panel	Formica	2525S		
2	8	Van Duct 4 1/4" x 4 1/4" Gray Formica Shd. B	Formica	1796/68	9687	
3	2	Van Duct 2 1/4" x 2 1/4" Gray Formica Shd. B	Formica	1796/68	9687	
4	1	2x4 x 1 1/2" x 1 1/2" W. Caped Oak Veneer 4 1/2" H. x 1 1/2" D.	Formica	0167 B	151-48	21002
5	1	Corona Maple Dovetail Veneer	Woodward	488-1205	21002	
6	1	Corona Maple Dovetail Veneer	Woodward	488-1205	21002	
7	1	Shawn 2 1/2" x 2 1/2" 2x2 Corners	Alloy Industry	55011675/09/001	22710	
8	1	2x4 2x2 Corners	Formica	1796/68	9687	

NOTE:
 1. REFER TO DWG 88-310-011V FOR FINISH DETAILS.
 2. RESERVE THIS WING DUCT FOR FIELD FINISH.

UNIFIED DRAWINGS ARE FOR REFERENCE ONLY

PROBABILITY FOR CUSTOMER REVIEW: App BY: _____ DATE: _____

AS BUILT: App BY: *RKH* DATE: *11/12*

ISSUED FOR CONSTRUCTION: App BY: _____ DATE: _____

NO DIMENSIONS OR CONSTRUCTION AND SHALL BE SUBJECT TO THE DISCRETION OF THE ARCHITECT AND ENGINEER. THE CONTRACTOR SHALL BE RESPONSIBLE FOR VERIFYING ALL DIMENSIONS AND CONDITIONS OF THE WORK. THE CONTRACTOR SHALL BE RESPONSIBLE FOR OBTAINING ALL NECESSARY PERMITS AND APPROVALS. THE CONTRACTOR SHALL BE RESPONSIBLE FOR OBTAINING ALL NECESSARY MATERIALS AND SUPPLIES. THE CONTRACTOR SHALL BE RESPONSIBLE FOR OBTAINING ALL NECESSARY LABORERS.

LEGEND

SYMBOL	DESCRIPTION
(Symbol)	EXISTING
(Symbol)	PROPOSED/REVISION
(Symbol)	NEW
(Symbol)	PHYSICAL DIMENSION

DRESSER-RAND
ENGINEERING
 4785 Mainway Ave. Suite 101
 Fort Collins, CO 80525 USA

ENCLOSURE & 1/4" FINISHES DRAWING FOR CABINET INTERIOR LAYOUT SHEET 2 OF 3

CABINET INTERIOR LAYOUT SHEET 2 OF 3

Control Wiring Diagram

E3 Air Fuel Ratio
 Controls Project
 Encana Oil & Gas
 Frenchie Draw, WY

Engine Manufacturer: Waukesha
 Engine Model: L7044GSI
 Engine Drive: Compressor
 Control Type: RELU

Pg#	Description
1	Cover Sheet and Index
2	General Notes and Symbols
3	Power Distribution
4	E3 Wiring
5	Communication Isolation / Conversion

UNFINISHED DRAWINGS ARE FOR REFERENCE ONLY

THESE DRAWINGS FOR CUSTOMER REVIEW DATE: _____
 REQUEST FOR CONSTRUCTION DATE: _____

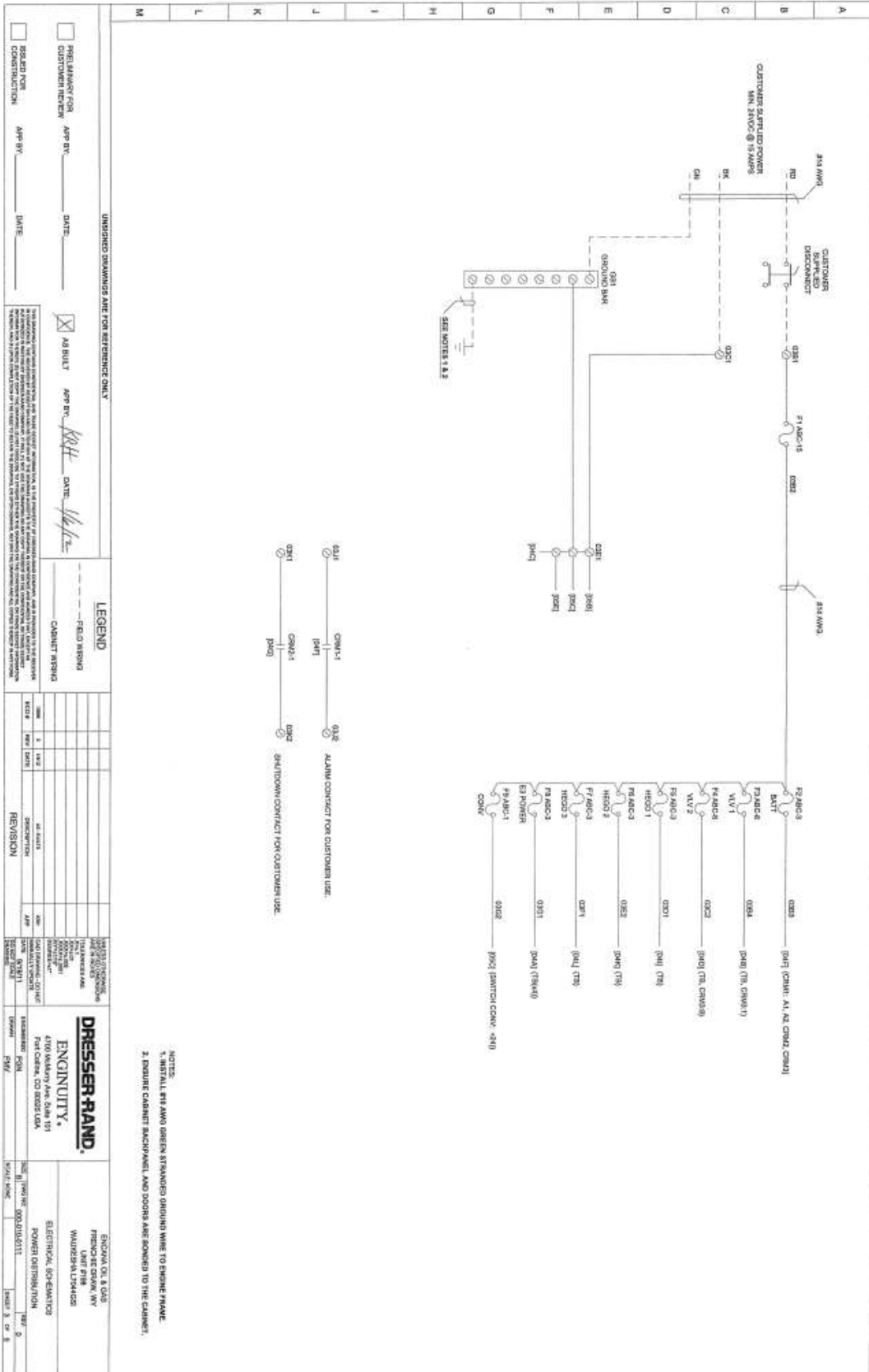
AS BUILT APP BY: *KEH* DATE: *4/6/12*

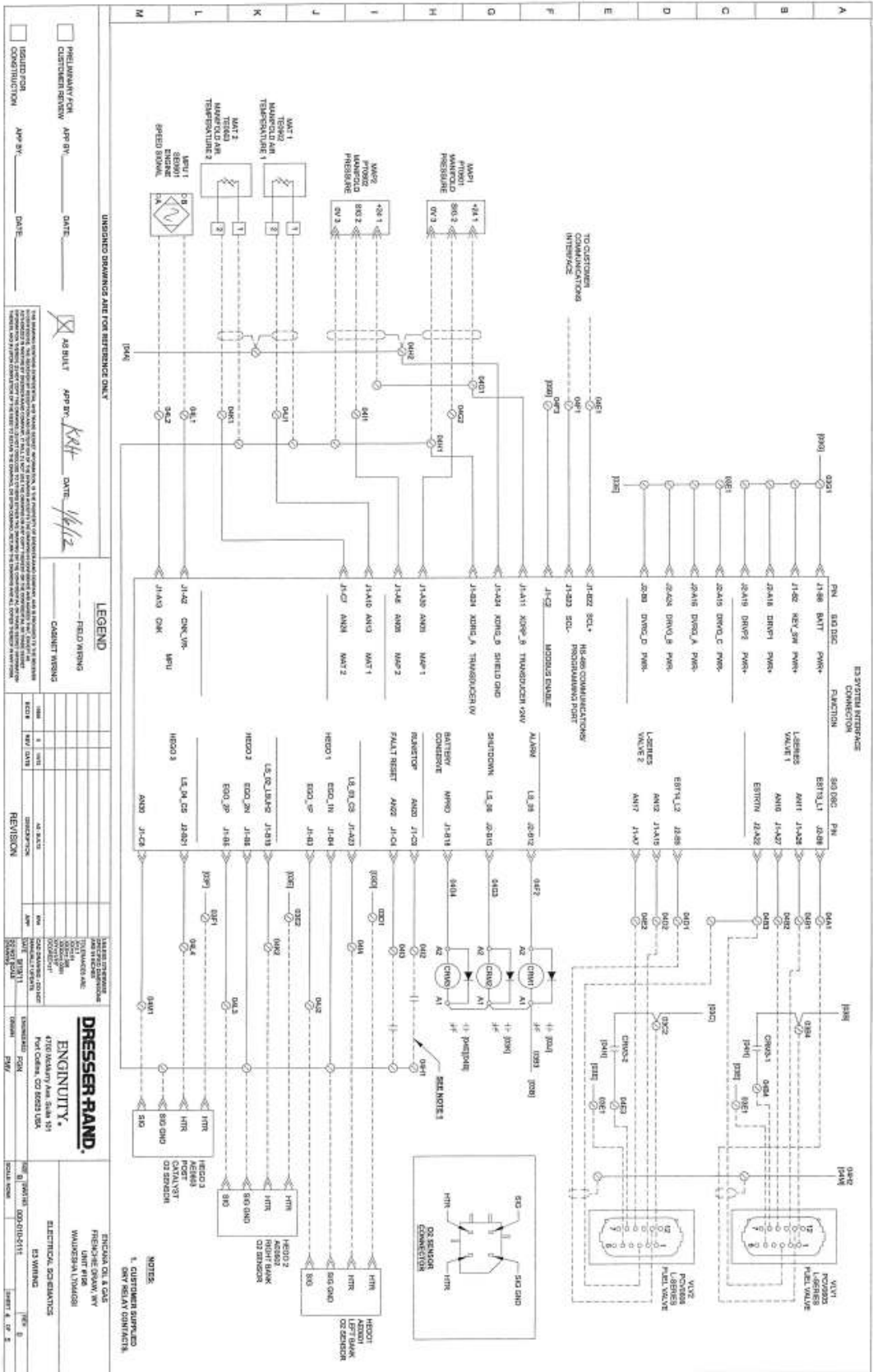
LEGEND FIELD WIRING CABINET WIRING

NO.	DESCRIPTION	DATE	BY	REVISION
1	AS BUILT	4/6/12	KEH	

DRESSER-RAND, ENGINE UTILITY, 4170 Oakley Ave. Ste. 501, Parkersburg, WV 26101
 PROJECT: ENGIN UTILITY

RECORD OR LOG: FRENCHES DRAWING UNIT #118 WARDEN WYOMING ELECTRICAL SCHEMATIC CONSTRUCTION AND INSULATION SHEET 1 OF 3







WOODWARD

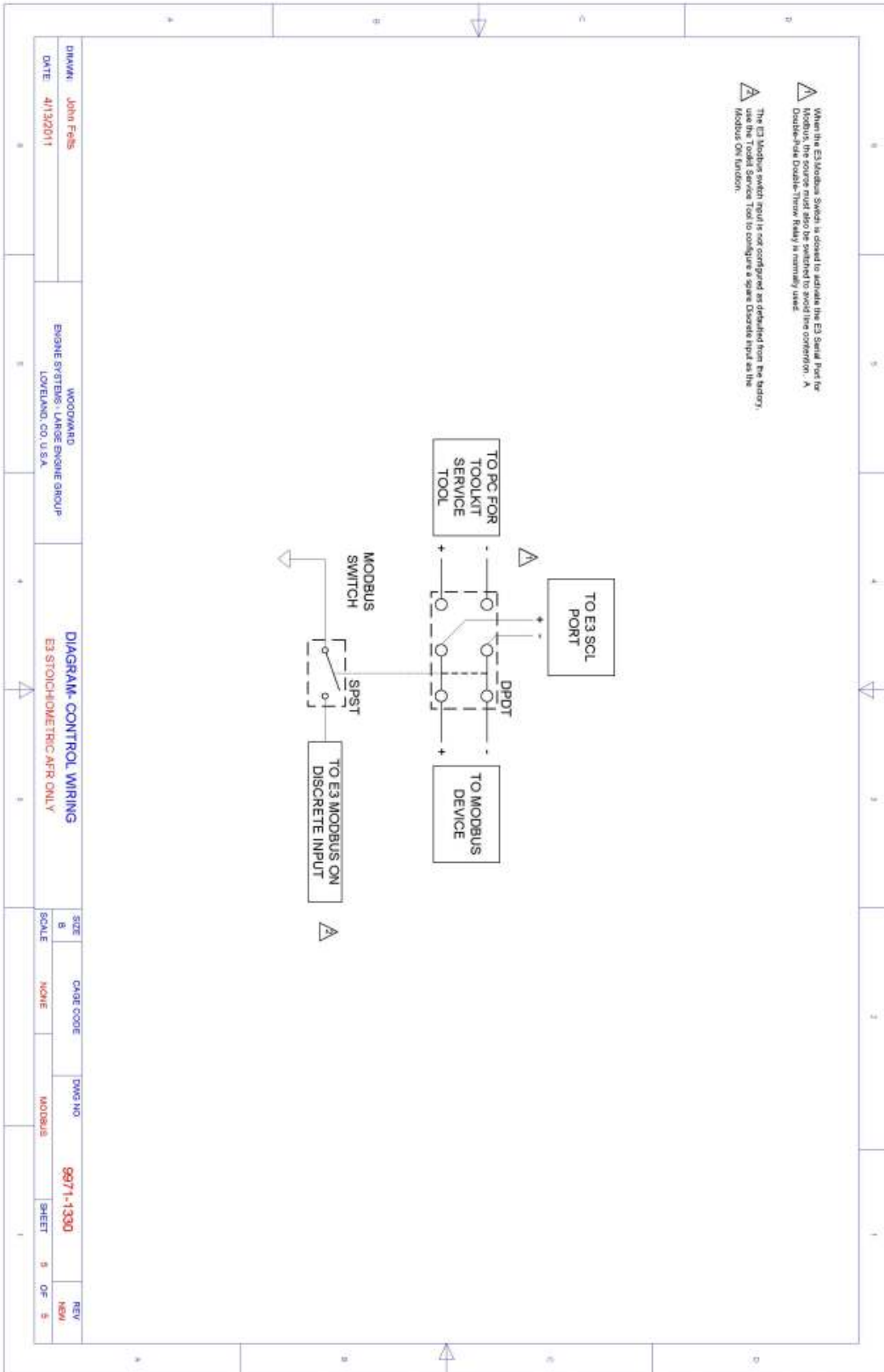
E3 STOICHIOMETRIC CONTROL SYSTEM WITH CATALYST AND ENGINE PROTECTION SYSTEM

Encana Gram Central #5 Unit 198
 Waukeshia L7044GSI SN C-15011/1
 E3 Stoichiometric AFR Only
 Woodward PN 8280-1104

CONTROL WIRING DIAGRAM

REVISION HISTORY			
REV	DESCRIPTION	DATE	APPROVED
0	PRELIMINARY FOR REVIEW	8/19/2011	CODEFOOR

DRAWN	Chris DeFoor	WOODWARD, INC.	DIAGRAM-CONTROL WIRING	SIZE	CAGE CODE	DWG NO.	REV
DATE	8/19/2011	LARGE ENGINE SYSTEMS LOWELAND, COLORADO, USA	E3 STOICHIOMETRIC AFR ONLY	B	NONE	XXXX-XXXX	0
				SCALE		TRUE	SHEET 1 OF 5



LIST OF ABBREVIATIONS

AFR	–	Air Fuel Ratio
BHP	–	Brake Horsepower
BSE	–	Brake Specific Emissions
CeO ₂	–	Ceria
CH ₄	–	Methane
CH ₂ O	–	Formaldehyde
CO ₂	–	Carbon Dioxide
CO	–	Carbon Monoxide
CSU	–	Colorado State University
EECL	–	Engines and Energy Conversion Laboratory
GC	–	Gas Chromatograph
H ₂	–	Hydrogen
HC	–	Hydrocarbons
HEGO	–	Heated Exhaust Gas Oxygen (sensor)
ICE	–	Internal Combustion Engine
LB	–	Lean Burn (engine)
MAP	–	Manifold Absolute Pressure
MAT	–	Manifold Air Temperature

MPU	–	Magnetic Pickup
N ₂	–	Nitrogen
NO	–	Nitric Oxide
NO ₂	–	Nitrogen Dioxide
NO _x	–	Oxides of Nitrogen
NSCR	–	Non-Selective Catalytic Reduction
O ₂	–	Oxygen
P&ID	–	Piping and Instrumentation Diagram
RB	–	Rich Burn (engine)
SI	–	Spark Ignited
STP	–	Standard Temperature and Pressure
THC	–	Total Hydrocarbons
TWC	–	Three-Way Catalyst
UHC	–	Unburnt Hydrocarbons
VOC	–	Volatile Organic Compound